NEWT LIMB AND SPINAL CORD REGENERATION

by

Katherine A. Zukor

A dissertation submitted to the faculty of
The University of Utah
in partial fulfillment of the requirements for the degree of

Doctor of Philosophy

Interdepartmental Program in Neuroscience

The University of Utah

December 2010

The University of Utah Graduate School

STATEMENT OF DISSERTATION APPROVAL

The dissertation of **Katherine A. Zukor**

has been approved by the following supervisory committee members:

Shannon J. Odelberg	, Chair	**10/21/10** Date Approved
Alejandro Sánchez Alvarado	, Member	**10/21/10** Date Approved
Maureen L. Condic	, Member	**10/21/10** Date Approved
Kristen A. Keefe	, Member	**10/21/10** Date Approved
Chi-Bin Chien	, Member	**10/21/10** Date Approved

and by **Mary T. Lucero** , Chair of

the Department of **Neuroscience**

and by Charles A. Wight, Dean of The Graduate School.

ABSTRACT

Newts have an amazing ability to regenerate lost structures and injured tissues. After a complete transection injury, which paralyzes the lower half of the animal, the newt spinal cord regenerates in as little as 4 weeks and re-establishes controlled movement. We have developed new methods of visualizing the cellular and molecular events of spinal cord regeneration and have used these to define six stages of axon regeneration. We also find that axon regeneration appears to be enabled, in part, because the lesion environment is permissive. The extracellular matrix is made up of canonically permissive and inhibitory proteins, but it remains loose and is not dense like it is in mammalian lesions. Meningeal cells and glia are most closely associated with regenerating axons and, instead of forming barriers to axon regeneration as they do in mammals, they appear to assist the regenerative process.

Amputated limbs are regenerated in about 7 – 10 weeks. After amputation, mature cells de-differentiate and form a proliferating pool of progenitor cells under the amputation plane called the regeneration blastema. The blastema then organizes itself into a new limb. Little is known about what molecular factors drive blastema formation and growth. We have identified a novel newt chemokine, NvCXCL, that is highly upregulated during limb regeneration and may play a role in this process. NvCXCL is expressed in de-differentiating tissues and the blastema, stimulates cells of mouse

fibroblastic and myoblastic cell lines to proliferate, and mildly induces the mouse fibroblasts to migrate, although not in a directed fashion.

This work establishes a detailed baseline of the events occurring during spinal cord regeneration and identifies a novel chemokine that may be involved in the formation and growth of the limb blastema. Further insights into the mechanisms driving limb and spinal cord regeneration will be greatly aided by the development of more powerful genetic tools. If the dream of regenerative medicine is to become a reality, it is imperative that we learn all we can about how nature has already derived a solution for regenerating injured structures and organs in this exceptional animal.

TABLE OF CONTENTS

LIST OF TABLES

ACKNOWLEDGMENTS

I thank Shannon Odelberg and the rest of my committee: Maureen Condic, Alejandro Sanchez Alvarado, Chi-Bin Chien, and Kristen Keefe for their excellent training, guidance, and support. I thank lab members David Kent, Tammy Stevenson, and Don Atkinson for their help and suggestions with experimental design and techniques. I thank Chris Rodesch and the University of Utah Cell Imaging Core for help with confocal microscopy; Robert Marc, Bryan Jones, Felix Vasquez-Chona, Drew Ferrell, Jia-Hui Yang, Carl Watt, and James Anderson for assistance with electron microscopy (EM) and the computational molecular phenotyping experiments; Larry Stensaas for his expertise in interpreting the EM data; Gerald Spangrude for his expertise with the analysis of the inflammatory response; and Namakkai and Vasanthi Rajasekaran for technical assistance with Western blots. I am also grateful to have been a part of such wonderful and supportive departments and groups: the Interdepartmental Program in Neuroscience, the Neurobiology and Anatomy Department, the Cardiology Division, and the Developmental Biology Interest Group. Many people in these departments and groups helped by loaning me their equipment, giving me aliquots of antibodies and various reagents to try, offering advice on protocols, giving feedback on proposals and presentations, organizing exciting retreats, symposia, seminars and social events, and providing lots of moral support. My research was funded by grants from the Craig H. Neilsen Foundation to SJO, NINDS to SJO (R01-NS43878), DARPA to SJO (W911NF-

06-1-0067), and by an NIH Developmental Biology Training Grant to KAZ (5T32 HD07491), as well as by funds from the Cardiology Division.

The authors for Chapter 2 are Tamara J. Stevenson, Katherine A. Zukor, Donald L. Atkinson, David T. Kent, and Shannon J. Odelberg, and this work has been submitted to Developmental Dynamics for publication. Chapter 3 is reprinted from Developmental Dynamics, 2010, 239:3048-3057. Katherine A. Zukor, David T. Kent, Shannon J. Odelberg. Fluorescent whole-mount method for visualizing three-dimensional relationships in intact and regenerating adult newt spinal cords. Reprinted with permission of Wiley-Liss, Inc. a subsidiary of John Wiley & Sons, Inc. Chapter 4 is reprinted from Neural Development (in press). Katherine A. Zukor, David T. Kent, Shannon J. Odelberg. Meningeal cells and glia establish a permissive environment for axon regeneration after spinal cord injury in newts. Reproduced with permission of BioMed Central, a part of Springer Science+Business Media.

CHAPTER 1

INTRODUCTION

The ability some animals have to scarlessly regenerate flesh wounds and complex structures such as limbs, eyes, spinal cords and even heads after they are lost or damaged rarely fails to invoke awe and stimulate the imagination. If only we could learn their secrets, maybe someday we too could regrow a limb or walk again after a spinal cord injury (SCI). Perhaps in the future doctors will be able to, as shown in the popular Star Trek television series, wave a device over an injured area that stimulates our own cells to flawlessly heal the damage. Such technology would make surgical interventions, cell-replacement therapies, and prosthetic devices appear crude and obsolete. While this reality may be relegated to the realm of science fiction for now, it is a seemingly impossible dream that, like the dream of flying once was, will not be extinguished.

1.1 Basic principles of regeneration

Regeneration, in a broad sense, is the ability to replace lost or damaged tissues to the extent that the restored tissues resemble and function as well as the original. This is in contrast to fibrotic wound healing, which walls off injuries and repairs them with scar tissue. This type of healing does not restore tissues to their original form and function (reviewed in Harty et al., 2003). For regeneration to occur, two principal components are needed: a source of cells and a genetic program that can control the cells and direct them to reconstruct the missing tissues. In other words, regeneration requires building blocks

and a blueprint. Stem cells, progenitor cells, and/or differentiated cells can be used as the cell source, and regeneration can take place in the presence or absence of significant cell proliferation.

When stem or progenitor cells are used as the cell source, injury induces these cells to proliferate and produce undifferentiated progeny that are capable of re-forming all of the lost cell types and tissues. Epithelial tissues in mammals are regenerated in this way if the damage is not so extensive that it eliminates the stem cells (Blanpain et al., 2007). Differentiated cells can be used similarly in that they can be induced to de-differentiate into progenitor cells that collectively can re-form all of the lost cell types and tissues. If the de-differentiated cells and/or stem cell progeny collect under the injury site and form a regeneration blastema, a structure that has self-organizing properties (reviewed in Nye et al., 2003), then the regenerative process is termed epimorphosis (reviewed in Brockes et al., 2001). Regeneration in planarians (freshwater flatworms) and regeneration of limbs and tails in salamanders occurs via epimorphosis. In planarians, the blastema is formed by stem cell progeny (reviewed in Reddien and Sanchez Alvarado, 2004). In salamanders, it is formed by a combination of stem cell progeny and de-differentiated cells (Morrison et al., 2006; Kragl et al., 2009).

More rarely, differentiated cells can be used to replace or repair tissues in the absence of proliferation in a process termed morphallaxis. The term indicates that tissues are repaired via a re-modeling process instead of a re-building from scratch, as is the case with epimorphosis (reviewed in Brockes et al., 2001). Regeneration in hydra (a freshwater polyp) occurs via morphallaxis. When the head is amputated, cells in the body column are re-modeled, or trans-differentiated, into head cells. This process does not

require proliferation (reviewed in: Bode, 2003; Bosch, 2007). Regeneration of axons in the nervous system can also be thought of as a type of morphallaxis. In this example, an axotomized neuron does not have to proliferate or trans-differentiate into another type of cell in order to restore form and function. It simply needs to be able to survive, re-grow an axon and re-establish functional synapses with appropriate targets.

Cells may be mobilized for regeneration primarily by one, or more likely a combination of these processes. What is essential, though, is that cells have the capacity to be mobilized. In other words, cells need to have enough flexibility or plasticity to be able to do what is required for regeneration (Brockes and Kumar, 2002; Odelberg, 2005).

After cells are mobilized, they need to be guided to re-form the missing parts. A sequence of events needs to be set in motion that can reliably reproduce the required form and function. Given that genetics governs the initial development of proper form and function and that regeneration of a structure often resembles its original development, it is thought that regeneration proceeds as a recapitulation of, or a variation on, developmental genetic programs (Brockes et al., 2001). For example, developing limb buds and regenerating limb blastemas progress through similar stages and utilize common molecular pathways to produce a functional limb (Muneoka and Bryant, 1982; Nye et al., 2003). In fact, it is thought that regenerative abilities are greater in animals that never stop growing, that is, in animals that exhibit indeterminate growth, because their developmental programs are always active (Holder and Clarke, 1988).

1.2 Regeneration in animals

All animals have some capacity for regeneration, although the extent tends to decline as the complexity of the animal increases. Invertebrates such as hydra and

planarians have such extensive regenerative abilities that they are said to be immortal under the knife. They can regenerate all of their tissues and organs, including their heads (reviewed in: Bode, 2003; Reddien and Sanchez Alvarado, 2004; Bosch, 2007). Vertebrates are more limited in their regenerative capacities with the more "primitive", cold-blooded classes having higher regenerative potentials than the more "advanced", warm-blooded classes. For example, many fish, amphibians and reptiles can regenerate complex structures such as limbs or tails, whereas regeneration in birds and mammals is much more limited. Mammals have only a modest capacity to regenerate epithelial, bone, and muscle tissues, as well as digit-tips and organs such as the liver (Sanchez Alvarado and Tsonis, 2006).

Regenerative abilities also tend to decline as a function of developmental age in individuals (Bryant et al., 2002; Ferretti et al., 2003; Carlson, 2007). For example, frogs can regenerate limbs and spinal cords before metamorphosis, but lose this ability after metamorphosis (Dent, 1962; Forehand and Farel, 1982; Beattie et al., 1990). Chicks and many mammals are able to regenerate limbs and spinal cords during development, but lose this ability before or shortly after birth (Bregman and Goldberger, 1983; Wanek et al., 1989; Kunkel-Bagden et al., 1992; Hasan et al., 1993; Kostakopoulou et al., 1996; Saunders et al., 1998). This may occur because, as noted above, genetic programs required for regeneration are irreversibly shut off as the animal matures.

The observation that regenerative abilities tend to decline as the complexity of species increases and an individual's development proceeds suggests that regeneration is an ancestral ability that was lost during the course of evolution (Brockes et al., 2001; Sanchez Alvarado and Tsonis, 2006). Thus, understanding how regeneration occurs in

more primitive species may enable us to unlock latent regenerative potentials in our own species. Invertebrate model systems are powerful tools because they are simpler organisms, making it easier to dissect the basic molecular and cellular principles of regeneration. If, however, we are ever to achieve the goal of being able to regenerate complex structures such as limbs and spinal cords in mammals, and ultimately in humans, it is equally imperative that we learn about how these complex structures regenerate in cold-blooded vertebrates. Because salamanders are regarded as the "champions" of vertebrate regeneration (Brockes et al., 2001), a salamander was the model system of choice for the studies presented herein.

1.3 Regeneration in salamanders

Salamanders (Urodeles) represent one of the three orders of amphibians, the other two being Anura (frogs and toads) and Gymnophiona (legless amphibians). Two main families of salamanders are commonly studied in the regeneration field: the mole salamanders (Ambystomatidae*)* and the newts (Salamandridae). More specifically, the axolotl (*Ambystoma mexicanum*) is the mole salamander commonly studied, and the newts commonly studied are those indigenous to various regions such as the Eastern newt (*Notophthalmus viridescens*), the Japanese newt (*Cynops pyrrhogaster*), and the European newt (*Pleurodeles waltl*).

Newts are aquatic, tailed amphibians. They hatch from eggs as aquatic larvae and after a few months undergo metamorphosis, during which they lose their gills, develop lungs and legs, and become terrestrial juveniles. One to 3 years later, they undergo a second metamorphosis, become sexually mature, and return to the water in their adult form. The Eastern newt has a lifespan of about 12 to 15 years. In contrast, axolotls are

said to be neotenic larval salamanders because they never complete the first metamorphosis. They develop legs and become sexually mature, but retain larval characteristics, such as gills, throughout their lives (Brockes and Kumar, 2005).

Newts and axolotls both have amazing regenerative abilities, but because newts complete metamorphosis and therefore may represent the most mature form that can regenerate, we preferred to study them so that lessons learned might be more applicable to the problem of regeneration in adult humans. An adult newt can regenerate its limbs (Brockes, 1997), tail (Iten and Bryant, 1976), jaw (Ghosh et al., 1994), retina (Mitashov, 1996), lens (Eguchi et al., 1974), portions of its heart (Oberpriller and Oberpriller, 1974) and even its spinal cord (Piatt, 1955).

Work presented in this dissertation focuses primarily on spinal cord regeneration, but also touches on limb regeneration in the Eastern newt, *Notophthalmus viridescens*. To reiterate, salamanders are the only vertebrates that can regenerate limbs as adults and the only order of tetrapod (four-limbed) vertebrates that can regenerate their spinal cords as adults. Fish can regenerate fins and their spinal cord as adults but do not have limbs (Zottoli et al., 1994; Becker et al., 1997; Akimenko et al., 2003). Frogs can regenerate their limbs and spinal cord, but not as adults: they lose the ability when they undergo metamorphosis (Dent, 1962; Forehand and Farel, 1982).

1.4 Newt limb regeneration

As mentioned above, newt limb regeneration is a prime example of epimorphic regeneration. It is completed in about 7 – 10 weeks and can be divided into three phases: wound healing (about 1 day), de-differentiation and blastema formation and growth (1 to 3 weeks), and differentiation and morphogenesis (3 to 10 weeks) (Iten and Bryant, 1976).

Immediately after amputation of a limb, epithelial cells migrate to cover the wound within 24 hours. This wound epidermis (WE) then thickens over the next few days to form an apical epithelial cap (AEC). As the WE thickens, cells from various tissues such as muscle, bone, and connective tissues de-differentiate and form a zone of immature mesenchymal cells under the AEC called the regeneration blastema. Muscle stem cells also contribute to the blastema. The blastema grows as de-differentiation proceeds and the blastemal cells divide. At about 3 to 4 weeks after amputation, de-differentiation and blastemal growth cease, and the blastema begins to develop into the new limb. Blastemal cells are patterned and re-differentiate to form all of the tissues of the limb such as muscle and bone.

The regeneration blastema plays a central role in newt limb regeneration and is a special structure that "knows" what to regenerate. For example, a bicep blastema is programmed to regenerate an elbow, forearm, wrist and hand, whereas a forearm blastema is programmed to regenerate only a wrist and hand (reviewed in Brockes, 1997; Nye et al., 2003). Likewise, a leg blastema will regenerate a leg. While much research has focused on cellular processes associated with and required for blastema formation and growth, the molecular mechanisms involved are only just beginning to be discovered. It is known that the early blastema requires nerves (Singer and Craven, 1948) for its survival and that the late blastema requires communication with the AEC (Mescher, 1976). Recent work has shown that Schwann cells in the nerve produce an anterior gradient protein (AG) that is sufficient to rescue blastemal survival and proliferation, and hence limb regeneration, in denervated limbs (Kumar et al., 2007). Much more work, however, is needed to determine what factors mobilize cells to produce this important

structure. To address this need, we performed a gene expression screen comparing genes expressed in intact and regenerating limbs and have begun to characterize one promising candidate that may play a role in cell proliferation and migration during limb regeneration. This is the topic of Chapter 2 of this dissertation.

1.5 Spinal cord regeneration

1.5.1 Spinal cord basics and requirements for functional recovery after SCI

The spinal cord is part of the central nervous system (CNS). When viewed in cross section, it is made up of a central canal that is filled with cerebral spinal fluid and surrounded by ependymal cells. Grey matter containing neuronal cell bodies and astrocytes surrounds the ependymal cells, and white matter containing myelinated axon tracts surrounds the grey matter. The whole cord is wrapped by the three layers of the meninges: the innermost pia mater and its associated basal lamina, the arachnoid mater, and the outermost dura mater.

The newt spinal cord histologically resembles the mammalian spinal cord. The main differences are that the newt spinal cord is smaller, has less grey matter, and its ependymal cells have the morphology of radial glia, the neuronal and glial progenitor cell of the developing mammalian neural cortex (Ferretti et al., 2003). Their radial processes extend to and maintain contact with the basal lamina of the pia mater. Therefore, newt ependymal cells are often referred to as radial ependymoglia or, more simply, ependymoglia (EG).

The spinal cord contains motor neurons that send axons to muscles in the periphery, propriospinal neurons whose axons never leave the spinal cord, and long

distance projection axons that transmit motor commands from the brain to the motor neurons in the spinal cord and sensory information from the periphery to the brain. When the spinal cord is injured, motor and propriospinal neurons in the injury site may die, but the main reason why spinal cord injuries are so devastating is because long distance axons are damaged and the brain is disconnected from the entire spinal cord distal to the injury. When a long distance axon is cut, the distal part of the axon degenerates and is phagocytosed in a process called Wallerian degeneration, and the proximal part, the part that is still connected to the cell body, has the opportunity to re-grow if the cell body does not die (reviewed in Bradbury and McMahon, 2006).

Therefore, to restore the bulk of the function lost after a spinal cord injury, new neurons do not necessarily need to be generated, but the following must be accomplished. 1) Axotomized long-distance projection neurons must survive, and the extent of the damage must be minimized. 2) Surviving neurons must regenerate their axons through and beyond the injury site. 3) The regenerating axons must be guided to proper targets. 4) They must re-establish functional synapses with those targets. 5) They must be able to conduct action potentials. 6) The re-established synapses must be able to restore function. Thus, functional regeneration of axons can be thought of as a type of morphallaxis. New cells may be required to assist the process, but the critical component is the proper remodeling of the surviving neurons' processes. In mammals, the first criterion is partially met in that some long distance projection neurons do survive the injury, but the subsequent criteria are not met (Sauve, 2005; Bradbury and McMahon, 2006).

1.5.2 Spinal cord injury in mammals and regeneration failure

Axons fail to regenerate through and beyond a spinal cord injury site in mammals for two primary reasons: 1) adult CNS neurons, though they do have some capacity for growth (David and Aguayo, 1981), are intrinsically inefficient at re-growing an axon (Cai et al., 2001; Blackmore and Letourneau, 2006) and 2) the environment of the injured spinal cord is inhibitory for axon regeneration (reviewed in Silver and Miller, 2004). A variety of cell types near an SCI lesion react to create physical barriers to axon regeneration, such as a scar, glia limitans, and cystic cavities, as well as chemical barriers, such as an extracellular matrix (ECM) that is repulsive for axon migration. Chondroitin sulfate proteoglycans (CSPGs) are a major component of the inhibitory ECM (Davies et al., 1999; Tang et al., 2003), and though permissive proteins such as laminin (LM) (Busch et al., 2010) and fibronectin (FN) (Bundesen et al., 2003; Herrmann et al., 2010) are also expressed, overall the matrix is dense and does not promote growth cone motility (Condic and Lemons, 2002). Beyond the injury site, axon regrowth is inhibited by proteins expressed on degenerating myelin such as Nogo-A (Chen et al., 2000), myelin associated glycoprotein (MAG) (McKerracher et al., 1994; Mukhopadhyay et al., 1994), and oligodendrocyte myelin glycoprotein (OMgp) (Wang et al., 2002). Axon regeneration can be modestly improved by a number of manipulations, including treatments that: enhance neuron-intrinsic growth potential, such as cyclic AMP injections (Qiu et al., 2002); degrade CSPGs, such as application of chondroitinase ABC (Bradbury et al., 2002); neutralize myelin inhibitors, such as application of function-blocking antibodies (Caroni and Schwab, 1988); or provide a bridge that does not contain

inhibitors, such as implantation of a peripheral nervous system bridge (David and Aguayo, 1981).

Three of the cell types that create an inhibitory environment in the lesion are astrocytes, meningeal fibroblasts, and macrophages (reviewed in Silver and Miller, 2004). Activated astrocytes become hypertrophic, meaning that they upregulate cytoskeletal proteins such as glial fibrillary acidic protein (GFAP) and their processes become thickened. Their hypertrophic processes wall off the injury and contribute to the formation of the barrier glia limitans between the cord and the injury site. Astrocytes also migrate into the injury site to contribute to the formation of a dense scar. Throughout all these activities, astrocytes secrete inhibitory CSPGs. Thus, the CSPGs are deposited in the scar, glia limitans, and in the spinal cord white matter in a gradient that increases as axons approach the edge of the lesion (Davies et al., 1999). Meningeal fibroblasts also invade the injury site, secrete high levels of ECM proteins including CSPGs, and participate in the formation of the scar and glia limitans. In fact, meningeal cells and astrocytes may communicate with each other to form the glia limitans (Bundesen et al., 2003; Shearer et al., 2003). Activated macrophages invade the lesion to phagocytose debris, contribute to the formation of the scar as well as cystic cavities (Fitch et al., 1999), and have even been shown to physically interact with axons to cause axon retraction (Horn et al., 2008). Disruption of the blood brain barrier (BBB) and release of cytokines as part of the inflammatory response likely play roles in activating these reactive cell behaviors (reviewed in Silver and Miller, 2004).

1.5.3 Spinal cord regeneration in newts

Unlike mammals, adult newts have the remarkable ability to regenerate their spinal cords. Their spinal cords regenerate with the regenerating tail after tail amputation (Singer et al., 1979), as well as after a gap-inducing SCI such as a complete transection (Piatt, 1955). For brevity, the term SCI will be used to refer to a gap-inducing SCI.

After a complete transection injury to the lower trunk region that paralyzes the hindlimbs, newts can regenerate their spinal cords and regain the use of their hindlimbs in as little as 4 weeks (Davis et al., 1990). When long-distance projection neurons in the brain are retrogradedly labeled 60 days after the injury, about 40% regenerate an axon across the lesion and to the hindlimb region compared to uninjured controls, and all brain regions that normally project to the hindlimb region regenerate axons across the lesion (Davis et al., 1989). Furthermore, the degree of functional recovery is correlated with the number of long projection axons that regenerate across the lesion, and recovery is abolished when these regenerated axons are once again severed (Davis et al., 1990). This implies that recovery requires long distance axons to regenerate across the lesion and re-establish functional connections with downstream targets. It is not simply due to a reorganization of circuits within the spinal cord. Thus, in the newt, all six criteria for functional spinal cord regeneration listed above are met. It should also be noted that functional recovery does not require neurogenesis. Davis et al (1990) found no evidence that new neurons are generated in the brain, and the grey matter at the injury site is not restored to its original volume at the time of recovery. While this indicates that regeneration of the adult newt spinal cord after SCI may not be perfect, there is evidence that, over time, the grey matter is at least partially reconstituted (Butler and Ward, 1967).

These findings led us to ask the questions: How do newt axons regenerate through and beyond the injury site? Do they have to be guided to and re-establish functional synapses with the same targets or can other targets be sufficient? Do the denervated targets rewire themselves such that functional recovery is re-established via a new type of circuit that includes propriospinal neurons? Answers to these questions will undoubtedly help us learn more about what may be necessary for functional recovery in mammals and how this may be achieved. Given that the first hurdle we must overcome in mammals relates to the second question, I focused on studying how newt axons regenerate through and beyond an injury site.

Axon regeneration may be enabled in the newt by axon intrinsic and/or axon extrinsic factors. Newt CNS neurons may be able to activate a high intrinsic growth potential, and/or the environment of the injured newt spinal cord may not be inhibitory for axon regeneration.

Much of the research on spinal cord regeneration in newts (and axolotls) has focused on spinal cord regeneration after tail amputation, because the surgical procedures are easier to perform. Additionally, because EG lining the central canal of the spinal cord have properties of neural progenitor cells, much research has focused on the EG response and on their potential to produce various cell types after injury. After tail amputation, a blastema forms and all of the tissues in the tail regenerate via epimorphosis, except the long distance axons that project from the brain. EG upregulate stem cell markers (Walder et al., 2003) and are thought to produce new neurons. Unlike regeneration after an SCI in newt, the grey matter is fully restored (Nordlander and Singer, 1978). There is even evidence that EG progeny contribute to the regeneration of structures outside of the

spinal cord, such as the spinal ganglia (Benraiss et al., 1999), muscle, and cartilage (Echeverri and Tanaka, 2002). EG also appear to play an important role in enabling axon regeneration following tail amputation. They elongate an ependymal tube that precedes and serves as a scaffold for regrowing axons (Nordlander and Singer, 1978). In distal portions of the regenerating tail, the channels formed by EG radial processes are devoid of axons. In more proximal regions, however, the channels contain more axons. The ECM associated with regenerating tail tissues, including the spinal cord, contains tenascin-C (TN-C), a protein that is sometimes permissive and sometimes inhibitory for axon growth, and there is mRNA *in situ* hybridization evidence that EG express this protein in their processes (Caubit et al., 1994). Overall, regeneration after tail amputation is thought to proceed as a recapitulation of developmental processes. Singer et al. (1979) compared spinal cord formation during development and spinal cord regeneration after tail amputation and found that the two processes appeared to be similar. In the context of tail regeneration, long distance projection axons grow into newly developing tissues.

Surprisingly, little is known about how axons regenerate after an SCI in the newt. In this context, axons must re-grow through an injury site having mature tissues on both sides of the lesion. This context is also more relevant to the problem of spinal cord injury in humans. Older studies of SCI in the newt have noted that a blastema and glial scar do not appear to form (Piatt, 1955), that axons can bridge large gaps in the cord before ependymal tubes elongate (Butler and Ward, 1967; Stensaas, 1983), and that, if left intact, the meninges can serve as a scaffold for axon regeneration (Stensaas, 1983). Thus, unlike regeneration after tail amputation, a pre-formed ependymal tube is not required for axon regrowth after an SCI in the trunk region of the animal (rostral to the hindlimbs). A

more recent study analyzed the EG response after an SCI to the tail region of the axolotl spinal cord (caudal to the hindlimbs) and found that EG appear to undergo an epithelial to mesenchymal transition, migrate into the injury site to form a solid mass of cells, and then undergo a mesenchymal to epithelial transition to re-form an ependymal tube that serves as a scaffold for axon regeneration (O'Hara et al., 1992; Chernoff et al., 2003). The mesenchymal "EG" in the injury site expressed the permissive ECM protein, FN. Though the conclusions of this study have dominated the literature as the model of regeneration after an SCI in salamanders, other interpretations of the data are possible. For example, cells in the injury site that Chernoff and colleagues call EG could, instead, be meningeal cells. Furthermore, processes occurring after an SCI to the caudal axolotl spinal cord may differ from those occurring after an SCI in the newt or following an SCI to the trunk region of the spinal cord.

In summary, previous studies of spinal cord regeneration in salamanders suggest that axon extrinsic factors enable axon regeneration. Physical barriers do not appear to form, EG and the meninges may help axons regenerate, and the ECM may contain permissive proteins. It is difficult to discern from these studies, however, a clear understanding of what happens after an SCI to the trunk region of the spinal cord in the newt. Some studies have used newts, others have used axolotls. Some have analyzed regeneration after tail amputation, while others have analyzed regeneration after an SCI. The SCI is usually in the trunk region but can be in the tail region, and the SCI is usually a simple transection but can also be a large ablation. Additionally, in the early studies of regeneration after SCI, many of the techniques used were less powerful than those available today, the quality of the images were less than optimal by today's standards, the

relationship of the images to the injury/amputation site or regenerating axons is not given, and the data presented fail to provide a comprehensive picture of the regenerative process.

To gain a clearer understanding of how axons regenerate through and beyond an SCI in the newt, I performed a comprehensive analysis of axon regeneration and the cellular and extracellular environment axons encounter within the lesion after an SCI. I chose to study regeneration after a complete transection injury to the trunk region of the cord so that my study could complement those done by Piatt (1955) and Davis et al (1989; 1990). The results are discussed in Chapter 4. To ensure that the images presented were of the highest quality, I adapted modern labeling and imaging techniques for use in the newt. These techniques are discussed in Chapters 3 and 4.

1.6 References

Akimenko MA, Mari-Beffa M, Becerra J, Geraudie J (2003) Old questions, new tools, and some answers to the mystery of fin regeneration. Dev Dyn 226:190-201.

Beattie MS, Bresnahan JC, Lopate G (1990) Metamorphosis alters the response to spinal cord transection in Xenopus laevis frogs. J Neurobiol 21:1108-1122.

Becker T, Wullimann MF, Becker CG, Bernhardt RR, Schachner M (1997) Axonal regrowth after spinal cord transection in adult zebrafish. J Comp Neurol 377:577-595.

Benraiss A, Arsanto JP, Coulon J, Thouveny Y (1999) Neurogenesis during caudal spinal cord regeneration in adult newts. Dev Genes Evol 209:363-369.

Blackmore M, Letourneau PC (2006) Changes within maturing neurons limit axonal regeneration in the developing spinal cordq. J Neurobiol 66:348-360.

Blanpain C, Horsley V, Fuchs E (2007) Epithelial stem cells: turning over new leaves. Cell 128:445-458.

Bode HR (2003) Head regeneration in Hydra. Dev Dyn 226:225-236.

Bosch TC (2007) Why polyps regenerate and we don't: towards a cellular and molecular framework for Hydra regeneration. Dev Biol 303:421-433.

Bradbury EJ, McMahon SB (2006) Spinal cord repair strategies: why do they work? Nat Rev Neurosci 7:644-653.

Bradbury EJ, Moon LD, Popat RJ, King VR, Bennett GS, Patel PN, Fawcett JW, McMahon SB (2002) Chondroitinase ABC promotes functional recovery after spinal cord injury. Nature 416:636-640.

Bregman BS, Goldberger ME (1983) Infant lesion effect: II. Sparing and recovery of function after spinal cord damage in newborn and adult cats. Brain Res 285:119-135.

Brockes J, Kumar A (2005) Newts. Curr Biol 15:R42-44.

Brockes JP (1997) Amphibian limb regeneration: rebuilding a complex structure. Science 276:81-87.

Brockes JP, Kumar A (2002) Plasticity and reprogramming of differentiated cells in amphibian regeneration. Nat Rev Mol Cell Biol 3:566-574.

Brockes JP, Kumar A, Velloso CP (2001) Regeneration as an evolutionary variable. J Anat 199:3-11.

Bryant SV, Endo T, Gardiner DM (2002) Vertebrate limb regeneration and the origin of limb stem cells. Int J Dev Biol 46:887-896.

Bundesen LQ, Scheel TA, Bregman BS, Kromer LF (2003) Ephrin-B2 and EphB2 regulation of astrocyte-meningeal fibroblast interactions in response to spinal cord lesions in adult rats. J Neurosci 23:7789-7800.

Busch SA, Horn KP, Cuascut FX, Hawthorne AL, Bai L, Miller RH, Silver J (2010) Adult NG2+ cells are permissive to neurite outgrowth and stabilize sensory axons during macrophage-induced axonal dieback after spinal cord injury. J Neurosci 30:255-265.

Butler EG, Ward MB (1967) Reconstitution of the spinal cord after ablation in adult *Triturus*. Dev Biol 15:464-486.

Cai D, Qiu J, Cao Z, McAtee M, Bregman S, Filbin MT (2001) Neuronal cyclic AMP controls the developmental loss of ability of axons to regenerate. J Neurosci 21:4731-4739.

Carlson BM (2007) Regeneration and aging. In: Princliples of Reneration Biology: Elsevier Inc.

Caroni P, Schwab ME (1988) Antibody against myelin-associated inhibitor of neurite growth neutralizes nonpermissive substrate properties of CNS white matter. Neuron 1:85-96.

Caubit X, Riou JF, Coulon J, Arsanto JP, Benraiss A, Boucaut JC, Thouveny Y (1994) Tenascin expression in developing, adult and regenerating caudal spinal cord in the urodele amphibians. Int J Dev Biol 38:661-672.

Chen MS, Huber AB, van der Haar ME, Frank M, Schnell L, Spillmann AA, Christ F, Schwab ME (2000) Nogo-A is a myelin-associated neurite outgrowth inhibitor and an antigen for monoclonal antibody IN-1. Nature 403:434-439.

Chernoff EA, Stocum DL, Nye HL, Cameron JA (2003) Urodele spinal cord regeneration and related processes. Dev Dyn 226:295-307.

Condic ML, Lemons ML (2002) Extracellular matrix in spinal cord regeneration: getting beyond attraction and inhibition. Neuroreport 13:A37-48.

David S, Aguayo AJ (1981) Axonal elongation into peripheral nervous system "bridges" after central nervous system injury in adult rats. Science 214:931-933.

Davies SJ, Goucher DR, Doller C, Silver J (1999) Robust regeneration of adult sensory axons in degenerating white matter of the adult rat spinal cord. J Neurosci 19:5810-5822.

Davis BM, Duffy MT, Simpson SB, Jr. (1989) Bulbospinal and intraspinal connections in normal and regenerated salamander spinal cord. Exp Neurol 103:41-51.

Davis BM, Ayers JL, Koran L, Carlson J, Anderson MC, Simpson SB, Jr. (1990) Time course of salamander spinal cord regeneration and recovery of swimming: HRP retrograde pathway tracing and kinematic analysis. Exp Neurol 108:198-213.

Dent JN (1962) Limb regeneration in larvae and metamorphosing individuals of the South African clawed toad. J Morphol 110:61-77.

Echeverri K, Tanaka EM (2002) Ectoderm to mesoderm lineage switching during axolotl tail regeneration. Science 298:1993-1996.

Eguchi G, Abe SI, Watanabe K (1974) Differentiation of lens-like structures from newt iris epithelial cells in vitro. Proc Natl Acad Sci U S A 71:5052-5056.

Ferretti P, Zhang F, O'Neill P (2003) Changes in spinal cord regenerative ability through phylogenesis and development: lessons to be learnt. Dev Dyn 226:245-256.

Fitch MT, Doller C, Combs CK, Landreth GE, Silver J (1999) Cellular and molecular mechanisms of glial scarring and progressive cavitation: in vivo and in vitro analysis of inflammation-induced secondary injury after CNS trauma. J Neurosci 19:8182-8198.

Forehand CJ, Farel PB (1982) Anatomical and behavioral recovery from the effects of spinal cord transection: dependence on metamorphosis in anuran larvae. J Neurosci 2:654-652.

Ghosh S, Thorogood P, Ferretti P (1994) Regenerative capability of upper and lower jaws in the newt. Int J Dev Biol 38:479-490.

Harty M, Neff AW, King MW, Mescher AL (2003) Regeneration or scarring: an immunologic perspective. Dev Dyn 226:268-279.

Hasan SJ, Keirstead HS, Muir GD, Steeves JD (1993) Axonal regeneration contributes to repair of injured brainstem-spinal neurons in embryonic chick. J Neurosci 13:492-507.

Herrmann JE, Shah RR, Chan AF, Zheng B (2010) EphA4 deficient mice maintain astroglial-fibrotic scar formation after spinal cord injury. Exp Neurol 223:582-598.

Holder N, Clarke JD (1988) Is there a correlation between continuous neurogenesis and directed axon regeneration in the vertebrate nervous system? Trends Neurosci 11:94-99.

Horn KP, Busch SA, Hawthorne AL, van Rooijen N, Silver J (2008) Another barrier to regeneration in the CNS: activated macrophages induce extensive retraction of dystrophic axons through direct physical interactions. J Neurosci 28:9330-9341.

Iten LE, Bryant SV (1976) Stages of tail regeneration in the adult newt, Notophthalmus viridescens. J Exp Zool 196:283-292.

Kostakopoulou K, Vogel A, Brickell P, Tickle C (1996) 'Regeneration' of wing bud stumps of chick embryos and reactivation of Msx-1 and Shh expression in response to FGF-4 and ridge signals. Mech Dev 55:119-131.

Kragl M, Knapp D, Nacu E, Khattak S, Maden M, Epperlein HH, Tanaka EM (2009) Cells keep a memory of their tissue origin during axolotl limb regeneration. Nature 460:60-65.

Kumar A, Godwin JW, Gates PB, Garza-Garcia AA, Brockes JP (2007) Molecular basis for the nerve dependence of limb regeneration in an adult vertebrate. Science 318:772-777.

Kunkel-Bagden E, Dai HN, Bregman BS (1992) Recovery of function after spinal cord hemisection in newborn and adult rats: differential effects on reflex and locomotor function. Exp Neurol 116:40-51.

McKerracher L, David S, Jackson DL, Kottis V, Dunn RJ, Braun PE (1994) Identification of myelin-associated glycoprotein as a major myelin-derived inhibitor of neurite growth. Neuron 13:805-811.

Mescher AL (1976) Effects on adult newt limb regeneration of partial and complete skin flaps over the amputation surface. J Exp Zool 195:117-128.

Mitashov VI (1996) Mechanisms of retina regeneration in urodeles. Int J Dev Biol 40:833-844.

Morrison JI, Loof S, He P, Simon A (2006) Salamander limb regeneration involves the activation of a multipotent skeletal muscle satellite cell population. J Cell Biol 172:433-440.

Mukhopadhyay G, Doherty P, Walsh FS, Crocker PR, Filbin MT (1994) A novel role for myelin-associated glycoprotein as an inhibitor of axonal regeneration. Neuron 13:757-767.

Muneoka K, Bryant SV (1982) Evidence that patterning mechanisms in developing and regenerating limbs are the same. Nature 298:369-371.

Nordlander RH, Singer M (1978) The role of ependyma in regeneration of the spinal cord in the urodele amphibian tail. J Comp Neurol 180:349-374.

Nye HL, Cameron JA, Chernoff EA, Stocum DL (2003) Regeneration of the urodele limb: a review. Dev Dyn 226:280-294.

O'Hara CM, Egar MW, Chernoff EA (1992) Reorganization of the ependyma during axolotl spinal cord regeneration: changes in intermediate filament and fibronectin expression. Dev Dyn 193:103-115.

Oberpriller JO, Oberpriller JC (1974) Response of the adult newt ventricle to injury. J Exp Zool 187:249-253.

Odelberg SJ (2005) Cellular plasticity in vertebrate regeneration. Anat Rec B New Anat 287:25-35.

Piatt J (1955) Regeneration of the spinal cord in the salamander. J Exp Zool 129:177-207.

Qiu J, Cai D, Dai H, McAtee M, Hoffman PN, Bregman BS, Filbin MT (2002) Spinal axon regeneration induced by elevation of cyclic AMP. Neuron 34:895-903.

Reddien PW, Sanchez Alvarado A (2004) Fundamentals of planarian regeneration. Annu Rev Cell Dev Biol 20:725-757.

Sanchez Alvarado A, Tsonis PA (2006) Bridging the regeneration gap: genetic insights from diverse animal models. Nat Rev Genet 7:873-884.

Saunders NR, Kitchener P, Knott GW, Nicholls JG, Potter A, Smith TJ (1998) Development of walking, swimming and neuronal connections after complete spinal cord transection in the neonatal opossum, Monodelphis domestica. J Neurosci 18:339-355.

Sauve Y (2005) Nervous system regeneration lecture. In: Developmental Neuroscience Course. University of Utah.

Shearer MC, Niclou SP, Brown D, Asher RA, Holtmaat AJ, Levine JM, Verhaagen J, Fawcett JW (2003) The astrocyte/meningeal cell interface is a barrier to neurite outgrowth which can be overcome by manipulation of inhibitory molecules or axonal signalling pathways. Mol Cell Neurosci 24:913-925.

Silver J, Miller JH (2004) Regeneration beyond the glial scar. Nat Rev Neurosci 5:146-156.

Singer M, Craven L (1948) The growth and morphogenesis of the regenerating forelimb of adult Triturus following denervation at various stages of development. J Exp Zool 108:279-308.

Singer M, Nordlander RH, Egar M (1979) Axonal guidance during embryogenesis and regeneration in the spinal cord of the newt: the blueprint hypothesis of neuronal pathway patterning. J Comp Neurol 185:1-21.

Stensaas LJ (1983) Regeneration in the spinal cord of the newt *Notopthalamus (Triturus) pyrrhogaster.* In: Spinal Cord Reconstruction (Kao CC, Bunge RP, Reier PJ, eds), pp 121-149. New York: Raven Press.

Tang X, Davies JE, Davies SJ (2003) Changes in distribution, cell associations, and protein expression levels of NG2, neurocan, phosphacan, brevican, versican V2, and tenascin-C during acute to chronic maturation of spinal cord scar tissue. J Neurosci Res 71:427-444.

Walder S, Zhang F, Ferretti P (2003) Up-regulation of neural stem cell markers suggests the occurrence of dedifferentiation in regenerating spinal cord. Dev Genes Evol 213:625-630.

Wanek N, Muneoka K, Bryant SV (1989) Evidence for regulation following amputation and tissue grafting in the developing mouse limb. J Exp Zool 249:55-61.

Wang KC, Koprivica V, Kim JA, Sivasankaran R, Guo Y, Neve RL, He Z (2002) Oligodendrocyte-myelin glycoprotein is a Nogo receptor ligand that inhibits neurite outgrowth. Nature 417:941-944.

Zottoli SJ, Bentley AP, Feiner DG, Hering JR, Prendergast BJ, Rieff HI (1994) Spinal cord regeneration in adult goldfish: implications for functional recovery in vertebrates. Prog Brain Res 103:219-228.

CHAPTER 2

A NOVEL MITOGENIC CXC CHEMOKINE IS INDUCED DURING NEWT LIMB REGENERATION

2.1 Abstract

Chemokines are cytokines that can induce chemotaxis and proliferation in target cell types and have been implicated in many biological processes such as wound healing, inflammation, cancer metastasis, stem cell recruitment, and angiogenesis. Here we show that a novel newt CXC chemokine (NvCXCL) is markedly upregulated during newt forelimb and hindlimb regeneration and that its expression levels peak at days 6-12 postamputation. NvCXCL is expressed in dedifferentiating tissues in 6-day regenerates and in the apical epithelial cap and blastema in 12-day regenerates. NvCXCL can act as a mitogen for mouse C2C12 and NIH-3T3 cells and, unlike the well-known mitogen IGF1, it can do so even in the absence of stimulating co-factors present in serum. Although we found no evidence that NvCXCL was chemotactic for any cell tested, it did appear to induce a chemokinetic response in NIH-3T3 fibroblasts. These results suggest that NvCXCL may be involved in the formation and growth of the limb blastema by promoting cell proliferation.

2.2 Introduction

Newts and other urodeles have the remarkable ability to regenerate lost appendages and injured organs, including limbs, tails, jaws, spinal cords, lenses, optic

nerves, heart ventricles, intestines, and parts of the brain (Piatt, 1955; O'Steen, 1958; Oberpriller and Oberpriller, 1974; Turner and Singer, 1974b, a; Brockes and Kumar, 2002). This regenerative ability is dependent upon an unusual degree of cellular plasticity at the site of injury. For example, during limb regeneration, differentiated cells just proximal to the amputation site lose their differentiated characteristics, re-enter the cell cycle, and migrate to the distal end of the stump to form a pool of proliferating progenitor cells known as the regeneration blastema (Thornton, 1938a, b; Bodemer and Everett, 1959; Hay and Fischman, 1961; Steen, 1968; Namenwirth, 1974; Lo et al., 1993; Kumar et al., 2000). Resident stem cells that express pax7 and resemble mammalian muscle satellite cells also migrate distally to participate in the formation of the blastema (Morrison et al., 2006). Once formed, the early blastema grows primarily through the proliferation of its progenitor cells until it reaches its maximum size around 21-25 days postamputation (dpa). At this time, chondrogenic condensations, which will eventually become the bones of the new limb, begin to form in the central region of the regenerate. Over about a 7-week period, the regenerate continues to grow and is patterned into the new limb as the blastemal cells differentiate into the various tissues that constitute the limb.

Although much has been learned about the cellular responses triggered by limb loss, very little is known about the genes that control blastema formation. In zebrafish, *fgf20* has been shown to be required for blastema formation during fin regeneration (Whitehead et al., 2005) but so far, this growth factor has not been implicated in urodele limb regeneration. However, other fibroblast growth factors (FGFs) are expressed during limb regeneration and beads soaked in FGFs can induce partial limb regeneration

following denervation (Mullen et al., 1996). Matrix metalloproteinases (MMPs) are required for successful regeneration in several species and tissues, including newt limbs (Leontovich et al., 2000; Quinones et al., 2002; Gourevitch et al., 2003; Bai et al., 2005; Vinarsky et al., 2005). MMPs may be functioning to prevent scar formation during newt limb regeneration (Vinarsky et al., 2005). However, it is not yet known whether MMPs play additional roles in the regenerative process that could aid in blastema formation. The homeobox gene *Msx1* has been implicated in several regenerative processes and may be involved in cellular dedifferentiation or the maintenance of the undifferentiated state in the blastema (Song et al., 1992; Reginelli et al., 1995; Simon et al., 1995; Odelberg et al., 2000; Hu et al., 2001; Beck et al., 2003; Han et al., 2003). The anterior gradient gene can replace the function of nerves in limb regeneration and rescue regeneration following denervation (Kumar et al., 2007). Wnts have also been shown to play a role in regeneration in *Xenopus* and zebrafish (Kawakami et al., 2006; Stoick-Cooper et al., 2007).

In an effort to identify additional factors that might be involved in blastema formation and growth, we have performed differential expression analyses between regenerating (1 to 21 dpa) and intact limbs in the newt species *Notophthalmus viridescens*. These screens have produced several candidate genes. One of these genes is a CXC chemokine that is similar yet distinct from mammalian CXCL9, CXCL10, and CXCL11.

CXC chemokines are small, secreted, chemotactic cytokines that are marked by four conserved cysteines of which the first two cysteines are separated by only one residue (Mortier et al., 2008). CXC chemokines are known to participate in several

biological processes including wound healing, inflammation, tumor metastases, cell migration, cell proliferation, angiogenesis, and axon guidance (Driscoll et al., 1995; Wang et al., 1996; Colletti et al., 1998; Vicari and Caux, 2002; Barbero et al., 2003; Ren et al., 2003; Li et al., 2005). CXCL9, 10 and 11 are three chemokines that bind to and activate the CXCR3 receptor, are regulated by interferon-γ, and have been shown to induce chemotaxis and proliferation in lymphocytes (Muller et al., 2010).

Given that blastema formation and growth requires both cell migration and proliferation, we decided to characterize this CXC chemokine, which we tentatively call NvCXCL. We found that NvCXCL is highly upregulated during newt limb regeneration and reaches maximum expression levels at 6 and 12 dpa in the regenerating newt hindlimb and forelimb, respectively. We show that it is expressed in dedifferentiating tissues, the regeneration blastema, and the AEC. Finally, we demonstrate that purified recombinant NvCXCL can act as a mitogen for both mouse myoblast and fibroblast cell lines and as a chemokinetic agent for the mouse fibroblast cell line. These data suggest that NvCXCL may play an important role in the formation and/or growth of the regeneration blastema.

2.3 Results

2.3.1 Cloning of the *NvCXCL* gene

We originally identified *NvCXCL* by differential display as a gene that was upregulated during the dedifferentiation stage of newt forelimb regeneration (1, 3 and 5 dpa). We used the 365 bp differential display product to generate a full-length cDNA clone of 737 bp using RNA Ligase Mediated-Rapid Amplification of cDNA Ends (RLM-

RACE) (Vinarsky et al., 2005; Stevenson et al., 2006). This clone was sequenced and an open reading frame of 324 nucleotides was identified having a predicted amino acid sequence that placed it in the family of CXC chemokines (Figure 2.1). Although we could not identify a true ortholog of the *NvCXCL* gene, we were able to show that it was most similar to the three mammalian interferon-γ inducible CXC chemokines CXCL9, CXCL10, and CXCL11, with amino acid identities varying between 27 and 34% and similarities between 45 and 57%.

2.3.2 *NvCXCL* is upregulated in regenerating newt limbs during blastema formation and growth

Microarray, real-time RT-PCR, and Northern blot analyses confirmed that *NvCXCL* was upregulated in both proximal (mid-stylopodial amputations) and distal (distal zeugopodial amputations) forelimbs during the period of dedifferentiation and blastema formation (Figure 2.2 and data not shown), suggesting that this chemokine might be involved in blastema formation and growth. Peak expression levels in the newt forelimb were reached at 12 dpa, with real-time RT-PCR revealing a 6.5-fold upregulation in the proximal limb and a 43.2-fold upregulation in the distal limb. Given this marked upregulation in the newt forelimb, we also examined expression levels in the newt hindlimb and found that a maximum 36.3-fold upregulation was reached by 6 dpa in the proximal hindlimb. Figure 2.2 also demonstrates that *NvCXCL* is markedly downregulated in the newt forelimb early in the regeneration process through at least day 6. However, this downregulation is not seen in the regenerating hindlimb and its significance, if any, has not yet been established. Repeated expression studies using a

Figure 2.1. Predicted amino acid sequence of NvCXCL and a comparison to other CXC chemokines. **A:** NvCXCL is a 107 amino acid (aa) protein that contains the four conserved cysteine residues (asterisks) indicative of CXC chemokines and a cleaved 21 aa signal peptide. Based on sequence homologies, it appears to be a novel CXCL similar to other interferon-γ inducible CXC chemokines but with no clear ortholog. Mammalian CXCL sequences were obtained from GenBank: Cow CXCL11, CXCL9, and CXCL10 (Accession numbers NM_001113173, NM001113172, and NM_001046551, respectively); Wild boar CXCL11, CXCL9, and CXCL10 (Accession numbers NM_001128491, NM_001114289, and NM_001008691, respectively); Human CXCL11, CXCL9, and CXCL10 (Accession numbers NM_005409, NM_002416, and NM_001565, respectively). **B:** A Phylip's tree phylogram based on ClustalW2 analysis showing that NvCXCL is most closely, though distantly, related to the interferon-γ-inducible CXC chemokines. Hs, human; Bt, cow; Ss, wild boar; Rn, rat; Mm, mouse; Cf, dog; Ec, horse; Oa, sheep; Ip, catfish; Dr, zebrafish; Xt, western clawed frog; El, northern pike; Hm, silver carp.

A


Signal peptide
NvCXCL MDMKG-ALLL-CAMLLLAADTQGSFINGKGRCLCTGPGSSSVRRTLVKSVHVYPESPGCE 58
Cow CXCL11 MSVKG-MAIV-LTVILCAAIVQGFPMFKGGRCLCIGPGVKAVKVADIEKVSIIYPTNNCD 58
Wild Boar CXCL11 MGVKG-MAIV-LAVIFCATTIQGFPMFKAGRCLCIGPGVKAVKVADIEKVSIIHPSNNCD 58
Human CXCL11 MSVKG-MAIA-LAVILCATVVQGFPMFKRGRCLCIGPGVKAVKVADIEKASIMYPSNNCD 58
Cow CXCL10 MNKSG-FLIF-CLILLTL--SQGVPLSRNTRCSCIEISNGSVNPRSLEKLEVIPASQSCP 56
Wild Boar CXCL10 MNQSA-VLIF-CLILLTLSGTQGIPLSRTVRCTCIKISDRPVNPRSLEKLEMIPASQSCP 58
Human CXCL10 MNQTA-ILIC-CLIFLTLSGIQGVPLSRTVRCTCISISNQPVNPRSLEKLEIIPASQFCP 58
Cow CXCL9 MKKSA-PLFL-GIIFLTLTGVQGVPAIRNGRCSCINTSQGMIHPKSLKDLKQFAPSPSCE 58
Wild Boar CXCL9 MKKSSVALLL-GIIFLTLIGVQGTLLMRNGRCSCINTSQRMIHLKSLRDLKQFAPSPSCE 59
Human CXCL9 MKKSG-VLFLLGIILLVLIGVQGTPVVRKGRCSCISTNQGTIHLQSLKDLKQFAPSPSCE 59
NvCXCL KNEVVAVMKKGQEKICLNWNSNKVQKLVQSMNKRSSRKAN----------K 99
Cow CXCL11 KTEVIITLKTHKGQRCLNPKAKQAKAIIKKVQRKNSEK---------- 96
Wild Boar CXCL11 KTEVIVTLKAHKGRRCLNPKSKQANVIMKKVERMNFLR---------- 96
Human CXCL11 KIEVIITLKENKGQRCLNPKSKQARLIIKKVERKN---------- 93
Cow CXCL10 RVEIIATMKKNGEKRCLNPESKTIKNLLKAINKQRTKRS---------- 95
Wild Boar CXCL10 HVEIIATMKKNGEKRCLNPESKTIKNLLKAISKERSKRS---------- 97
Human CXCL10 RVEIIATMKKKGEKRCLNPESKAIKNLLKAVSKE---------- 92
Cow CXCL9 KTEIIATMK-NGNEACLNPDLPEVKELIKEWEKQVNQKKKQRKGKKYKKTKKVPKVKRSQ 117
Wild Boar CXCL9 KMEVIATMK-NGDQTCLNPDSPDVKKLIKEWEKQVSLKKKQKKGKKHPKTKKVRKVKKSQ 118
Human CXCL9 KIEIIATLK-NGVQTCLNPDSADVKELIKKWEKQVSQKKKQKNGKKHQK-KKVLKVRKSQ 117
NvCXCL KSKAKKSA 107
Cow CXCL11 ----YKNI 100
Wild Boar CXCL11 ----YQNV 100
Human CXCL11 -------F 97
Cow CXCL10 -PRTRKEA 102
Wild Boar CXCL10 -PRTQREA 104
Human CXCL10 --RSKRSP 98
Cow CXCL9 RPSQKKTT 125
Wild Boar CXCL9 RPDQKKMT 126
Human CXCL9 RSRQKKTT 125

B

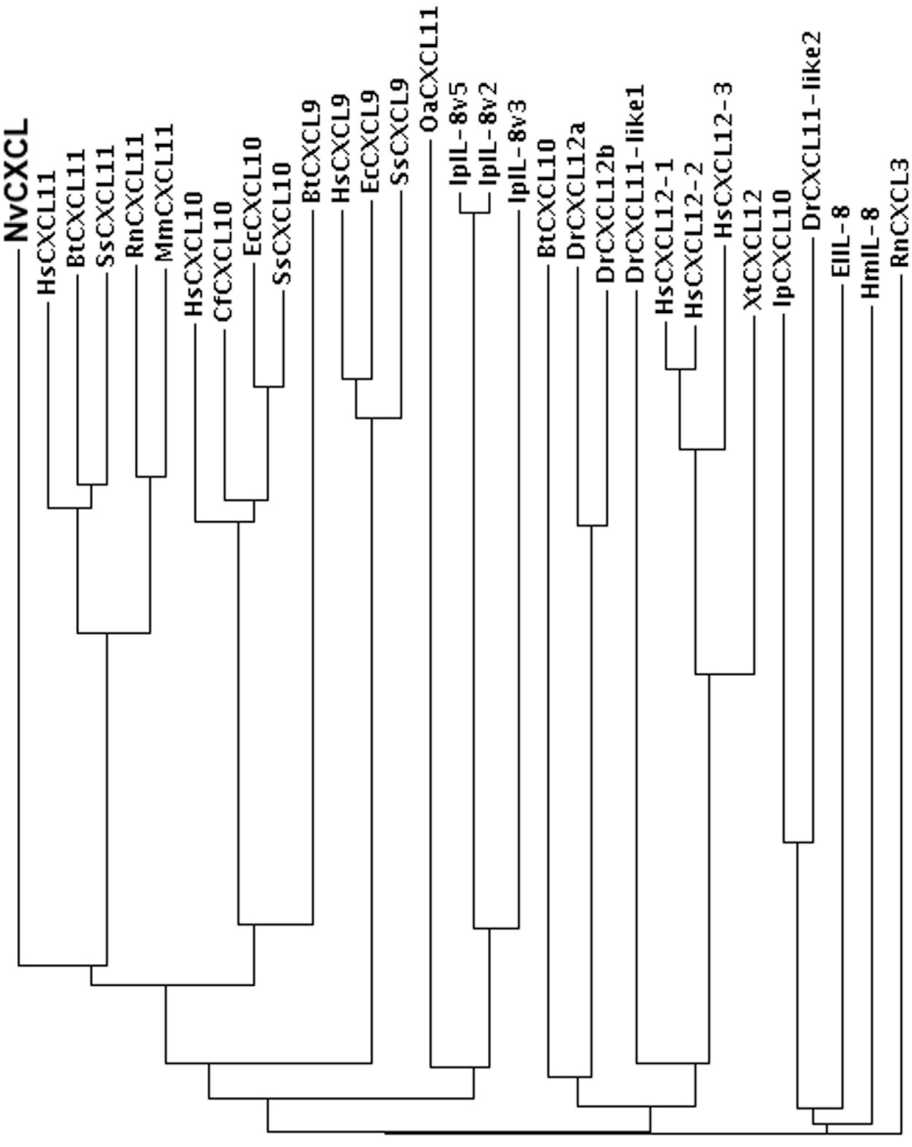
NvCXCL
HsCXCL11
BtCXCL11
SsCXCL11
RnCXCL11
MmCXCL11
HsCXCL10
CfCXCL10
EcCXCL10
SsCXCL10
BtCXCL9
HsCXCL9
EcCXCL9
SsCXCL9
OaCXCL11
IpIL-8v5
IpIL-8v2
IpIL-8v3
BtCXCL10
DrCXCL12a
DrCXCL12b
DrCXCL11-like1
HsCXCL12-1
HsCXCL12-2
HsCXCL12-3
XtCXCL12
IpCXCL10
DrCXCL11-like2
EllL-8
HmlL-8
RnCXCL3

Figure 2.2. Dynamic expression of *NvCXCL* during newt limb regeneration. **A:** Microarray analysis reveals that *NvCXCL* expression is downregulated in the newt forelimb over the first 6 days of regeneration, then rapidly upregulated by day 12 dpa, and drops by 21 dpa. During hindlimb regeneration, *NvCXCL* appears to be upregulated by 3 dpa, reaches peak expression levels by 6 dpa, and then slowly declines in expression through 21 dpa. **B:** Real-time RT-PCR confirms the microarray expression data. *y*-axis is in $\log_{10}$ scale. The numbers above the bars indicate the fold-change in linear scale. *stylopod* = proximal limb; *zeugopod* = distal limb.

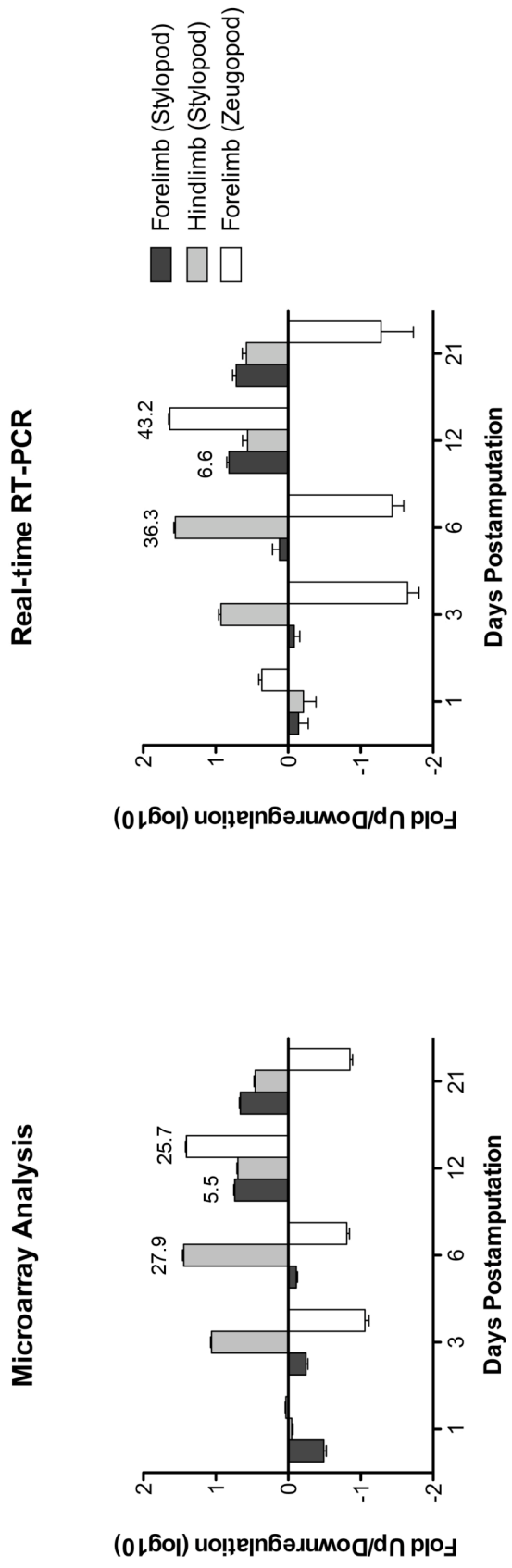
Real-time RT-PCR
Forelimb (Stylopod)
Hindlimb (Stylopod)
Forelimb (Zeugopod)
43.2
6.6
36.3
Fold Up/Downregulation (log10)
Days Postamputation
Microarray Analysis
25.7
5.5
27.9
Fold Up/Downregulation (log10)
Days Postamputation

variety of experimental techniques including microarray and Northern blot analyses (data not shown) have revealed a variable expression pattern in regards to the timing and level of *NvCXCL* up- or downregulation following limb amputation. However, in all studies, *NvCXCL* was consistently observed to be upregulated during the late dedifferentiation/early blastema stage at 12 dpa.

2.3.3 *NvCXCL* is expressed in dedifferentiating tissues and in the blastema and AEC

RNA *in situ* hybridization at days 6 (hindlimb stylopod) and 12 (forelimb zeugopod) using three different newts for each analysis confirmed that *NvCXCL* is consistently upregulated at these time points and also revealed the spatial expression patterns of this chemokine (Figure 2.3). At 6 dpa, the hindlimb stylopod expresses *NvCXCL* in the dedifferentiating muscle tissues, while at 12 dpa, *NvCXCL* is expressed in the nascent blastema, AEC, and dedifferentiating muscle tissues of the regenerating forelimb zeugopod. These expression data are consistent with a possible role for *NvCXCL* in limb regeneration during the periods of dedifferentiation/blastema formation and blastemal growth.

2.3.4 Purification of recombinant NvCXCL protein

Using affinity chromatography, we purified a recombinant NvCXCL protein possessing a FLAG-tag on its C-terminal end from the conditioned medium of transfected HEK293 cells. Western blot analysis revealed a protein with an apparent molecular weight of ~13 kDa (Figure 2.4). Given that the predicted weight of secreted NvCXCL, based on amino acid composition, is about ~10.5 kDa, it is likely that the mature protein

Figure 2.3. Spatial expression patterns of NvCXCL mRNA during newt limb regeneration. Longitudinal sections were imaged on a confocal microscope and 2-3 confocal planes were z-projected into one image to represent signal from the full thickness of the section. NvCXCL mRNA is shown in red and nuclei are shown in green. **A:** NvCXCL is expressed at very low levels in at 0 dpa (intact limb). **B:** At 6 dpa (dedifferentiation stage), the proximal hindlimb (stylopod) expresses NvCXCL in the dedifferentiating mesodermal tissues (especially the muscle) of the limb stump. **C:** At 12 dpa (early blastemal stage), the distal forelimb (zeugopod) expresses high levels of NvCXCL in the blastema, apical epithelial cap, and dedifferentiating muscle of the limb stump. **D:** A 12 dpa, the distal forelimb hybridized with a sense NvCXCL probe to confirm specificity of the signal. e = epithelium; m = muscle; b = bone; bl = blastema; aec = apical epithelial cap.

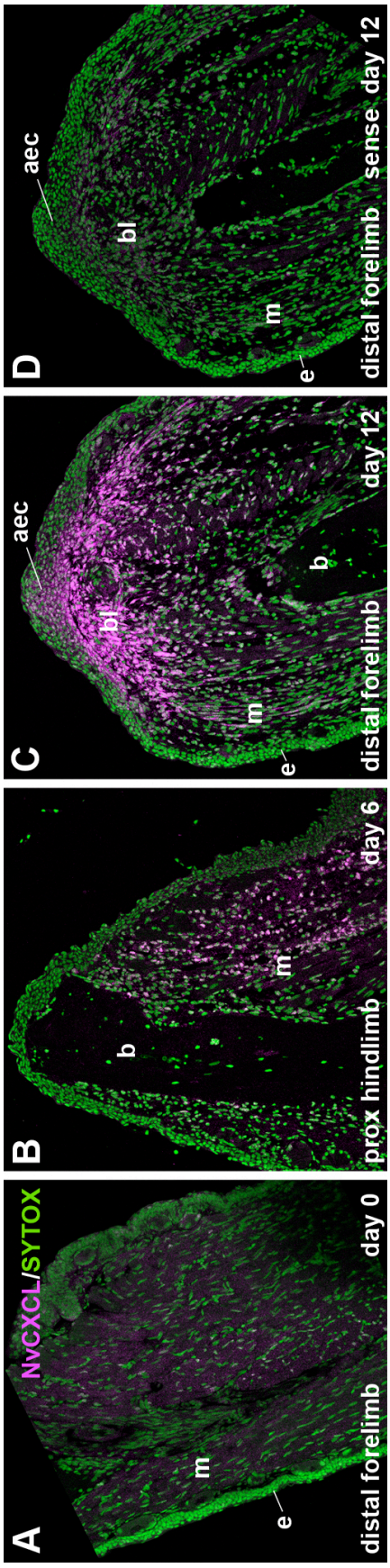
A
NvCXCL/SYTOX
m
e
distal forelimb
day 0
B
b
m
prox hindlimb
day 6
C
aec
bl
m
e
b
distal forelimb
day 12
D
aec
bl
m
e
distal forelimb
sense day 12

Figure 2.4. Western blot of affinity chromatography purified NvCXCL. Secreted FLAG tagged-NvCXCL migrates as a 13 kDa protein during reducing SDS-polyacrylamide gel electrophoresis.

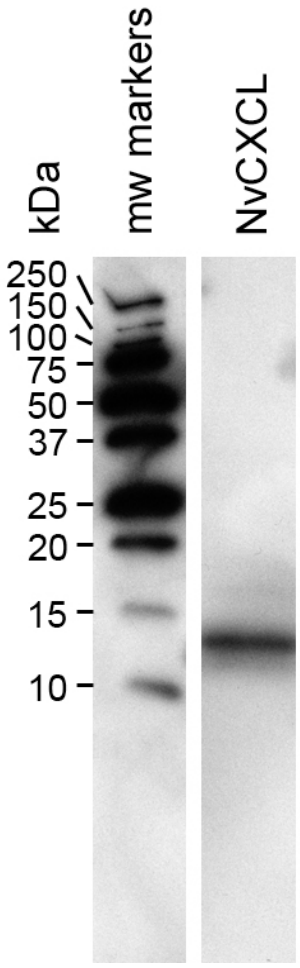
kDa
mw markers
NvCXCL
250
150
100
75
50
37
25
20
15
10

is either co- or posttranslationally modified. N-linked glycosylation is unlikely given that no cognate N-X-S/T motifs (where X is any amino acid except proline) are found in NvCXCL (see Figure 2.1). However, there is one theoretical O-linked glycosylation site at S79. It remains to be determined whether this site is glycosylated or some other protein modification is responsible for the apparent upward shift in the molecular weight of NvCXCL.

2.3.5 NvCXCL can act as mitogen on mouse myoblast and fibroblast cell lines

Several recent studies have shown that CXC chemokines can act as mitogens on certain cell types (Bajetto et al., 2001; Barbero et al., 2002; Murphy et al., 2005; Porcile et al., 2005; Bajetto et al., 2006; Barbieri et al., 2006). To determine whether NvCXCL can function as a mitogen on cell types known to contribute to blastema formation, such as myoblasts and fibroblasts, we used the WST-8 assay to assess cell proliferation *in vitro*. We found that NvCXCL acts as a potent mitogen on mouse C2C12 myoblasts and mouse NIH/3T3 fibroblasts (Figure 2.5). In this assay, subconfluent cell cultures were deprived of serum for 24 hours to arrest and synchronize the cell cycle. The cells were then stimulated with various concentrations of either NvCXCL or IGF1 (positive mitogenic control) for 2 days and then treated with WST-8 for 2 hours at 37°C. Viable cells cleave the WST-8 reagent to produce a chromogenic substance that can be detected and quantified by measuring absorbance at 450 nm. The absorbance is directly proportional to the number of viable cells and can be used to assess relative cell number and therefore the degree of cell proliferation relative to untreated controls. We observed a

Figure 2.5. NvCXCL acts as a mitogen on mouse myoblast and fibroblast cell lines. **A-B:** NvCXCL acts as a mitogen on mouse C2C12 myoblasts in a dose-dependent manner both in the presence of low serum concentrations (A) and in the absence of serum co-factors (B). **C-D:** NvCXCL acts as a mitogen on mouse NIH/3T3 fibroblasts in a dose dependent manner in the presence of low serum concentrations (C) and in the absence of serum cofactors (D). IGF = IGF1 (mitogen positive control). Results for NvCXCL were compared to the no protein control using one-way ANOVA and Tukey-Kramer post hoc test, while results for IGF were compared to the no protein control using Student's t-test. * $p < 0.05$; ** $p < 0.01$; *** $p < 0.001$; **** $p < 0.0001$.

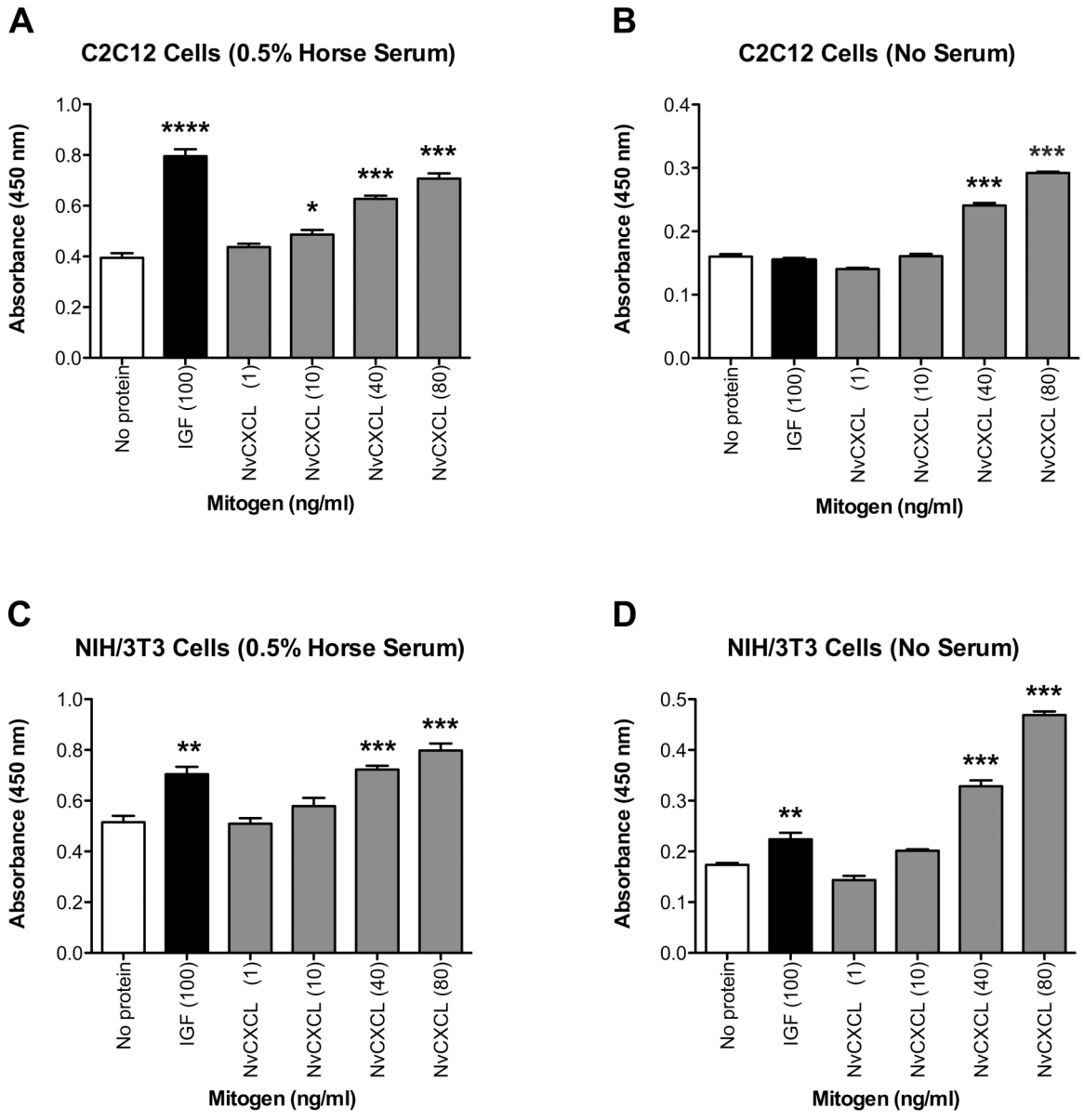
A
C2C12 Cells (0.5% Horse Serum)
Absorbance (450 nm)
1.0
0.8
0.6
0.4
0.2
0.0
****
*
***
***
No protein
IGF (100)
NvCXCL (1)
NvCXCL (10)
NvCXCL (40)
NvCXCL (80)
Mitogen (ng/ml)
B
C2C12 Cells (No Serum)
Absorbance (450 nm)
0.4
0.3
0.2
0.1
0.0
***
***
No protein
IGF (100)
NvCXCL (1)
NvCXCL (10)
NvCXCL (40)
NvCXCL (80)
Mitogen (ng/ml)
C
NIH/3T3 Cells (0.5% Horse Serum)
Absorbance (450 nm)
1.0
0.8
0.6
0.4
0.2
0.0
**
***
***
No protein
IGF (100)
NvCXCL (1)
NvCXCL (10)
NvCXCL (40)
NvCXCL (80)
Mitogen (ng/ml)
D
NIH/3T3 Cells (No Serum)
Absorbance (450 nm)
0.5
0.4
0.3
0.2
0.1
0.0
**
***
***
No protein
IGF (100)
NvCXCL (1)
NvCXCL (10)
NvCXCL (40)
NvCXCL (80)
Mitogen (ng/ml)

dose-dependent proliferative response following stimulation of mouse C2C12 myoblasts and NIH/3T3 fibroblasts with NvCXCL both in the absence of serum and in the presence of low serum concentrations. At 40-80 ng/ml NvCXCL, both cell types exhibited a robust response, while at 10 ng/ml, C2C12 cells proliferated when cultured in the presence of 0.5% horse serum. The magnitude of the proliferative response was similar to that observed when the cells were exposed to the mitogen IGF1 (100 ng/ml) in the presence of low serum concentrations indicating that NvCXCL is a potent mitogen for these mammalian cell types. However, unlike IGF1, which requires a serum cofactor for mitogenic activity (Napier et al., 1999), NvCXCL acted as mitogen even in the absence of serum cofactors.

Chemokines are also known to be chemotactic factors. To test whether NvCXCL might also be chemotactic, we used a Neuro Probe chemotaxis assay to determine whether NvCXCL could promote the directed migration of NIH/3T3 fibroblasts (Figure 2.6). Although we observed a statistically significant 2.5-fold increase in cell migration upon stimulation of NIH/3T3 cells with 80 ng/ml NvCXCL, the chemokinetic control suggested that the limited migratory effect was not due to chemotaxis but rather to a general stimulation cell motility (Figure 2.6). Furthermore, the observed 2.5-fold increase in cell migration was small when compared to the 9-fold increase in cell migration we observed upon stimulation of NIH/3T3 cells with 1 nM (~30 ng/ml) of human recombinant PDGF-BB (positive chemotactic control). These results suggest that NvCXCL does not act as a chemotactic agent for NIH/3T3 cells, although we do not yet know whether it induces chemotaxis of cell types important for newt limb regeneration.

Figure 2.6. NvCXCL acts as chemokinetic but not chemotactic factor on a mouse fibroblast cell line. NvCXCL induced chemokinesis (random nondirectional migration) of mouse NIH/3T3 fibroblasts at the highest concentration tested (80 ng/ml), but did not induce chemotaxis (directional migration), given that there was no statistically significant difference in cell migration between the chemokinetic control and the test for chemotaxis. PDGF-BB was used as a positive control for chemotaxis. Results were analyzed using one-way ANOVA and Tukey-Kramer post hoc test. ***$p < 0.001$.

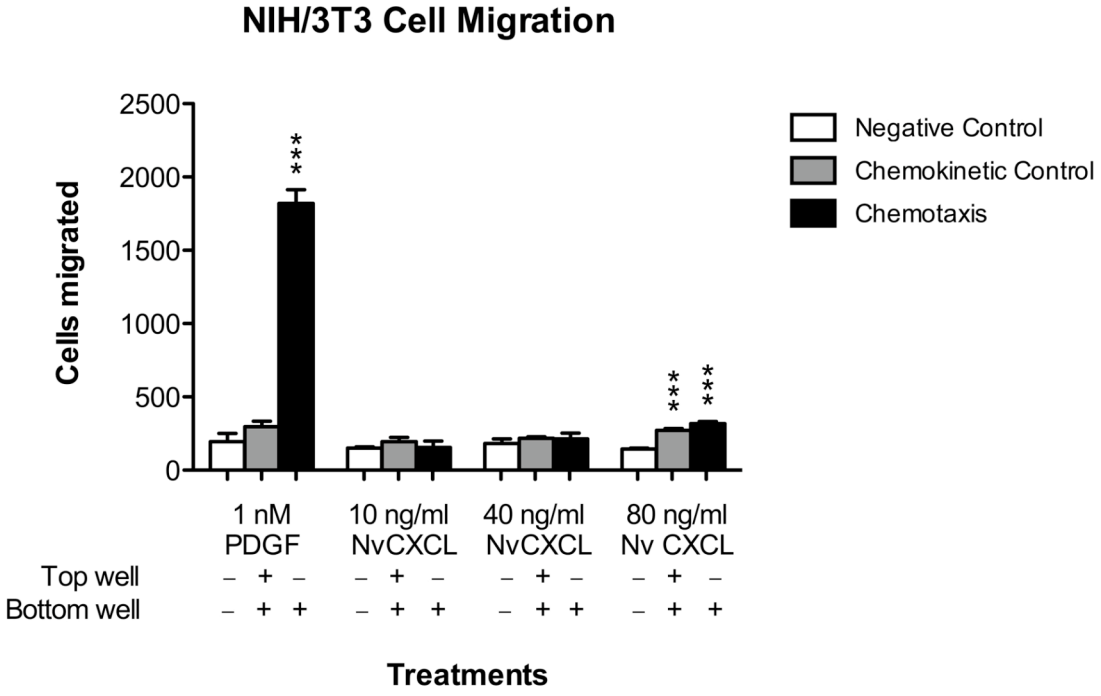
NIH/3T3 Cell Migration
Cells migrated
2500
2000
1500
1000
500
0
***
***
***
Negative Control
Chemokinetic Control
Chemotaxis
1 nM PDGF
10 ng/ml NvCXCL
40 ng/ml NvCXCL
80 ng/ml Nv CXCL
Top well – + – – + – – + – – + –
Bottom well – + + – + + – + + – + +
Treatments

2.4 Discussion

During newt limb regeneration, a blastema consisting of proliferating progenitor cells is formed at the distal tip of the limb stump. Although the blastemal cells are thought to be derived from the combined effects of tissue dedifferentiation and activation of resident stem cells (Lo et al., 1993; Kumar et al., 2000; Morrison et al., 2006), the mitogenic factors that drive the proliferative response have not yet been identified. Here, we identify a mitogenic CXC chemokine, NvCXCL, which is expressed in the regenerating limb during the dedifferentiation and blastemal stages and could therefore play a role in the proliferative response. NvCXCL is expressed in the AEC, in muscle tissue that is undergoing tissue dedifferentiation, and in the early blastema. This spatial expression pattern suggests that this chemokine may function in blastema formation and growth. We have shown that NvCXCL can function as a potent mitogen for C2C12 myoblasts and NIH/3T3 fibroblasts.

Newt myoblasts and fibroblasts are thought to play a major role in blastema formation (Muneoka et al., 1986; Morrison et al., 2006), so observing these proliferative effects on mammalian myoblasts and fibroblasts suggests that NvCXCL might be playing a role in establishing the regeneration blastema by inducing the proliferation of cells that will contribute to the blastema. We tested this hypothesis by treating the newt A1 cell line (limb myoblasts) (Ferretti and Brockes, 1988) and a blastemal cell line with NvCXCL *in vitro*. We were unable, however, to observe any signs of a proliferative response (data not shown). These negative results could indicate that newt limb myoblasts and blastemal cells are not induced by NvCXCL to proliferate *in vivo*. It is also possible, however, that prolonged culture of these cell lines has altered them so they are no longer able to

respond to this potent mitogen. Additionally, blastemal cell types competent to respond to NvCXCL may not be represented in the blastemal cell line used in this study. Blastemal cells are likely a mixture of different types of progenitor cells, including progenitors for muscle, cartilage, bone, and connective tissue. Once cultured and subjected to multiple passages, certain cell types would be expected to predominate, while others would be lost due to differential proliferation. Therefore, newt cell types that might be responsive to the mitogenic effects of NvCXCL could be absent from the pool of surviving blastemal cells. It would be interesting to determine whether Pax7+ primary myoblasts derived from newt muscles express the NvCXCL receptor and are responsive to the mitogen. This intriguing possibility awaits testing.

Though chemokines are known to have potent chemotactic properties, we were unable to confirm that NvCXCL is chemotactic for the mammalian or newt cell lines tested. This may indicate, again, that potentially responsive cell types were not tested. Chemokines are known to be especially chemotactic for immune cells. CC chemokines often induce chemotaxis of monocytes, eosinophils, basophils, B and T lymphocytes, natural killer cells, or dendritic cells, while CXC chemokines induce chemotaxis of neutrophils, monocytes, T cells, and B cells with the interferon-γ inducible CXC chemokines (CXCL9, CXCL 10, and CXCL11) acting as potent activators of T cell and monocyte migration (Proost et al., 2001). We did not test whether NvCXCL could induce chemotaxis of immune cells, primarily because its expression levels do not peak until 6-12 dpa, which is well after the inflammatory reaction has been initiated (Mescher and Neff, 2006). It is also possible that we were unable to detect NvCXCL's chemotactic properties because they were lost as a result of post-translational modifications. It is

known that such modifications, especially peptidase cleavages, can alter a chemokine's ability to act as a chemotactic agent. For example, cleavage of the N-terminal amino acids of CXCL9, CXCL10, and CXCL11 decreases the chemotactic activity of these chemokines and can even cause them to become chemotactic antagonists, while still retaining their other normal biological functions (Proost et al., 2006). Although our Western blot data indicate that post-translational modifications of NvCXCL increase the apparent molecular weight of the protein, we cannot rule out the possibility that concurrent modifications, such as minimal N-terminal cleavage coupled with glycosylation, could produce a larger than expected protein that has lost its chemotactic properties. In this regard, it is interesting to note that the NvCXCL protein does not have an N-terminal penultimate proline following removal of the signal peptide (amino acid 23 of the full-length protein shown in Figure 2.1). Instead, the newt protein has a phenylalanine at this position. A proline at the penultimate position is thought to confer protection from aminopeptidase cleavage (Proost et al., 2006). Most interferon-γ inducible chemokines possess this protective proline (see Figure 2.1). Therefore, NvCXCL may be more susceptible to N-terminal degradation and therefore loss of any chemotactic properties it might have originally possessed.

Further analyses will be required to determine the precise role of NvCXCL in the regenerative process. An intriguing possibility may be that different types of blastemal cells require different mitogens for their propagation. NvCXCL might be an important mitogen for fibroblasts and Pax7+ myoblasts, while other mitogens could be required to induce proliferation of other blastemal cell types. Furthermore, it has recently been shown that the transitional matrix of the early limb regenerate contains ECM molecules

such as tenascin-C and fibronectin that can enhance cell proliferation (Calve et al., 2010). How these ECM molecules interact with other growth factors and mitogens, such as NvCXCL, to establish the blastema is not yet known. As additional regeneration-associated mitogens are identified, it will be important to determine the interactive roles these mitogens and ECM molecules play in establishing a pool of programmed progenitor cells capable of replacing a lost limb.

2.5 Experimental procedures

2.5.1 Newt limb amputations

All procedures involving newts were approved by the University of Utah Institutional Animal Care and Use Committee. Anesthesia was accomplished by immersing the newts in 0.1% ethyl 3-aminobenzoate methanesulfonic acid and limb amputations were performed as previously described (McGann et al., 2001; Vinarsky et al., 2005). At the designated time points, regenerating limbs were reamputated approximately 1.5 mm proximal to the limb stump.

2.5.2 Differential display

Differential display was performed according to manufacturer's instructions (GenHunter) as previously described using RNA isolated from intact forelimbs and forelimbs at 1, 3, and 5 dpa (Vinarsky et al., 2005).

2.5.3 RNA ligase-mediated-RACE and cloning full-length *NvCXCL*

RNA Ligase-Mediated-RACE (RLM-RACE) was performed as previously described (Vinarsky et al., 2005; Stevenson et al., 2006) using nested 3'-primers specific

to *NvCXCL* and nested 5'-primers specific to the RNA linker that had been ligated to the 5'-end of the *NvCXCL* transcript. RLM-RACE products were TA-cloned into pBluescript II and sequenced.

2.5.4 Microarray analysis

Custom microarrays were prepared by Agilent Technologies using both in-house DNA sequence data and data from public databases. Each microarray represented 1,876 putative transcripts from 6 newt species with 93% of the transcript sequences being derived from *Notophthalmus viridescens*. The majority of the *N. viridescens* genes were cloned from mRNA isolated from regenerating tissues; therefore this microarray is enriched for genes that are expressed during regeneration. A 60-mer probe was designed for each transcript using Agilent eArray software, and each probe was represented 23 times on a grid containing 44,000 oligonucleotide probes. Newt limbs were amputated through the stylopod or zeugopod of the forelimb and hindlimb and RNA was isolated from regenerating tissues collected at 0 (intact), 1, 3, 6, 12, or 21 days. The Huntsman Cancer Institute Microarray Core Facility at the University of Utah prepared the RNA probes and performed the hybridizations. RNA probes were generated by amplifying the isolated RNA and labeling with Cy3 or Cy5. Microarrays were competitively hybridized with Cy3- and Cy5-labeled probes from regenerating and day 0 (intact) tissues. Following hybridization, the quality reports for each microarray were examined to ensure uniformity of median signal intensities, to determine the number of bad features on each array, and to confirm that radiometric controls were performing as expected. All bad features were eliminated from further analysis (bad features typically represented < 0.1% of all spots on the array). The microarrays were Lowess normalized, the Cy5:Cy3 ratio

(regenerating vs. intact tissues) for each hybridization was $\log_{10}$ transformed, and geometric means and standard deviations were obtained for repetitive hybridizations.

2.5.5 Real-time RT-PCR

Real-time RT-PCR was performed as previously described (Atkinson et al., 2006; Stevenson et al., 2006) using the Bio-Rad iScript cDNA Synthesis Kit, a mixture of poly-dT and random primers, iTaq SYBR Green Supermix with ROX (Bio-Rad), and the ABI Prism 7700 Sequence Detection System. Data were analyzed using the standard curve method and normalized to the control gene *Nvg00818*. *Nvg00818* is a newt gene expressed in regenerating limbs that exhibits no differential expression over regeneration time as assessed by microarray analysis. No homology to any other cloned gene has yet been identified. Specific primers for *NvCXCL* and the control gene were designed using the Beacon Designer 3.01 program (Premier Biosoft International): 1) *NvCXCL* fwd (175cf1) 5'-ACTGCTTAGAAACCCTGAG-3'; 2) *NvCXCL* rev (175cr1), 5'-GTGGACGGATTTGACTAAAG-3'; *Nvg00818* fwd (4n02a-2f) 5'-GCAGTTGACTGCAGATATTCAA -3'; and *Nvg00818* rev (4n02a-1r) 5'-TCGGCGTAAGATGTTTATTGTAA-3'.

2.5.6 *In situ* hybridization

All steps were performed at room temperature (RT) unless otherwise specified. Intact and 6-day regenerating proximal hindlimbs (stylopod) and intact and 12-day regenerating distal forelimbs (zeugopod) were harvested from anesthetized animals, fixed with 4% paraformaldehyde (PFA) in PBS overnight at 4°C, and rinsed with PBS. Limbs were decalcified with Morse's solution (22.5% formic acid, 10% sodium citrate) for 24

hrs, rinsed with PBS, dehydrated in a series of solutions containing increasing concentrations of ethanol (50%, 70%, 95%, 100%, 30 min each; 100%, 1 hr), infiltrated with paraffin (75% Hemo-De in EtOH, 20 min; 100% Hemo-De, 1 hr; paraffin, 1 hr, 60°C, 15 Hg vacuum), and embedded in paraffin. Sections 10-12 μm thick were mounted onto slides, left on a 37°C slide warmer overnight, and stored at 4°C. Prior to ISH, sections were dewaxed (Hemo-De, 10 min, 2 times; 75% Hemo-De in EtOH, 5 min; 100% EtOH briefly, then 3 min) and rehydrated into PBS (95% EtOH, 3 min; 70% EtOH, 3 min; PBS, 5 min). Sections were then post-fixed with 4% PFA in PBS for 15 min, washed with PBS for 5 min, quenched of endogenous peroxidases with 1% H_2O_2 in PBS for 30 min, washed with PBS for 5 min, and permeabilized with 5 μg/ml Proteinase K in TE (100 mM Tris-HCl, 50 mM EDTA, pH 8.0) for 15 min at 37°C. Sections were washed with PBS for 5 min, briefly equilibrated in TEA (0.1 M triethanolamine, pH 8.0), acetylated with 0.25% acetic anhydride in TEA for 15 min, washed in PBS for 5 min, and pre-hybridized in hybridization buffer (4X SSC, 50% formamide, 1X Denhardt's solution, 200 μg/ml yeast RNA, 500 μg/ml heat denatured herring sperm DNA, 10% PEG6000) for 30 min at 55°C. Digoxigenin-labeled riboprobes were diluted in hybridization buffer to 500 μg/ml, heat denatured for 3 min at 80°C, and added to the sections. Sections were hybridized in a humidified box overnight at 55°C. After hybridization, sections were briefly washed at 55°C in wash solution (4X SSC, 50% formamide, 1X Denhardt's solution). Subsequent washes included a series of solutions with lowering concentrations of wash solution (100% wash solution, 75% wash solution/25% 2X SSC, 50% wash solution/ 50% 2X SSC, and 25% wash solution/75% 2X SSC) for 10 min each, two washes with 2X SSC for 20 min each, two washes with

0.2X SSC for 20 min each, and then two washes at RT in MABT (100 mM maleic acid, 150 mM NaCl, 0.1% Tween-20, pH 7.5) for 10 min. Sections were then blocked with MABTB (MABT with 1% BSA and 10% heat inactivated horse serum) for 1hr, incubated overnight at 4°C with anti-DIG-POD (HRP) antibody (Roche, 11207733910, 150 U/ml) diluted 1:1000 in MABTB, rinsed five times with MABT for 10 min, rinsed with TNT (100 mM Tris-HCl, 150 mM NaCl, 0.05% Tween-20, pH 7.5) for 10 min. The signal was then amplified by incubating the sections in tyramide-Cy5 (PerkinElmer, NEL745001KT; Waltham, MA) diluted 1:50 in diluent for 20 min. Sections were washed 5 times with TNT for 10 min, incubated with SYTOX green nucleic acid stain (Invitrogen, S7020; Carlsbad, CA) diluted 1:50,000 in 2% in DMSO in TNT for 15 min, washed with TNT, then 50% TNT, then water for 5 min each wash. Sections were mounted with Fluoromount G (Thermo Fisher Scientific, OB100-01; Rockford, IL) and coverslips were sealed with clear nail polish. Sections were imaged on an Olympus FV300 laser scanning confocal microscope using a 10X or 20X air objective. Images were processed with Image J, version 1.40g (W. Rasband; http://rsb.info.nih.gov/ij; NIH, Bethesda, MD) and Adobe Photoshop CS2. Levels were adjusted in Photoshop to maximize the signal to noise ratio but the same adjustments were made to experimental and control images.

2.5.7 Expression and purification of recombinant NvCXCL

cDNA containing the complete open reading frame of *NvCXCL* and a 3'-FLAG sequence (coding for the C-terminal sequence DYKDDDDK) was cloned into the pCMV-SPORT6 vector (Invitrogen, Carlsbad, CA). The recombinant clone was transfected into human embryonic kidney 293H cells using Lipofectamine 2000

(Invitrogen, Carlsbad, CA), 100-200 ml of serum-free conditioned medium was collected at 24-96 hours posttransfection, and FLAG-tagged NvCXCL was purified by affinity chromatography using the anti-FLAG M2 antibody (Sigma-Aldrich, St. Louis, MO) as previously described (Vinarsky et al., 2005). Concentration of the protein was estimated by comparison to a FLAG-tagged bovine alkaline phosphatase standard (Sigma-Aldrich, St. Louis, MO) following Western blotting and chemiluminescence detection using the SuperSignal West Femto reagent (Thermo Fisher Scientific—Pierce, Rockford, IL).

2.5.8 Proliferation assay

C2C12 and NIH/3T3 cells (mouse myoblast and fibroblast cell lines, respectively) were purchased from the American Type Culture Collection (ATCC, Rockville, MD) and grown at 37°C/5% CO_2 in DMEM (high glucose, 4.5 g/l) supplemented with 4 mM glutamine, 10% FBS, 100 U/ml penicillin, and 100 µg/ml streptomycin. Cells were plated in quadruplicate in 100 µl volumes on 96-well tissue culture plates at 5,000 cells/well. Cells were allowed to attached overnight, rinsed once with PBS and synchronized for 20-24 hours with either serum-free medium or medium containing 0.5% horse serum. Cells were then treated with synchronization medium alone (negative control) or synchronization medium supplemented with either 100 ng/ml insulin growth factor 1A (IGF1A; positive control) or varying concentrations of NvCXCL (1, 10, 40, or 80 ng/ml). After 2 days of treatment, the cells were assayed for cell number using the WST-8 assay (Dojindo) as described previously (Stevenson et al., 2006). ANOVA was used to assess the differences between the cell number means and a Tukey-Kramer post hoc test was used to assess statistical differences between the individual treatment groups.

2.5.9 Chemotactic assay

Chemotactic function was assessed according to manufacturer's instructions using a Neuro Probe chemotactic system (Gaithersburg, MD) and fibronectin-coated membranes having 8 μm diameter pores. NIH/3T3 cells were treated with serum-free medium overnight to ensure quiescence. The lower chambers of the system were loaded with serum-free medium (negative control), 1 nM (~30 ng/ml) PDGF-BB (positive control), or varying concentrations of NvCXCL (10 ng/ml, 40 ng/ml, or 80 ng/ml). Upper chambers were loaded with 30,000 quiescent NIH/3T3 cells either in the absence (chemotactic test) or presence (chemokinetic control) of equimolar concentrations of the protein (NvCXCL or PDGF-BB). Each condition was done in quadruplicate. Cell migration was allowed to proceed at 37°C/5% CO_2 for 4 hours. Membranes were fixed, stained with hematoxylin and eosin, and nonmigrated cells from the upper chamber side of the membrane were removed with a moist cotton swab before mounting the membrane using Permount. For each well, cell counts were obtained and summed for four randomly selected regions of the membrane. Mean and standard error of the mean were calculated for the quadruplicate samples and ANOVA and Tukey-Kramer posthoc tests were performed to assess statistical significance of the results.

2.6 References

Atkinson DL, Stevenson TJ, Park EJ, Riedy MD, Milash B, Odelberg SJ (2006) Cellular electroporation induces dedifferentiation in intact newt limbs. Dev Biol 299:257-271.

Bai S, Thummel R, Godwin AR, Nagase H, Itoh Y, Li L, Evans R, McDermott J, Seiki M, Sarras MP, Jr. (2005) Matrix metalloproteinase expression and function during fin regeneration in zebrafish: analysis of MT1-MMP, MMP2 and TIMP2. Matrix Biol 24:247-260.

Bajetto A, Barbero S, Bonavia R, Piccioli P, Pirani P, Florio T, Schettini G (2001) Stromal cell-derived factor-1alpha induces astrocyte proliferation through the activation of extracellular signal-regulated kinases 1/2 pathway. J Neurochem 77:1226-1236.

Bajetto A, Barbieri F, Dorcaratto A, Barbero S, Daga A, Porcile C, Ravetti JL, Zona G, Spaziante R, Corte G, Schettini G, Florio T (2006) Expression of CXC chemokine receptors 1-5 and their ligands in human glioma tissues: role of CXCR4 and SDF1 in glioma cell proliferation and migration. Neurochem Int 49:423-432.

Barbero S, Bonavia R, Bajetto A, Porcile C, Pirani P, Ravetti JL, Zona GL, Spaziante R, Florio T, Schettini G (2003) Stromal cell-derived factor 1alpha stimulates human glioblastoma cell growth through the activation of both extracellular signal-regulated kinases 1/2 and Akt. Cancer Res 63:1969-1974.

Barbero S, Bajetto A, Bonavia R, Porcile C, Piccioli P, Pirani P, Ravetti JL, Zona G, Spaziante R, Florio T, Schettini G (2002) Expression of the chemokine receptor CXCR4 and its ligand stromal cell-derived factor 1 in human brain tumors and their involvement in glial proliferation in vitro. Ann N Y Acad Sci 973:60-69.

Barbieri F, Bajetto A, Porcile C, Pattarozzi A, Massa A, Lunardi G, Zona G, Dorcaratto A, Ravetti JL, Spaziante R, Schettini G, Florio T (2006) CXC receptor and chemokine expression in human meningioma: SDF1/CXCR4 signaling activates ERK1/2 and stimulates meningioma cell proliferation. Ann N Y Acad Sci 1090:332-343.

Beck CW, Christen B, Slack JM (2003) Molecular pathways needed for regeneration of spinal cord and muscle in a vertebrate. Dev Cell 5:429-439.

Bodemer CW, Everett NB (1959) Localization of newly synthesized proteins in regenerating newt limbs as determined by radioautographic localization of injected methionine-S^{35}. Dev Biol 1:327-342.

Brockes JP, Kumar A (2002) Plasticity and reprogramming of differentiated cells in amphibian regeneration. Nat Rev Mol Cell Biol 3:566-574.

Calve S, Odelberg SJ, Simon HG (2010) A transitional extracellular matrix instructs cell behavior during muscle regeneration. Dev Biol 344:259-271.

Colletti LM, Green M, Burdick MD, Kunkel SL, Strieter RM (1998) Proliferative effects of CXC chemokines in rat hepatocytes in vitro and in vivo. Shock 10:248-257.

Driscoll KE, Hassenbein DG, Howard BW, Isfort RJ, Cody D, Tindal MH, Suchanek M, Carter JM (1995) Cloning, expression, and functional characterization of rat MIP-2: a neutrophil chemoattractant and epithelial cell mitogen. J Leukoc Biol 58:359-364.

Ferretti P, Brockes JP (1988) Culture of newt cells from different tissues and their expression of a regeneration-associated antigen. J Exp Zool 247:77-91.

Gourevitch D, Clark L, Chen P, Seitz A, Samulewicz SJ, Heber-Katz E (2003) Matrix metalloproteinase activity correlates with blastema formation in the regenerating MRL mouse ear hole model. Dev Dyn 226:377-387.

Han M, Yang X, Farrington JE, Muneoka K (2003) Digit regeneration is regulated by Msx1 and BMP4 in fetal mice. Development 130:5123-5132.

Hay ED, Fischman DA (1961) Origin of the blastema in regenerating limbs of the newt Triturus viridescens. An autoradiographic study using tritiated thymidine to follow cell proliferation and migration. Dev Biol 3:26-59.

Hu G, Lee H, Price SM, Shen MM, Abate-Shen C (2001) Msx homeobox genes inhibit differentiation through upregulation of cyclin D1. Development 128:2373-2384.

Kawakami Y, Rodriguez Esteban C, Raya M, Kawakami H, Marti M, Dubova I, Izpisua Belmonte JC (2006) Wnt/beta-catenin signaling regulates vertebrate limb regeneration. Genes Dev 20:3232-3237.

Kumar A, Velloso CP, Imokawa Y, Brockes JP (2000) Plasticity of retrovirus-labelled myotubes in the newt limb regeneration blastema. Dev Biol 218:125-136.

Kumar A, Godwin JW, Gates PB, Garza-Garcia AA, Brockes JP (2007) Molecular basis for the nerve dependence of limb regeneration in an adult vertebrate. Science 318:772-777.

Leontovich AA, Zhang J, Shimokawa K, Nagase H, Sarras MP, Jr. (2000) A novel hydra matrix metalloproteinase (HMMP) functions in extracellular matrix degradation, morphogenesis and the maintenance of differentiated cells in the foot process. Development 127:907-920.

Li Q, Shirabe K, Thisse C, Thisse B, Okamoto H, Masai I, Kuwada JY (2005) Chemokine signaling guides axons within the retina in zebrafish. J Neurosci 25:1711-1717.

Lo DC, Allen F, Brockes JP (1993) Reversal of muscle differentiation during urodele limb regeneration. Proc Natl Acad Sci U S A 90:7230-7234.

McGann CJ, Odelberg SJ, Keating MT (2001) Mammalian myotube dedifferentiation induced by newt regeneration extract. Proc Natl Acad Sci U S A 98:13699-13704.

Mescher AL, Neff AW (2006) Limb regeneration in amphibians: immunological considerations. ScientificWorldJournal 6 Suppl 1:1-11.

Morrison JI, Loof S, He P, Simon A (2006) Salamander limb regeneration involves the activation of a multipotent skeletal muscle satellite cell population. J Cell Biol 172:433-440.

Mortier A, Van Damme J, Proost P (2008) Regulation of chemokine activity by posttranslational modification. Pharmacol Ther 120:197-217.

Mullen LM, Bryant SV, Torok MA, Blumberg B, Gardiner DM (1996) Nerve dependency of regeneration: the role of Distal-less and FGF signaling in amphibian limb regeneration. Development 122:3487-3497.

Muller M, Carter S, Hofer MJ, Campbell IL (2010) Review: The chemokine receptor CXCR3 and its ligands CXCL9, CXCL10 and CXCL11 in neuroimmunity--a tale of conflict and conundrum. Neuropathol Appl Neurobiol 36:368-387.

Muneoka K, Fox WF, Bryant SV (1986) Cellular contribution from dermis and cartilage to the regenerating limb blastema in axolotls. Dev Biol 116:256-260.

Murphy C, McGurk M, Pettigrew J, Santinelli A, Mazzucchelli R, Johnston PG, Montironi R, Waugh DJ (2005) Nonapical and cytoplasmic expression of interleukin-8, CXCR1, and CXCR2 correlates with cell proliferation and microvessel density in prostate cancer. Clin Cancer Res 11:4117-4127.

Namenwirth M (1974) The inheritance of cell differentiation during limb regeneration in the axolotl. Dev Biol 41:42-56.

Napier JR, Thomas MF, Sharma M, Hodgkinson SC, Bass JJ (1999) Insulin-like growth factor-I protects myoblasts from apoptosis but requires other factors to stimulate proliferation. J Endocrinol 163:63-68.

O'Steen WK (1958) Regeneration of the intestine in adult urodeles. J Morphol 103:435-477.

Oberpriller JO, Oberpriller JC (1974) Response of the adult newt ventricle to injury. J Exp Zool 187:249-253.

Odelberg SJ, Kollhoff A, Keating MT (2000) Dedifferentiation of mammalian myotubes induced by msx1. Cell 103:1099-1109.

Piatt J (1955) Regeneration of the spinal cord in the salamander. J Exp Zool 129:177-207.

Porcile C, Bajetto A, Barbieri F, Barbero S, Bonavia R, Biglieri M, Pirani P, Florio T, Schettini G (2005) Stromal cell-derived factor-1alpha (SDF-1alpha/CXCL12) stimulates ovarian cancer cell growth through the EGF receptor transactivation. Exp Cell Res 308:241-253.

Proost P, Struyf S, Van Damme J (2006) Natural post-translational modifications of chemokines. Biochem Soc Trans 34:997-1001.

Proost P, Schutyser E, Menten P, Struyf S, Wuyts A, Opdenakker G, Detheux M, Parmentier M, Durinx C, Lambeir AM, Neyts J, Liekens S, Maudgal PC, Billiau A, Van Damme J (2001) Amino-terminal truncation of CXCR3 agonists impairs receptor signaling and lymphocyte chemotaxis, while preserving antiangiogenic properties. Blood 98:3554-3561.

Quinones JL, Rosa R, Ruiz DL, Garcia-Arraras JE (2002) Extracellular matrix remodeling and metalloproteinase involvement during intestine regeneration in the sea cucumber Holothuria glaberrima. Dev Biol 250:181-197.

Reginelli AD, Wang YQ, Sassoon D, Muneoka K (1995) Digit tip regeneration correlates with regions of Msx1 (Hox 7) expression in fetal and newborn mice. Development 121:1065-1076.

Ren X, Carpenter A, Hogaboam C, Colletti L (2003) Mitogenic properties of endogenous and pharmacological doses of macrophage inflammatory protein-2 after 70% hepatectomy in the mouse. Am J Pathol 163:563-570.

Simon HG, Nelson C, Goff D, Laufer E, Morgan BA, Tabin C (1995) Differential expression of myogenic regulatory genes and Msx-1 during dedifferentiation and redifferentiation of regenerating amphibian limbs. Dev Dyn 202:1-12.

Song K, Wang Y, Sassoon D (1992) Expression of Hox-7.1 in myoblasts inhibits terminal differentiation and induces cell transformation. Nature 360:477-481.

Steen TP (1968) Stability of chondrocyte differentiation and contribution of muscle to cartilage during limb regeneration in the axolotl (Siredon mexicanum). J Exp Zool 167:49-78.

Stevenson TJ, Vinarsky V, Atkinson DL, Keating MT, Odelberg SJ (2006) Tissue inhibitor of metalloproteinase 1 regulates matrix metalloproteinase activity during newt limb regeneration. Dev Dyn 235:606-616.

Stoick-Cooper CL, Weidinger G, Riehle KJ, Hubbert C, Major MB, Fausto N, Moon RT (2007) Distinct Wnt signaling pathways have opposing roles in appendage regeneration. Development 134:479-489.

Thornton CS (1938a) The histogenesis of the regenerating forelimb of larval Amblystoma after exarticulation of the humerus. J Morphol 62:219-235.

Thornton CS (1938b) The histogenesis of muscle in the regenerating fore limb of larval amblystoma punctatum. J Morphol 62:17-47.

Turner JE, Singer M (1974a) The ultrastructure of regeneration in the severed newt optic nerve. J Exp Zool 190:249-268.

Turner JE, Singer M (1974b) An electron microscopic study of the newt (Triturus viridescens) optic nerve. J Comp Neurol 156:1-18.

Vicari AP, Caux C (2002) Chemokines in cancer. Cytokine Growth Factor Rev 13:143-154.

Vinarsky V, Atkinson DL, Stevenson TJ, Keating MT, Odelberg SJ (2005) Normal newt limb regeneration requires matrix metalloproteinase function. Dev Biol 279:86-98.

Wang X, Yue TL, Ohlstein EH, Sung CP, Feuerstein GZ (1996) Interferon-inducible protein-10 involves vascular smooth muscle cell migration, proliferation, and inflammatory response. J Biol Chem 271:24286-24293.

Whitehead GG, Makino S, Lien CL, Keating MT (2005) fgf20 is essential for initiating zebrafish fin regeneration. Science 310:1957-1960.

CHAPTER 3

FLUORESCENT WHOLE-MOUNT METHOD FOR VISUALIZING THREE-DIMENSIONAL RELATIONSHIPS IN INTACT AND REGENERATING ADULT NEWT SPINAL CORDS

3.1 Abstract

Adult newts have the remarkable ability to regenerate their spinal cords after a complete transection injury. In order to understand this process, we have developed a method for visualizing the cellular and molecular events during regeneration in whole-mount preparations using fluorescent probes (streptavidins and antibodies) and confocal microscopy. This method was optimized by varying parameters associated with fixation, tissue trimming, fluorescent probe penetration, and clearing and represents a significant advance in our ability to observe the intact and regenerating newt spinal cord. These methods should also be widely applicable to the study of other newt tissues and adult tissues from other model systems.

3.2 Introduction

Often, the first step in understanding a complex biological process is to carefully observe the process, to identify the structural, cellular or molecular players and watch their behaviors. Ideally, this is best done in a way that maintains three-dimensional (3D) relationships. While 3D relationships can be reconstructed from images of serial sections, this method is time consuming and introduces artifacts. Individual sections can be warped

or torn, and this can make it difficult to faithfully reconstruct the 3D image. A better and more efficient way to observe 3D relationships is to image tissues in whole-mount on a confocal microscope. For this method, the tissue must be fluorescently labeled, optically clear, and not more than about 300 μm thick. Thus, zebrafish embryos, which are clear and small, are ideal for confocal microscopy and can even be imaged live if fluorescent labels are introduced *in vivo*. Many specimens, however, must be trimmed, fluorescently labeled *ex vivo*, and cleared after an animal has been sacrificed and its tissues fixed. While methods for performing each of these steps have been established for many developmental model organisms (Klymkowsky and Hanken, 1991; Kardon, 1998), these methods have not been optimized for use in many adult tissues, which are larger and less permeable, or for use in many less common model organisms, such as the newt.

Newts are remarkable for their ability to regenerate body parts after they are lost or damaged. A newt can regenerate its limbs (Brockes, 1997), tail (Iten and Bryant, 1976), jaw (Ghosh et al., 1994), retina (Mitashov, 1996), lens (Eguchi et al., 1974), portions of its heart (Oberpriller and Oberpriller, 1974) and even its spinal cord (Piatt, 1955). After a complete transection injury to the spinal cord, the newt can regenerate its spinal cord and regain the use of its hindlimbs and tail in as little as 4 weeks (Davis et al., 1990). To begin to understand how newts are able to do this, we sought to develop methods that would allow us to visualize with unprecedented clarity the cellular and molecular events after a spinal cord transection injury in the adult newt.

Here we report a method for obtaining 3D images of intact and regenerating spinal cords of adult newts via confocal microscopy that was optimized by varying parameters associated with fixation, tissue trimming, fluorescent labeling, and clearing.

This method will be invaluable for future studies of spinal cord regeneration in the newt, as well as for the development of methods for obtaining 3D images of other newt or adult tissues.

3.3 Results and discussion

The sequential steps to our method are as follows: fixation, bone decalcification (to prepare for trimming), bleaching (part of clearing), embedding and vibratome sectioning (to trim the tissue), permeabilization and incubation with fluorescent probes, and clearing (Table 3.1). Parameters tested for each step were evaluated on 4 mm segments of spinal cord from the lower trunk region of the animal. Spinal cords were intact or regenerating after a transection injury. In some animals, the axon tracer, biotinylated dextran amine (BDA), was applied *in vivo* and visualized with streptavidin-Cy5. The method was first optimized for the streptavidin probe because of its smaller size (about 60 kDa) and was then later modified to work with antibodies, which are much larger (150 kDa for IgG, 900 kDa for IgM). Spinal cords were imaged on a confocal microscope through the dorsal-ventral axis, such that each confocal plane is a longitudinal section. Table 3.1 shows the parameters that were tried for each step and identifies the preferred conditions for streptavidin and antibody labeling.

3.3.1 Fixation

We sought a fixative that would preserve cellular morphology and molecular antigenicity and still allow fluorescent probes to penetrate fully into the newt spinal cord. Fixatives tried included glutaraldehyde (GA), paraformaldehyde (PFA), and periodate lysine paraformaldehyde (PLP). GA is commonly used for electron microscopy because

Table 3.1. Sequential steps, parameters tested for each step and preferred conditions for streptavidin and antibody labeling

Sequential Steps	Parameters Tested	Preferred Conditions for:	
		Streptavidin Labeling	Antibody Labeling
fixation	PLP with 0.5% PFA PLP with 2% PFA 2% glutaraldehyde/ 2% PFA perfusion vs nonperfusion	perfuse & post-fix PLP with 0.5% PFA	post-fix without perfusion PLP with 0.5% PFA
decalcification	Morse's solution	Morse's solution	Morse's solution
bleaching	modified Dent's bleach formamide bleach	formamide bleach	formamide bleach
embedding	3%, 4%, and 6% agarose	4% agarose	4% agarose
sectioning	100 – 400 um razor blades, feather blades	400 um feather blades	350-375 um feather blades
permeabilization	20% DMSO with one of: 0.5 – 2% Triton X-100 (non-ionic) 1% Tween-20 (weaker non-ionic) 1% NP-40 (stronger non-ionic) 1% CHAPS (zwitterionic) 1% SDS in pretreatment (ionic)	20% DMSO 0.5% Triton X-100	20% DMSO 2% Triton X-100
incubation	1 – 10 days 96 well plate small centrifuge tubes	7 days 96 well plate or centrifuge tubes	10 days 1° 10 days 2° centrifuge tubes
clearing	glycerol BABB	BABB	BABB

it preserves morphology very well, but because it interacts strongly with proteins, it tends to disrupt antigen-antibody interactions. PFA does not preserve morphology as well as GA, but it is more commonly used for immunohistochemistry because it does not cross-link proteins and disrupt antigenicity as much as GA. PFA, however, tends to add autofluorescence to the already highly autofluorescent newt tissues. Finally, PLP was tried because it was found to preserve morphology as well as GA (McLean and Nakane, 1974), and because it can be effective with lower concentrations of PFA, it may reduce autofluorescence and allow fluorescent probes to more readily enter the tissue, while still preserving antigenicity. Alcohol-based fixatives were not tried because they tend to denature antigens, and molecules that are soluble in alcohol are lost. (McLean and Nakane, 1974; Klymkowsky and Hanken, 1991; Rogers, 1999).

The fixatives were evaluated in newt spinal cords that had regenerated 3 days after a spinal cord transection (Figure 3.1). BDA was applied rostral or caudal to the injury site to label descending or ascending axons, respectively. Animals were perfused with 2% GA/2% PFA, PLP with 2% PFA or PLP with 0.5% PFA, and 4 mm of spinal column containing the injury site was postfixed in PLP with 2% PFA (after GA/PFA and PLP with 2% PFA perfusion) or PLP with 0.5% PFA (after PLP with 0.5% PFA perfusion). One animal was not perfused, but was only postfixed with PLP with 2% PFA. All tissues were trimmed to a thickness of 400 μm, except the nonperfused tissue which was trimmed to 300 μm, and incubated with streptavidin-Cy5 for 4.5 days.

As shown in Figure 3.1, morphology was well preserved and the amount of autofluorescence was low in all animals, regardless of which fixative was used and whether or not the tissue was perfusion-fixed (Figure 3.1A-D). The different

Figure 3.1. Comparison of different methods of fixation. **A-E:** Dorsal views of 3 day regenerating spinal cords, fixed as indicated above each panel, imaged on a confocal microscope and 3D-rendered in Fluorender. The axon tracer, BDA, was applied rostral (**C**) or caudal (**A,B,D,E**) to the injury site (asterisk in **B**), labeled with streptavidin-Cy5 for the duration indicated above each panel, and is shown in white. Arrowheads in **B** mark the end of the cut spinal cord. **A'-E':** Cross sectional views of the same cords shown in **A-E**. R, rostral; C, caudal; D, dorsal; V, ventral. Scale bars: 100 μm.

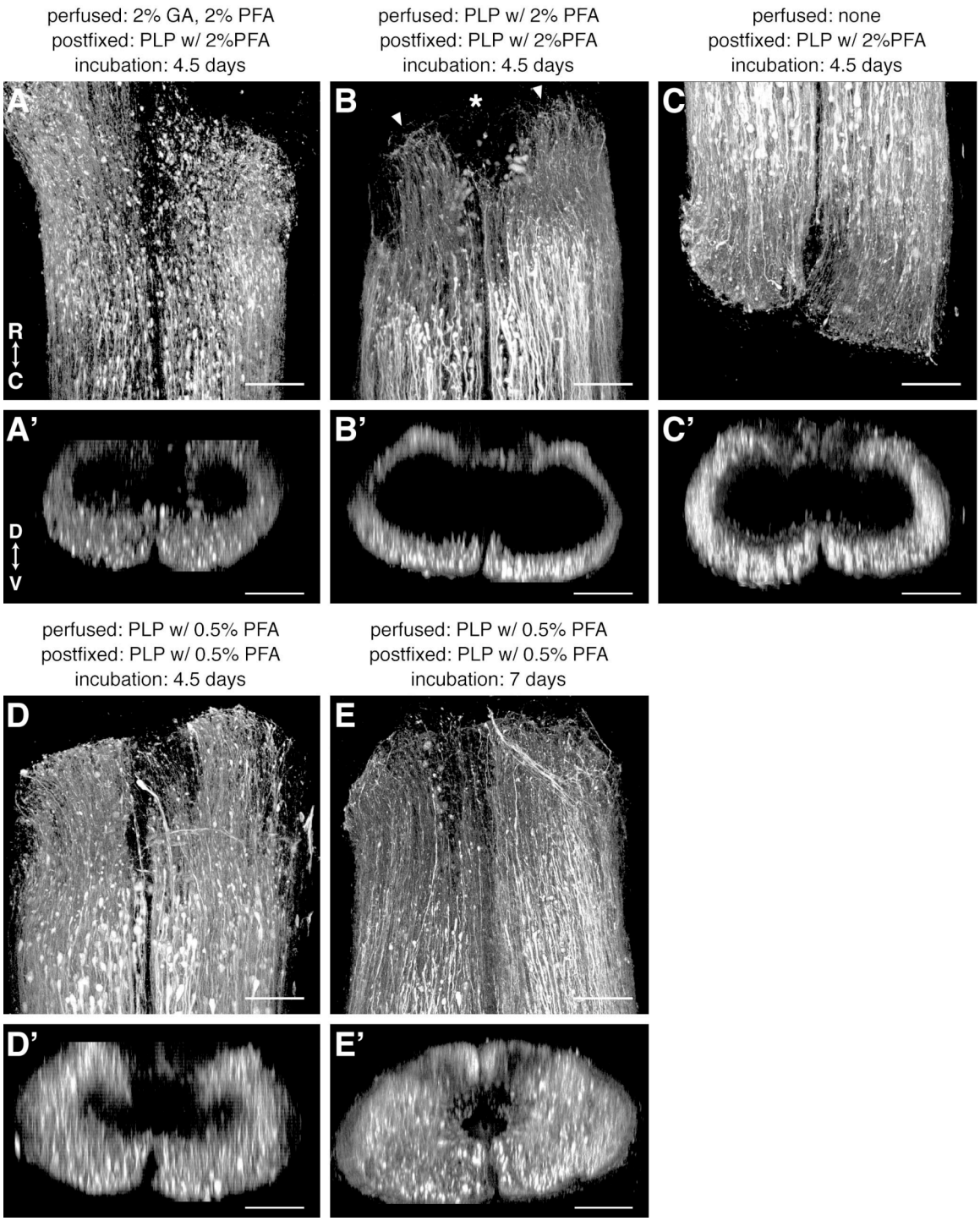
perfused: 2% GA, 2% PFA
postfixed: PLP w/ 2%PFA
incubation: 4.5 days
perfused: PLP w/ 2% PFA
postfixed: PLP w/ 2%PFA
incubation: 4.5 days
perfused: none
postfixed: PLP w/ 2%PFA
incubation: 4.5 days
A
B
C
R
C
A'
B'
C'
D
V
perfused: PLP w/ 0.5% PFA
postfixed: PLP w/ 0.5% PFA
incubation: 4.5 days
perfused: PLP w/ 0.5% PFA
postfixed: PLP w/ 0.5% PFA
incubation: 7 days
D
E
D'
E'

fixatives did have an effect, however, on how far the streptavidin probe was able to penetrate into the spinal cord. This is evident when the spinal cords are viewed in cross section (Figure 3.1A'-D'). Though not complete after 4.5 days of incubation, penetrance was best when the fixative with the least amount of formaldehyde was used, namely, PLP with 0.5% PFA.

Therefore, we favored the PLP with 0.5% PFA fixative and found that we could improve streptavidin penetration without detrimentally affecting morphology by increasing the incubation duration to 7 days (Figure 3.1E, E'). Perfusion fixation does not appear to be necessary to preserve morphology (compare Figure 3.1B, C) and it may hinder probe penetrance (compare Figure 3.1B', C'), but because perfusion makes the tissue stiffer and, therefore, easier to section, we preferred to include this step for streptavidin-only labeling. We preferred to omit perfusion, however, on tissue that was labeled with antibodies in order to optimize their penetration into the spinal cord (see below).

3.3.2 Tissue trimming

In order to minimize the amount of tissue the confocal laser and fluorescent probes must penetrate, we used a vibratome to remove tissue dorsal and ventral to the spinal cord. We preferred to do this rather than dissect the cord out of the spinal column because dissection would disrupt the 3D relationships of a spinal cord injury site.

To prepare for vibratome sectioning, segments of spinal column were decalcified with Morse's solution and embedded in agarose. The agarose served as a support for the tissue during sectioning and in order for it to provide sufficient support, it needed to have a density similar to that of the spinal column. This is a challenge because spinal column

tissues have heterogeneous densities: the spinal cord is very soft compared to the muscle and decalcified bone around it. We tried 3%, 4%, and 6% agarose and found that, when sections are cut with thin, sharp blades, 4% worked best and enabled us to reliably obtain good sections. Agarose-embedded tissue blocks were glued onto vibratome chucks, ventral side down, and the dorsal tissue was trimmed until the spinal cord was exposed. A 350 to 400 μm thick section was then cut which contained the entire spinal cord. The ventral side of the spinal cord was not always exposed in a 400 μm thick cut, but nonetheless this was adequate for streptavidin labeling. For antibody labeling, however, we preferred to risk losing a little of the ventral spinal cord to ensure that both sides were exposed and, therefore, cut 350 – 375 μm thick sections. It was not possible to obtain sections much thinner than about 100 μm because of the heterogeneous nature of the spinal column.

3.3.3 Fluorescent Labeling

Specific probes, such as antibodies and streptavidin, bind with high affinity to their specific binding sites and with low affinity to nonspecific sites. To obtain efficient, specific and even labeling of whole-mount preparations with such probes, specific binding sites must be made accessible throughout the tissue. Methods for making the tissue permeable to probes include the use of detergents, heat, enzymes, and carrier agents such as dimethyl sulfoxide (DMSO). At the same time, conditions for non-specific binding must be made unfavorable either with blocking reagents or by incubation at lower temperatures or both.

In initial experiments, we used phosphate buffered saline (PBS) with 0.5% of the detergent Triton X-100 and 20% of the carrier agent DMSO to permeabilize the newt spinal cord and incubated the sections at room temperature (RT) for 7 days. To block non-specific binding, we used 1% BSA and 0.1% fish gelatin. This was sufficient to allow the streptavidin probe to penetrate fully into a 400 μm section and label the axon tracer specifically with minimal background signal (Figure 3.1E). This was not sufficient, however, for antibody labeling. Using these same parameters and a 7d incubation with primary antibody followed by a 7d incubation with secondary antibody at RT, there were regions in the middle of the spinal cord that were not labeled with the 3A10 antibody, which is an axonal marker (Figure 3.2A).

To improve antibody penetration, therefore, we tested whether increasing the amount or strength of the detergent could improve antibody labeling, compared to 0.5% Triton X-100, without detrimentally affecting morphology. We did not consider enzyme treatments, such as trypsin or collagenase, because we were interested in studying the expression of extracellular matrix proteins. Detergents tested, in order of increasing strength, were Tween-20 (weaker non-ionic), Triton X-100 (non-ionic), NP-40 (stronger non-ionic), CHAPS (zwitterionic), and SDS (ionic) (Bhairi and Mohan, 2007). SDS was only used during the pre-treatment period since it is a denaturing detergent. The detergents were evaluated in intact newt spinal cords that were labeled with the 3A10 antibody and an antibody against glial fibrillary acidic protein (GFAP), which is an ependymoglial and astrocytic marker in the newt. None of the other detergents out-performed Triton X-100. CHAPS and NP-40 worked about as well as similar concentrations of Triton X-100 (compare Figure 3.2B, C with D, E; and F with G) and, as

Figure 3.2. Comparison of detergents and incubation times. **A-O:** Longitudinal sections of intact spinal cords were imaged through the dorsal-ventral axis, 3D-rendered in Fluorender and rotated to reveal cross sectional morphology. Dorsal is up. Axons were labeled with the 3A10 antibody (green) and nuclei with SYTOX green (magenta). Headings above each panel indicate the amount and type of detergent used to permeabilize the section (Tx, Triton X-100; NP40, NP-40; CHP, CHAPS; SDS, SDS; Tw, Tween-20), the incubation times with primary and secondary antibodies (10/7 indicates 10 days with primary and 7 days with secondary), and whether the tissue was perfused (P) or not perfused (NP). Headings to left of each row group images into their respective experiments. Details of each experiment are summarized in Table 3.2. SA, streptavidin; cc, central canal; eg, ependymoglia; gm, grey matter; wm, white matter; D, dorsal; V, ventral. Scale bars: 100 μm.

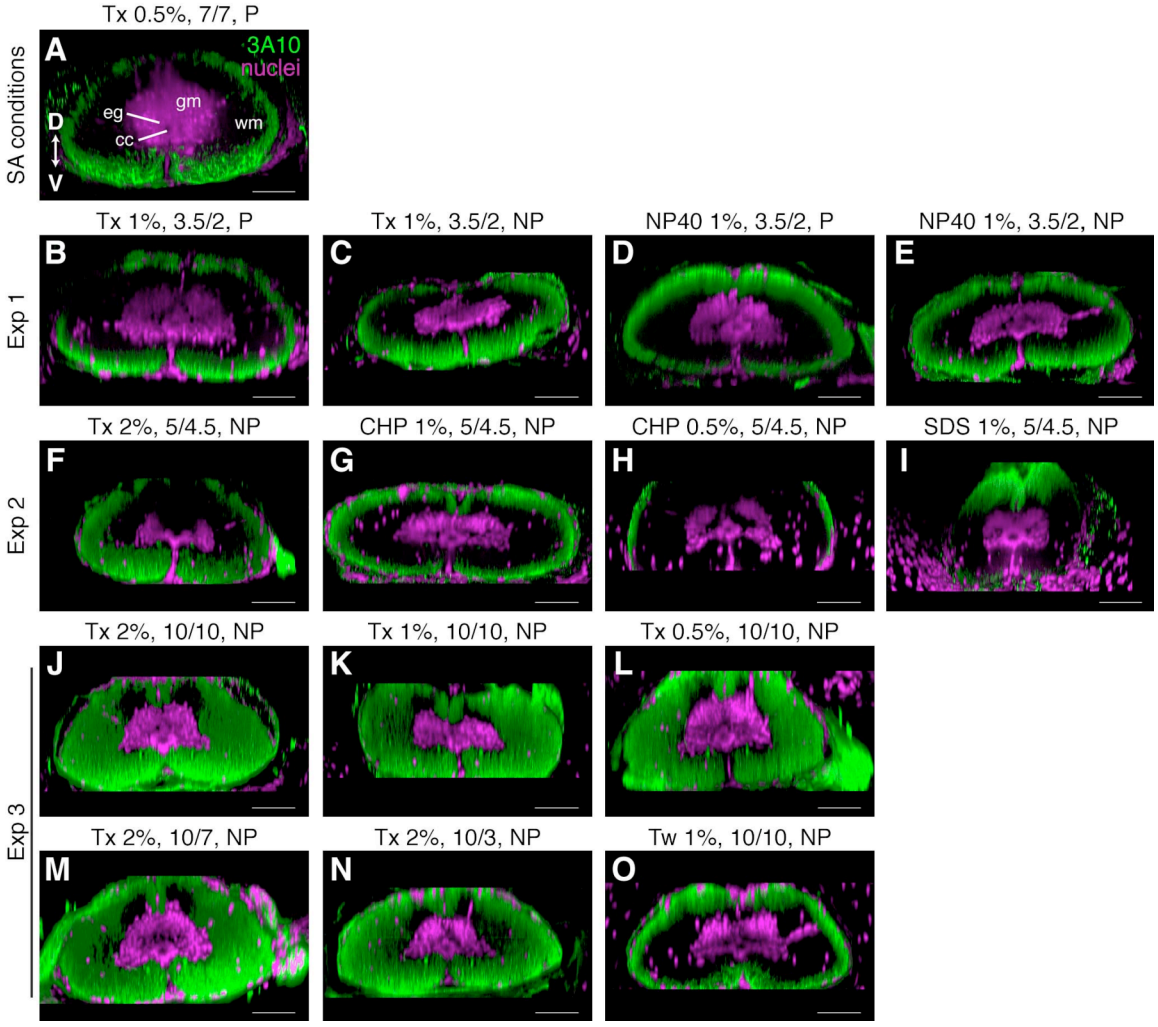
SA conditions
Exp 1
Exp 2
Exp 3
Tx 0.5%, 7/7, P
A
3A10
nuclei
gm
eg
cc
wm
D
V
Tx 1%, 3.5/2, P
B
Tx 1%, 3.5/2, NP
C
NP40 1%, 3.5/2, P
D
NP40 1%, 3.5/2, NP
E
Tx 2%, 5/4.5, NP
F
CHP 1%, 5/4.5, NP
G
CHP 0.5%, 5/4.5, NP
H
SDS 1%, 5/4.5, NP
I
Tx 2%, 10/10, NP
J
Tx 1%, 10/10, NP
K
Tx 0.5%, 10/10, NP
L
Tx 2%, 10/7, NP
M
Tx 2%, 10/3, NP
N
Tw 1%, 10/10, NP
O

expected, Tween-20 did not work as well (compare Figure 3.2K with O). SDS disrupted the morphology of the spinal cord, in that the cord appeared stretched and warped, without improving antibody penetration (Figure 3.2I).

Thus, Triton X-100 remained our detergent of choice and we were able to modestly improve antibody penetration by increasing the amount of Triton X-100 to 2% (compare Figure 3.2A and F). This, however, was still not sufficient. In order to get labeling throughout the spinal cord, we increased incubation times to 10 days with primary and 10 days with secondary antibodies and improved the ability of the antibody solution to mix with the sections by incubating sections in higher volumes of antibody solution and in small centrifuge tubes, rather than in 96-well plates (Figure 3.2J-L). In fact, these adjustments appeared to have a greater effect on antibody penetrance than the amount of detergent, for these conditions enabled full penetrance with even 0.5% Triton X-100 (Figure 3.2L). The quality of labeling, though, was best with 2% Triton X-100. The fine GFAP positive processes emanating from ependymoglia and astrocytes are most clearly labeled in sections permeabilized with 2% Triton X-100 (compare Figure 3.3A-C).

Given that secondary antibodies often require less incubation time than primary antibodies, we tested whether this might be true in our sections. We permeabilized sections with 2% Triton X-100 and incubated them with primary antibody for 10 days and compared secondary incubation times of 3, 7 and 10 days. While antibody penetration was complete for all three time points (Figure 3.2J, M, N), the quality of labeling was best when incubation with secondary antibody was 10 days (compare GFAP labeling in Figure 3.3C, D, E).

Figure 3.3. Comparison of the quality of antibody labeling in experiment 3. **A-E:** Single confocal planes, representing longitudinal sections through intact spinal cords at the level of the central canal (cc). Rostral is up. Axons were labeled with the 3A10 antibody (red), astrocytes and ependymoglia (eg) with a GFAP antibody (green), and nuclei with SYTOX green (blue). gm, grey matter; wm, white matter. Headings above each panel indicate the amount of Triton X-100 (Tx) detergent used to permeabilize the section and the incubation times with primary and secondary antibodies (10/7 indicates 10 days with primary and 7 days with secondary). Details of experiment 3 are summarized in Table 3.2. R, rostral; D, dorsal. Scale bar: 100 μm (all images are the same scale).

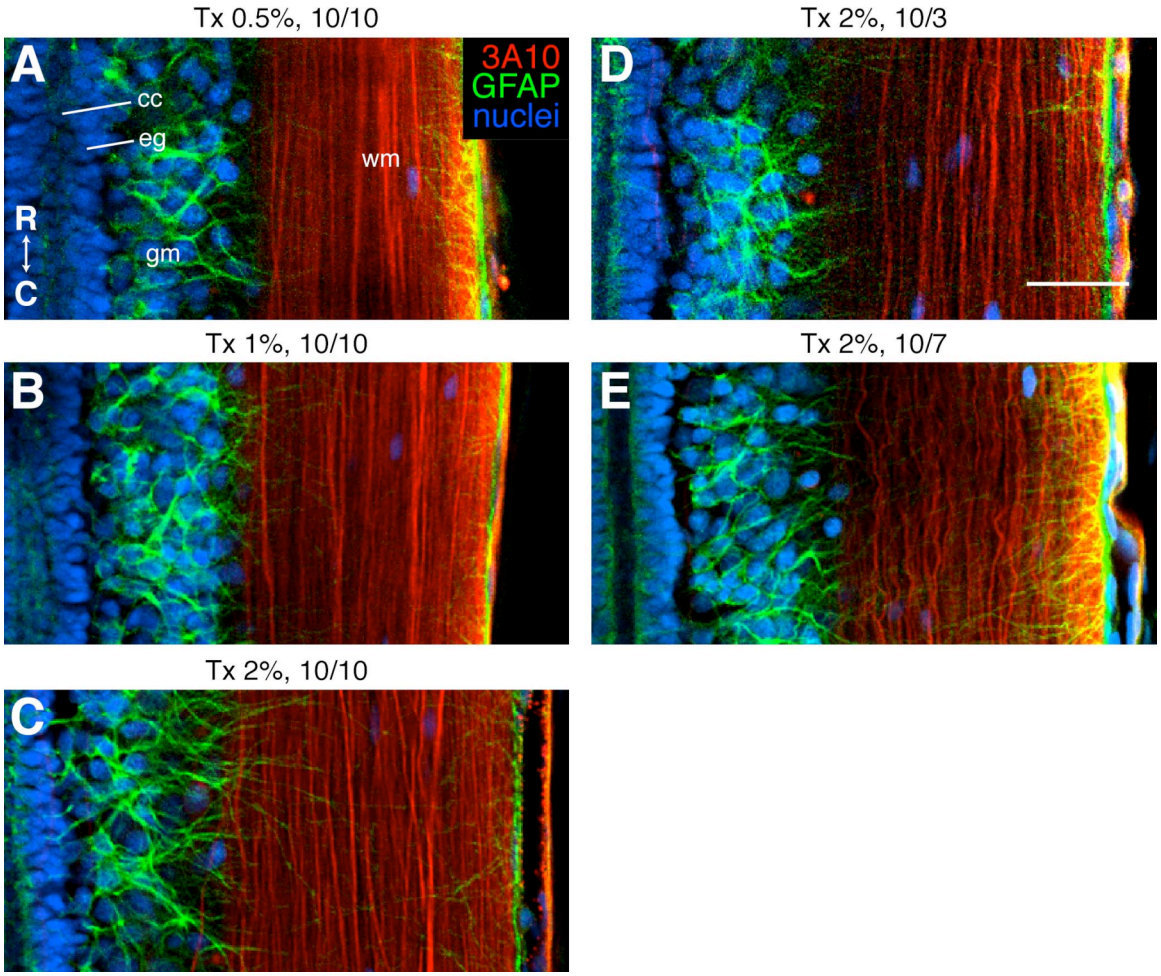
Tx 0.5%, 10/10
A
3A10
GFAP
nuclei
cc
eg
wm
gm
R
C
Tx 2%, 10/3
D
Tx 1%, 10/10
B
Tx 2%, 10/7
E
Tx 2%, 10/10
C

These results are summarized in Table 3.2. We optimized antibody labeling by increasing the amount of Triton X-100 detergent to 2%, increasing the incubation times to 10 days each with primary and secondary antibody, and improving the ability of the antibody solution to mix with the sections. This increased signal without adding background noise and without detrimental effects to morphology. Permeabilizing the tissue at a higher temperature (37°C) before the addition of antibodies did not appear to have a large effect on the efficiency of antibody penetration. Other factors that likely promote antibody labeling include decreasing the section thickness to 350 – 375 μm to ensure that the spinal cord is exposed on both sides of the section and omitting the perfusion fixation step and fixing the tissue after harvest only.

3.3.4 Clearing

Whole-mount specimens must be free of light scattering pigment and optically clear before high-quality confocal images through the entire specimen can be obtained. For this, bleaching and clearing agents are used (Klymkowsky and Hanken, 1991).

We tried two types of bleach, a modified Dent's bleach containing 15% hydrogen peroxide and a formamide bleach containing 6% hydrogen peroxide and 3% formamide. The formamide bleach was superior. All pigment was completely gone after just 2 hours in the formamide bleach while the Dent's bleach was unable to remove all pigment even after a 2 day incubation period.

To clear our whole-mounts, we tried glycerol and BABB. Despite the disadvantages to working with BABB, namely that it is a caustic solution and makes the tissue brittle, we found it to work exceptionally well and preferred to use it over glycerol.

Table 3.2. Amount of antibody penetrance obtained with various detergents and incubation times

exp	perfuse	detergent	thick-ness	1° Ab time	2° Ab time	penetrance	quality of labeling
initial	yes	0.5% Tx	400 μm	7d	7d	fair	–
1	no	1% Tx	300 μm	3.5d	2d	fair	–
1	yes	1% Tx	300 μm	3.5d	2d	fair	–
1	no	1% NP40	400 μm	3.5d	2d	fair	–
1	yes	1% NP40	400 μm	3.5d	2d	fair	–
2	no	0.5% Chp	350 μm	5d	4.5d	poor	–
2	no	1% Chp	350 μm	5d	4.5d	fair	–
2	no	1% SDS in pre-tr, then 2% Tx	350 μm	5d	4.5d	fair	poor morphology
2	no	2% Tx	300 μm	5d	4.5d	fair	–
3	no	0.5% Tw	350 μm	10d	10d	fair	–
3	no	0.5% Tx	350 μm	10d	10d	complete	ok
3	no	1% Tx	350 μm	10d	10d	complete	good
3	no	2% Tx	350 μm	10d	3d	complete	ok
3	no	2% Tx	350 μm	10d	7d	complete	good
3	no	2% Tx	350 μm	10d	10d	complete	best

Conditions for each experiment (exp) are listed below.

Initial: permeabilize 2 hours, RT; incubate in 250 μl in 96-well plate

Exp 1: permeabilize 2 hours, 37°C; incubate in 250 μl in 96-well plate

Exp 2: permeabilize 5 hours, 37°C; incubate in 250 μl in 96-well plate

Exp 3: permeabilize 4.5 hours, RT; incubate in 400 μl in small centrifuge tubes

Ab, antibody; tr, treatment; Tx, Triton X-100; Tw, Tween-20; Chp, CHAPS

Care was taken to always wear gloves and avoid the use of plastics when working with BABB. Sections were transferred to glass vials before they were cleared. Cleared sections were transferred to metal slides for imaging and transferred back to the glass vials containing BABB for storage at 4°C. Sections stored in this way have remained well preserved for up to 2 years.

3.3.5 Viewing 3D relationships

As mentioned above, spinal cords were imaged on a confocal microscope in 2 to 5 μm steps through the dorsal-ventral axis. 3D relationships were then visualized with ImageJ or Fluorender software. This is demonstrated on a 3-week regenerating spinal cord that was prepared with the optimized method outlined in Table 3.1 and labeled with the 3A10 antibody and an antibody against the extracellular matrix protein, tenascin C (TN-C). In ImageJ, the planes of the confocal z-stack can be viewed individually in rapid succession to allow one to visualize the detail in each confocal plane in relationship to the whole stack (Figure 3.4A-A", Movie 3.1). Using this view, one can appreciate that some of the TN-C in this injured spinal cord lines tube-like structures that are connected (*arrowheads* in Figure 3.4A-A"). This type of 3D structure would not be as well appreciated if it were viewed in a single 2D image. In Fluorender, the whole volume is rendered in 3D and it can be rotated to reveal, for example, cross-sectional morphologies and 3D shapes (Figure 3.4B-B", Movie 3.2).

This method of visualizing the cellular and molecular structure of the regenerating newt spinal cord represents a significant advance in the field of newt regeneration biology and will be a useful tool for future studies into the mechanisms of spinal cord

Figure 3.4. Visualizing 3D relationships. A 3-week regenerating spinal cord was prepared for antibody labeling as outlined in Table 3.1 and longitudinal planes through the dorsal-ventral axis were imaged on a confocal microscope. Axons were labeled with the 3A10 antibody (red), the extracellular matrix with a TN-C antibody (green), and nuclei with SYTOX green (blue). Rostral is up. **A-A":** Single confocal planes through the level of the terminal vesicles (TV, **A**), and 40 μm (**A'**) and 60 μm (**A"**) dorsal to the TVs. The arrowheads mark TN-C-lined, tube-like structures that can be seen to be connected when the whole z-stack is viewed (Movie 3.1). The asterisk marks the injury site. **B-B":** Snapshots of Movie 3.2 of the entire z-stack rendered in 3D with Fluorender and rotated around the horizontal axis. **B:** A dorsal view rotated 20° to reveal a cross section of the spinal cord caudal to the injury (arrow). **B':** A flat dorsal view. **B":** A dorsal view rotated 20° to reveal a cross section of the spinal cord rostral to the injury (arrow). Scale bars: 100 μm (**A-A"** are the same scale).

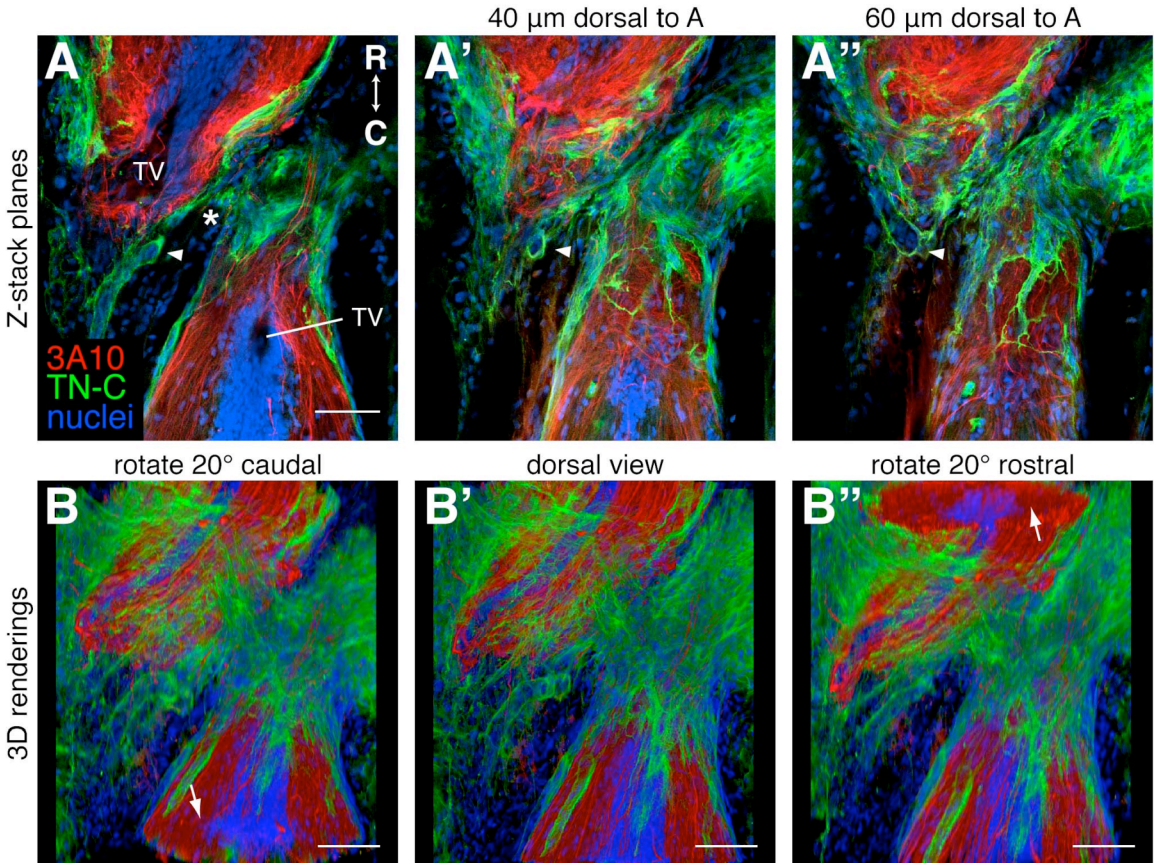
40 µm dorsal to A
60 µm dorsal to A
A
A'
A''
R
C
TV
TV
*
3A10
TN-C
nuclei
Z-stack planes
rotate 20° caudal
dorsal view
rotate 20° rostral
B
B'
B''
3D renderings

regeneration. These methods should also be widely adaptable for anyone wishing to study 3D relationships in other adult tissues.

3.4 Detailed methods

3.4.1 Animals

Adult newts, *Notophthalmus viridescens*, were purchased from Charles D. Sullivan Co. Inc., (Nashville, TN), housed at 22°C in glass aquariums equipped with water filters, and fed live blackworms, Lumbriculus varietgatus (Eastern Aquatics, PA). All animal protocols were approved by the University of Utah Institutional Animal Care and Use Committee.

3.4.2 Spinal cord injury surgery

Transect the spinal cord and allow it to regenerate for the desired length of time, if applicable. Perform transection injuries as described in Davis et al (1989; 1990). Anesthetize newts in Tricaine solution for 10 min and then place in ice for 30 min. Place the animal prone on a sylgard dish with its trunk region propped up slightly. Cover the head and tail with moist kimwipes. Swab the skin with 10% providone iodine and make a deep incision between two vertebral bones about 1 cm rostral to the hindlimbs. Using forceps, gently separate the vertebrae and remove the dorsal lamina of the caudal-most vertebra to expose the spinal cord. Cut the cord completely with fine spring scissors. Irrigate blood with sterile 85% PBS, if necessary. Place newts on ice for 15 min after the surgery and allow them to recover in bins that are tilted to produce a shallow area of water. Clean bins every day or two during the recovery period and replace the water with fresh de-chlorinated tap water.

3.4.3 Tissue preparation

3.4.3.1 Day 1 (Apply axon tracer, harvest tissue, and fix).

1. Apply the axon tracer to the spinal cord and allow it to travel for 6 hours, if applicable. Our procedure was modified from that used in zebrafish (Becker et al., 1997; Becker and Becker, 2001). Prepare tracer-soaked pieces of gel foam ahead of time: soak a small piece of gel foam in 1.5 μl of a 10% solution of biotinylated dextran amine (BDA, 3kD, lysine fixable, Invitrogen, D7135) and let it air dry in a tissue culture hood for 40 min to further concentrate the solution. Add fast green dye (Fisher, F-99) to the tracer solution at 0.05 mg/ml to make it visible *in vivo*, if desired. To apply the tracer, anesthetize newts as above and place in ice for 30 min. Transect the spinal cord as above one segment rostral or caudal to the original injury site (or targeted injury site if the cord is still intact) and insert a piece of tracer-soaked gel foam into the wound. Control excessive bleeding before adding the tracer, if necessary, by inserting a piece of fresh gel foam into the wound and allowing the animal to sit on ice for a few minutes. Minimize use of this technique as it decreases the efficiency of tracer uptake.

2. Once the tracer dye has labeled the spinal cord, perfuse the newts through the heart with 1.5 ml 85% PBS followed by 3 ml PLP with 0.5% PFA (omit if labeling with antibodies). We use a micromanipulator to control the needle and an infusion pump set to run at about 1 ml per 1.5 min. Anesthetize newts in Tricaine solution for 10 min and then place on ice for 15 min. To perfuse, place the newt supine on a sylgard dish and pin the arms apart. Make a rostral-caudal incision between the forelimbs up to the jaw/neck to expose the heart. Position the perfusion needle near the heart, turn on the perfusion pump to run 85% PBS, nick the sinus venosus and insert the needle into the ventricle. After 1.5

ml of 85% PBS has run through the animal, switch the pump to the fixative and run 3 ml of it through the animal. The liver should be cleared of blood and the animal should feel stiff after perfusion.

3. Harvest about 4 mm of lower trunk spinal column. If the animal has not been perfused, then sacrifice via decapitation after the animal is fully anesthetized. Use a microtome blade (extremely sharp; Ted Pella, 27237, Accu-Edge blades) to separate about 4 mm of the lower trunk spinal column from the rest of the spinal column and scissors to remove the 4 mm long segment from the rest of the animal. Trim away tissue lateral to the spinal column so that the specimen is about 2 mm wide. Always use a very sharp blade when cutting or trimming the spinal column so that you do not pull the very soft spinal cord out of the spinal column.

Note: All incubations are at RT and with rocking unless otherwise specified.

4. Post-fix in PLP with 0.5% PFA for 2 hours. Use 3 ml in a small vial if fixing 1 or 2 segments together. Use 10 ml in 15 ml conical tube if fixing 3 to 8 segments together.

5. Rinse with PBS briefly, then for 30 min (3 times), then overnight at 4°C.

3.4.3.2 Day 2 (Decalcify).

6. Decalcify with Morse's solution for 24 hours.

3.4.3.3 Day3 (Bleach, embed, section, permeabilize).

7. Rinse with PBS briefly, then for 30 min (3 times).

8. Bleach with formamide bleach for 2 hours or until all pigment is gone.

9. Rinse with PBS briefly, then for 30 min (3 times).

10. Embed in 4% agarose for longitudinal sections. Dissolve agarose in PBS by heating in a microwave and stabilize the temperature to 60°C in an oven prior to embedding. Keep agarose liquefied during embedding by putting it on a hot plate at the bench. Dab tissue on a kimwipe, fill the mold with agarose, quickly position the tissue in the mold, and place the mold on ice to let the agarose congeal.

11. Use a vibratome to obtain thick sections containing the entire spinal cord. Fill the collection bath with pre-chilled PBS and keep it cold with PBS ice cubes. Use feather thin blades (Ted Pella, 121-6, Double Edge, Breakable Style) rather than razor blades to section and always use a fresh part of the blade for each block. Remove agarose block from the mold, trim, and use Super Glue to glue the block to the chuck so that the ventral side of the spinal column is down. We used a Leica VT1000S vibratome and set the speed to 6.5 (out of 10) and the amplitude to 9 (out of 10). Trim the dorsal tissue until the spinal cord is exposed. Set the machine to cut a 400 μm (for streptavidin only labeling) or a 350-375 μm (for antibody labeling) thick section that contains the whole spinal cord. The spinal cord should be exposed on both sides for antibody labeling. Trim agarose away from the sides of the section and transfer the section to a small centrifuge tube containing PBS.

3.4.4 Fluorescent labeling

Note: Use at least 400 μl per small centrifuge tube. PBS-TxD or PBS-TxDB solutions should be made fresh and have 0.5% Triton X-100 for streptavidin staining and 2% Triton X-100 for antibody staining. If labeling with both streptavidin and antibodies, then use the parameters for antibody labeling.

12. Permeabilize with PBS-TxD for 4 hours to overnight.

13. Incubate in streptavidin-Cy5 or primary antibody diluted in PBS-TxDB for 7 or 10 days, respectively.

14. Rinse with PBS-Tx briefly, then for 30 min (5 times).

15. Incubate in secondary antibody diluted in PBS-TxDB for 10 days.

16. Rinse with PBS-Tx briefly, then for 30 min (4 times). Then rinse with TNT for 30 min.

17. Incubate in SYTOX green solution for 2-3 hours to stain nuclei.

3.4.5 Dehydration and clearing

18. Rinse with TN for 10 min (3 times) and transfer sections to glass vials.

19. Dehydrate through a methanol (MeOH)/TN series: 20%, 50%, 75%, 100% MeOH, 15 min each. These times are critical. Once dehydrated, move sections into the clearing agent as soon as possible.

20. Clear with BABB (1 part benzyl alcohol, 2 parts benyzl benzoate) and store in BABB at 4°C. When working with BABB, wear gloves and do not use plastics. Dispose of used BABB via incineration.

3.4.6 Confocal imaging and image analysis

The metal slides made for imaging are 77 x 26 mm^2 and 1 mm thick and have a 13 mm diameter hole drilled through the center. A glass coverslip covers the hole on one side to create a well and is glued in place with clear nail polish. Before imaging, dump a cleared section and the BABB in which it is stored into a glass petri dish, and use forceps to transfer the section to the well in the metal slide. Use a glass pipette to fill the well

with BABB, and cover the well with another coverslip. Transfer the remaining BABB back into the glass vial. After imaging, remove the top coverslip and transfer the section back to the BABB in the glass vial for storage at 4°C.

Spinal cords were imaged on an Olympus FV300 laser scanning confocal microscope using a 20X air objective. Images were processed with ImageJ, version 1.40g (W. Rasband; http://rsb.info.nih.gov/ij; NIH, Bethesda, MD), Fluorender, version 2.5.0 (Otsuna and Wan; http://www.sci.utah.edu/software/13-software/127-fluorender.html; University of Utah, Salt Lake City, UT) and Adobe Photoshop CS2. Levels were adjusted in ImageJ and/or Photoshop to maximize the signal to noise ratio.

3.4.7 Solutions

Tricaine solution: 0.1% w/v Tricaine (Ethyl 3-aminobenzoate methanesulfonate salt, Sigma, A5040) in 20 mM Tris-HCl, pH 7.5.

PBS: 137 mM NaCl, 2.7 mM KCl, 8.1 mM Na_2HPO_4, 1.15 mM KH_2PO_4, pH 7.4.

PLP fixative: 75 mM lysine, 0.5-2% PFA, 10 mM $NaIO_4$ in 85% PBS. Prepare by mixing 3 parts 0.1 M lysine stock with 1 part 4X PFA, then add solid $NaIO_4$. Make fresh and use within 2 hours. Make stock solutions ahead of time and store at -20°C: 0.1 M lysine in 85% PBS; 16% PFA in 85% PBS, pH 7.4.

GA/PFA fixative: 2% GA, 2% PFA in 85% PBS, pH 7.4.

Morse's solution: 22.5% formic acid, 10% sodium citrate.

Formamide bleach: 6% H_2O_2, 3% formamide, 0.1% Triton X-100 in PBS.

Modified Dent's bleach: 15% H_2O_2, 40% MeOH, 10% DMSO.

PBS-TxD: PBS with 0.5% or 2% Triton X-100 and 20% DMSO.

PBS-TxDB: PBS-TxD with the blocking reagents 1% BSA (EMD, OmniPur, Fraction V, Heat Shock Isolation, 2960) and 0.1% fish skin gelatin (Sigma G7765, 45% solution).

TN: 100 mM Tris-HCl, pH 7.5, 150 mM NaCl.

TNT: TN with 0.05% Tween-20

SYTOX green solution: Dilute SYTOX green (Invitrogen, S7020) 1:1000 in DMSO to make a stock solution and store at -20°C. Before use, dilute the stock another 1:25 in TNT.

3.4.8 Antibodies and streptavidin

Primary antibodies and dilutions used are as follows: 3A10 (mouse anti-chick neurofilament associated protein IgG1 monoclonal, DSHB, 3A10) 1:25; GFAP (rabbit anti-cow GFAP polyclonal, Dako, Z0334), 1:200; TN-C (rabbit anti-chick tenascin C polyclonal, Chemicon, AB19013) 1:100. Secondary antibodies (Invitrogen, whole antibodies, 2 mg/ml, conjugated to Alexa 568 or 633) were diluted 1:100. Streptavidin-Cy5 (Invitrogen, SA1011) and Streptavidin-Alexa 633 (Invitrogen, S21375) were diluted to 4 μg/ml. Lyophilized streptavidin-Alexa 633 was reconstituted with PBS to make a 1 mg/ml stock.

3.5 Movie legends

Movie 3.1. Movie through whole confocal z-stack of the 3 week regenerate shown in Figure 3.4A-A". It begins on the ventral side of the cord and moves in 2 μm increments through to the dorsal side. Rostral is up. Axons were labeled with the 3A10 antibody (red), the extracellular matrix with a TN-C antibody (green), and nuclei with SYTOX green (blue).

Movie 3.2. A movie of the Fluorender 3D rendering of the 3 week regenerate shown in Figure 3.4B-B". Axons were labeled with the 3A10 antibody (red), the extracellular matrix with a TN-C antibody (green), and nuclei with SYTOX green (blue). It begins with a dorsal view in which rostral is up. Scale bar: 100 μm.

3.6 References

Becker T, Becker CG (2001) Regenerating descending axons preferentially reroute to the gray matter in the presence of a general macrophage/microglial reaction caudal to a spinal transection in adult zebrafish. J Comp Neurol 433:131-147.

Becker T, Wullimann MF, Becker CG, Bernhardt RR, Schachner M (1997) Axonal regrowth after spinal cord transection in adult zebrafish. J Comp Neurol 377:577-595.

Bhairi SM, Mohan CM (2007) Calbiochem detergents: a guide to the properties and uses of detergents in biology and biochemistry. In: http://www.emdchemicals.com/life-science-research/request-literature/. EMD Biosciences, San Diego, CA.

Brockes JP (1997) Amphibian limb regeneration: rebuilding a complex structure. Science 276:81-87.

Davis BM, Duffy MT, Simpson SB, Jr. (1989) Bulbospinal and intraspinal connections in normal and regenerated salamander spinal cord. Exp Neurol 103:41-51.

Davis BM, Ayers JL, Koran L, Carlson J, Anderson MC, Simpson SB, Jr. (1990) Time course of salamander spinal cord regeneration and recovery of swimming: HRP retrograde pathway tracing and kinematic analysis. Exp Neurol 108:198-213.

Eguchi G, Abe SI, Watanabe K (1974) Differentiation of lens-like structures from newt iris epithelial cells in vitro. Proc Natl Acad Sci U S A 71:5052-5056.

Ghosh S, Thorogood P, Ferretti P (1994) Regenerative capability of upper and lower jaws in the newt. Int J Dev Biol 38:479-490.

Iten LE, Bryant SV (1976) Stages of tail regeneration in the adult newt, Notophthalmus viridescens. J Exp Zool 196:283-292.

Kardon G (1998) Muscle and tendon morphogenesis in the avian hind limb. Development 125:4019-4032.

Klymkowsky MW, Hanken J (1991) Whole-mount staining of Xenopus and other vertebrates. In: Methods in Cell Biology, pp 419-441: Academic Press, Inc.

McLean IW, Nakane PK (1974) Periodate-lysine-paraformaldehyde fixative. A new fixation for immunoelectron microscopy. J Histochem Cytochem 22:1077-1083.

Mitashov VI (1996) Mechanisms of retina regeneration in urodeles. Int J Dev Biol 40:833-844.

Oberpriller JO, Oberpriller JC (1974) Response of the adult newt ventricle to injury. J Exp Zool 187:249-253.

Piatt J (1955) Regeneration of the spinal cord in the salamander. J Exp Zool 129:177.

Rogers S (1999) Cell biological applications of fluorescence microscopy. In: http://www.itg.uiuc.edu/publications/techreports/99-006/. University of Illinois at Urbana-Champaign, Urbana, IL: Imaging Technology Group, Beckman Institute for Advanced Science and Technology.

CHAPTER 4

MENINGEAL CELLS AND GLIA ESTABLISH A PERMISSIVE ENVIRONMENT FOR AXON REGENERATION AFTER SPINAL CORD INJURY IN NEWTS

4.1 Abstract

4.1.1 Background

Newts have the remarkable ability to regenerate their spinal cords as adults. Their spinal cords regenerate with the regenerating tail after tail amputation, as well as after a gap-inducing spinal cord injury (SCI) such as a complete transection. While most studies on newt spinal cord regeneration have focused on events occurring after tail amputation, less attention has been given to events occurring after an SCI, a context that is more relevant to human SCI. Our goal was to use modern labeling and imaging techniques to observe axons regenerating across a complete transection injury and determine how cells and the extracellular matrix in the injury site might contribute to the regenerative process.

4.1.2 Results

We identify stages of axon regeneration following a spinal cord transection and find that axon regrowth across the lesion appears to be enabled, in part, because meningeal cells and glia form a permissive environment for axon regeneration. Meningeal and endothelial cells regenerate into the lesion first and are associated with a loose extracellular matrix that allows axon growth cone migration. This matrix,

paradoxically, consists of both permissive and inhibitory proteins. Axons grow into the injury site next and are closely associated with meningeal cells and glial processes extending from cell bodies surrounding the central canal. Later, ependymal tubes lined with glia extend into the lesion as well. Finally, the meningeal cells, axons, and glia move as a unit to close the gap in the spinal cord. After crossing the injury site, axons travel through white matter to reach synaptic targets, and though ascending axons regenerate, sensory axons do not appear to be among them. This entire regenerative process occurs even in the presence of an inflammatory response.

4.1.3 Conclusions

These data reveal, in detail, the cellular and extracellular events that occur during newt spinal cord regeneration after a transection injury and uncover an important role for meningeal and glial cells in facilitating axon regeneration. Given that these cell types interact to form inhibitory barriers in mammals, identifying the mechanisms underlying their permissive behaviors in the newt will provide new insights for improving spinal cord regeneration in mammals.

4.2 Background

Unlike mammals, adult newts have the remarkable ability to recover function after they are paralyzed by a spinal cord injury (SCI). After a complete transection injury, newts regenerate their spinal cords and regain use of their hindlimbs in as little as 4 wks (Davis et al., 1990) (see Movie 4.1). This recovery requires supraspinal axons to regenerate across the lesion and re-establish connections with downstream targets and is not simply due to a reorganization of circuits within the spinal cord (Davis et al., 1990).

This finding led us to ask the question: why do axons regenerate across an injury site in the newt when they do not in mammals?

One of the main reasons why regeneration fails in mammals is because the environment of the injured spinal cord is inhibitory for axon regeneration (Silver and Miller, 2004). After SCI, a variety of cell types, including astrocytes and meningeal fibroblasts, react in ways that prevent axons from regenerating across the injury site. These reactive cells create physical barriers to regeneration such as a glial scar and a glial limitans at the border between the cord and the injury site. They also create an extracellular matrix (ECM) that is inhibitory or repulsive for axon growth cone migration.

Therefore, axon regeneration may be enabled in the newt, in part, because the environment of the injury site is not inhibitory. Cells may respond in ways that help rather than hinder axon regeneration such that physical barriers are not created and the ECM is not inhibitory.

Much of what is known about spinal cord regeneration in salamanders comes from studies of tail regeneration. After tail amputation, a blastema forms and ependymoglia (EG) lining the central canal of the spinal cord elongate an ependymal tube that precedes and serves as scaffold for axon regeneration (Singer et al., 1979). Regeneration in this context is thought to proceed as a recapitulation of developmental processes as axons grow into newly developing tissues. Surprisingly, little is known about how axons regenerate after an SCI in the newt. In this context, axons must re-grow through an injury site having mature tissues on both sides of the lesion. This context is more relevant to the problem of spinal cord injury in humans. Older studies of SCI in the

newt have noted that a blastema and glial scar do not appear to form (Piatt, 1955), that axons can bridge large gaps in the cord before ependymal tubes elongate (Butler and Ward, 1967), and that, if left intact, the meninges can serve as a scaffold for axon regeneration (Stensaas, 1983). A more recent study of SCI in the axolotl, a neotenic larval salamander, found that EG appear to undergo an epithelial to mesenchymal transition, migrate into the injury site to form a solid mass, and then undergo a mesenchymal to epithelial transition to re-form an ependymal tube that serves as a scaffold for axon regeneration (O'Hara et al., 1992; Chernoff et al., 2003). In summary, previous studies suggest that physical barriers do not appear to form and EG and the meninges may help axons regenerate. Though O'Hare et al (1992) demonstrated that mesenchymal cells in the axolotl injury site were associated with fibronectin (FN), a permissive ECM protein, little else is known about the nature of the ECM of the injured newt spinal cord.

A focused and detailed study of axon regeneration and the cellular and extracellular environment axons encounter after an SCI in the newt has not been conducted. We, therefore, took advantage of modern labeling and imaging techniques to define, for the first time, stages of newt axon regeneration after a spinal cord transection injury and find that meningeal cells and glia, instead of interacting to form barriers to axon regeneration as they do in mammals (Shearer and Fawcett, 2001; Bundesen et al., 2003), appear to interact to form a permissive environment for axon regeneration in the newt. Our study examines many aspects of newt spinal cord regeneration, establishes the required foundation for further investigation into the cellular and molecular mechanisms

controlling this naturally occurring process, and may inform new therapeutic approaches in regenerative medicine.

4.3 Results and discussion

To understand how newt axons regenerate after an SCI we carefully observed axons regenerating across a complete transection injury, which severed all innervation to the tail and hindlimbs. Animals were allowed to regenerate for 1 d, 3 d, 1 wk, 2 wks, 3 wks, 4 wks, 6 wks or 9 wks, and prior to tissue harvest an axon tracer was applied rostral or caudal to the original injury site in order to label descending or ascending regenerating axons, respectively. The tracer and nuclei were labeled fluorescently, and the injury site was analyzed in whole-mount preparation on a confocal microscope. At least 3 animals were observed per tracer application site and time point (Table 4.1).

4.3.1 Spinal cord transection injury and axon tracer application

The spinal column in *Notophthalmus viridescens* contains one cervical (the atlas), about 13 trunk, 1-2 sacral, and 22-25 caudal vertebrae (Figure 4.1A) (Francis, 2002). The number of trunk, sacral and caudal vertebrae appears to be variable. The hindlimbs are innervated primarily by the last 2 trunk (T-1 and T-2) and first sacral (S1) spinal nerves, though there can be contributions from the third to last trunk (T-3) vertebra and the vertebra after S1 (S2/C1) (Figure 4.1D) (Francis, 2002). This is supported by the fact that the largest spinal nerves are associated with T-2, T-1 and S (see Figure S4.1) and axon tracer applied to the sciatic nerve labels primarily neurons in these spinal ganglia (see Figure 4.3A, B). To be sure all innervation to the hindlimbs was severed, we aimed to transect the spinal cord between T-4 and T-3 (Figure 4.1A, D), about 1 cm rostral to

Table 4.1. The number of animals observed at each stage and time point*

time point	total	retraction	growth initiation	wrapping	wrapping/ wisping	wisping	wisping/ spiking (no et)	spiking (no et)	spiking (with et)	contact	growth beyond injury (not recovered)	growth beyond injury (recovered)
1d	**6** **(3/3)**	6 (3/3)										
3d	**8** **(4/4)**	6 (4/2)	2 (-/2)									
1wk	**15** **(11/4)**	3 (3/-)	12 (8/4)									
2wk	**11** **(6/5)**		2 (1/1)	3 (1/2)	2 (1/1)	4 (3/1)						
3wk	**10** **(5/5)**			2 (2/-)		4 (-/4)			1 (1/-)	1 (1/-)	2 (1/1)	
4wk	**8** **(4/4)**			4 (3/1)					1 (1/-)		3 (-/3)	
6wk	**7** **(4/3)**					1 (-/1)	1 (-/1)	1 (-/1)	2 (2/-)	1 (1/-)		1 (1/-)
9wk	**6** **(4/2)**										2 (1/1)	4 (3/1)
totals	**71** **(41/30)**	**15** **(10/5)**	**16** **(9/7)**	**9** **(6/3)**	**2** **(1/1)**	**9** **(3/6)**	**1** **(-/1)**	**1** **(-/1)**	**4** **(4/-)**	**2** **(2/-)**	**7** **(2/5)**	**5** **(4/1)**

***** The numbers in parentheses break the totals for each category into rostral and caudal tracer application, respectively. For example, (4/2) indicates 4 animals received rostral tracer and 2 received caudal tracer. Animals that had recovered function were chosen preferentially for rostral tracer application. et, ependymal tube.

Figure 4.1. Spinal cord transection injury and axon tracer application. **(A)** Newt skeleton showing targeted location of injury. Note, the sacroiliac (SI) joints are not associated with the same vertebra in this animal, thus there are two sacral (S) vertebrae where there is usually one. T, trunk; C, caudal. **(B)** Intact and **(C)** completely transected spinal cord viewed from dorsal side. **(D)** Cartoon showing the location of the targeted injury, the spinal ganglia that supply innervation to the hindlimbs (solid line, primary contribution; dotted line, occasional contribution), and rostral tracer application site. **(E)** Cross section of spinal cord about 500 μm away from a tracer application site showing the tracer labels axons and neurons specifically. **(F, G)** Longitudinal sections through 1 wk regenerates. Asterisk, injury site. The tracer was applied to the animal in (F) and not to the animal in (G). Axons were also labeled with the 3A10 antibody. Application of the tracer 6 hours prior to tissue harvest did not alter the overall appearance of the axons at the injury site. cc, central canal; eg, ependymoglia; gm, grey matter; wm, white matter; m, meninges; D, dorsal; V, ventral; R, rostral; C, caudal. Scale bars: 200 μm (F, G, same scale).

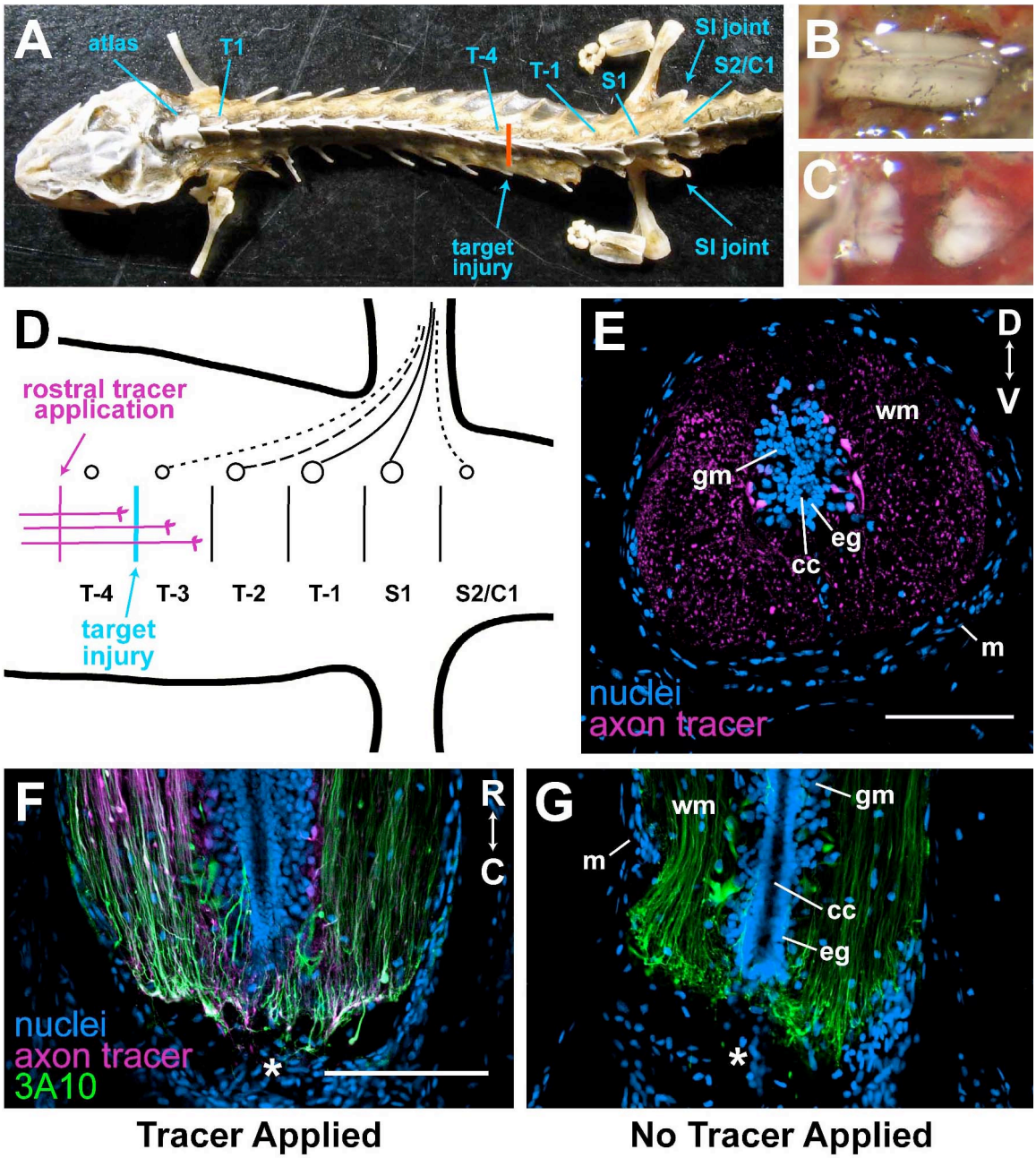
A
atlas
T1
T-4
T-1
S1
SI joint
S2/C1
target injury
SI joint
B
C
D
rostral tracer application
T-4
T-3
T-2
T-1
S1
S2/C1
target injury
E
D
V
wm
gm
eg
cc
m
nuclei
axon tracer
F
R
C
nuclei
axon tracer
3A10
*
G
wm
gm
m
cc
eg
*
Tracer Applied
No Tracer Applied

the hindlimbs. Upon dissection, it was often found that the injury was actually 1 or 2 segments rostral to the targeted site (see Figure S4.1B). Figure 4.1B shows what the intact spinal cord looks like when exposed from the dorsal side. After a complete transection injury, the two ends of the cut cord spring away from each other leaving a gap in the cord (Figure 4.1C). This type of injury was chosen because it is simple to perform consistently, spares no axons, severs the meninges as well as axons, and allows our studies to more seamlessly complement those done by previous investigators (Piatt, 1955; Davis et al., 1989; 1990). All injured animals were paralyzed (see Movie 4.1) and unable to swim for at least 3 wks, though the typical reflexive movements of the hindlimbs and tail were observed. Recovery of swimming function was scored and filmed in 6 and 9 wk regenerates. One out of seven (14%) 6 wk regenerates and 4 /6 (67%) 9 wk regenerates recovered swimming function (Table 4.1). This recovery rate is consistent with that reported in Davis et al (1990).

To label descending regenerating axons, a piece of gel foam saturated with the axon tracer, biotinylated dextran amine (BDA) was inserted into a transection injury 1 segment (about 2 mm) rostral to the original injury site (Figure 4.1D), and the tracer was allowed to travel for 6 hours. Ascending axons were similarly labeled by applying the tracer 1 segment caudal to the original injury. BDA travels 3 – 4 mm in 6 hours (see Figure 4.2K, L), produces a strong signal, and labels only neurons and their processes in the nervous system (Figure 4.1E). It does not diffuse across an injury site to label axons that have not regenerated across it (see Figure 4.2A-D). Transecting the spinal cord to apply the tracer rostral or caudal to the original injury site 6 to 24 hours prior to tissue

harvest does not appear to alter the general appearance of axons in the injury site (compare Figure 4.1F and G; see also Figure 4.4F, J, N, R vs. B, V).

4.3.2 Stages of axon regeneration

Our tracer analyses uncovered six stages of axon regeneration (Figure 4.2) that appeared to be typical and sequential. The timing for all but the first two stages was highly variable (Table 4.1). The times in parentheses after each stage in the text indicate the earliest and latest time points at which the stage was observed.

4.3.2.1 Retraction stage (1 d – 1 wk, most often before 1 wk)

Axons appear to have retracted away from the end of the cut cord (Figure 4.2A, B), and many axon tips have a balled-up morphology that is reminiscent of the dystrophic end-bulbs seen on axons that are unable to regenerate (Figure 4.2B") (Ramon y Cajal, 1928; Tom et al., 2004). Axon growth cones, however, can also be identified at this stage (Figure 4.2B').

4.3.2.2 Growth initiation stage (3 d – 2 wk, most often at 1 wk)

Axons appear to have initiated growth and grown back to the end of the cut cord (Figure 4.2C, D). As in the retraction stage, dystrophic axons and growth cones can be identified (Figure 4.2D', D"). The main difference between the first two stages is that many more axons extend to the end of the cut cord in the growth initiation stage. This difference is apparent even when all axons from the spinal cord are viewed in z-projections (see Figure S4.2). Also in this stage, the central canal, especially on the rostral side, begins to enlarge to form the terminal vesicle (TV).

Figure 4.2. Stages of axon regeneration. Images are montages of single confocal planes (except where indicated) of longitudinal thick sections. Rostral is to the left. Descending (A, C, E, G, I, K) or ascending (B, D, F, H, J, L) axons were labeled with the axon tracer (magenta), and nuclei are shown in green. Time after injury is indicated in the upper right corner of each panel. **(A, B)** Retraction and **(C, D)** growth initiation stages. Arrowheads, end of cord; asterisk, injury site; dotted line, unlabeled cord opposite the injury site. (B) is a z-projection of 4 planes to highlight growth cones. **(B', B", D', D")** Enlargements of dotted boxes in (B) and (D) showing that growth cones (primed boxes) and dystrophic axons (double primed boxes) are present at both stages. **(E, F)** Wrapping stage. **(G, H)** Wisping stage. **(I, J)** Spiking stage. (H) and (I) are z-projections of 2 confocal planes to show wrapping axons with wisping (H) or spiking (I) axons. **(K, L)** Contact and growth beyond the injury site stage. The animal in (K) had recovered swimming function, while the one in (L) had not. Open arrowheads, residual wrapping axons; arrows, meninges; TV, terminal vesicle. R, rostral; C, caudal. Scale bars: 200 μm (A-L), 50 μm (B', B", D', D").

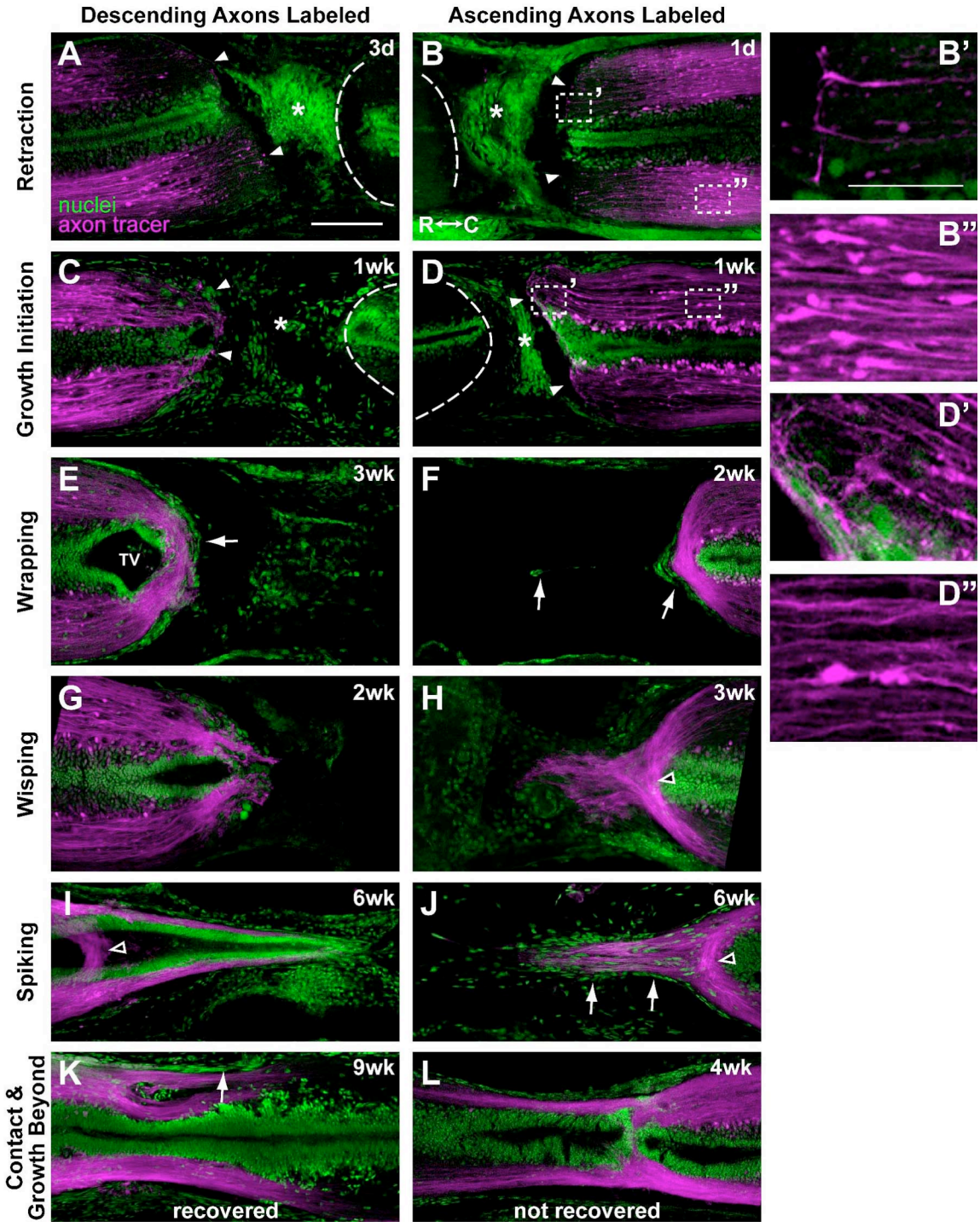
Descending Axons Labeled
Ascending Axons Labeled
Retraction
Growth Initiation
Wrapping
Wisping
Spiking
Contact & Growth Beyond
A
3d
nuclei
axon tracer
B
1d
R↔C
B'
B''
C
1wk
D
1wk
D'
D''
E
3wk
TV
F
2wk
G
2wk
H
3wk
I
6wk
J
6wk
K
9wk
recovered
L
4wk
not recovered

4.3.2.3 Wrapping stage (2 wk – 4 wk)

Axons continue to grow and wrap around the end of the TV (Figure 4.2E, F). Residual numbers of dystrophic axons can still be seen at this and all subsequent stages. The meninges also wrap around, or bound, the end of the cord (Figure 4.2E, F) and often begin regenerating across the injury site ahead of the axons and TV (Figure 4.2F). The low density of cells within the injury site suggests that a scar is not forming. The size of the gap in the cord is also larger at this stage than at all other stages (see Figure S4.3). This could indicate that the wrapping stage is an abortive stage seen only in animals that do not recover function. We do not favor this interpretation, however, because wrapping axons are still evident at all subsequent stages. This observation suggests that wrapping is a typical stage through which all regenerating spinal cords progress. The gap in the cord may get bigger before it gets smaller, simply as a result of body movements of the animal.

4.3.2.4 Wisping stage (2 wk – 6 wk)

Axons begin growing, or wisping, into the injury site ahead of the EG-lined TV (Figure 4.2G, H). Thus, as seen in previous studies of SCI in the newt, a pre-formed ependymal tube is not required for axon regeneration into the injury site (Butler and Ward, 1967; Stensaas, 1983). Wisping axons, however, do not grow into the ECM of the injury site alone but rather remain associated with cells. Many of these cells appear to be continuous with the meninges. At this stage, the meninges do not bound the end of the cord as they did in the wrapping stage but continue regenerating across the injury site, preceding the regenerating axons. Some wisping axons even appear to follow the regenerating meninges (see Figure 4.5D and Movie 4.2).

4.3.2.5 Spiking stage (3 wk – 6 wk)

As wisping axons continue to grow, they may fasciculate to form a spike (Figure 4.2I, J; see also Movies 4.3, 4.4). Spiking axons are still associated with cells in the injury site and cells that are continuous with the meninges. Some spikes do not contain an ependymal tube (Figure 4.2J), while others do (Figure 4.2I). In spikes with an ependymal tube, the ependymal tube appears to have elongated from the end of the cut cord because the largest part of the TV and residual wrapping axons are seen well behind the tip of the spike (Figure 4.2I; see also Movie 4.4). It is conceivable that a spike may not need to form. For example, if the gap in the cord is not large, wisping axons may be able to grow through the lesion and enter the cord on the opposite side without forming a spike.

4.3.2.6 Contact and growth beyond the injury site stage (3 wk – 9 wk)

In this stage, the two ends of the cord make contact with each other, and axons begin growing through the cord on the opposite side of the injury to re-establish functional connections (Figure 4.2K, L). All animals that had recovered swimming ability were in this stage, although not all animals in this stage had recovered function. Also, in all animals that had recovered, the ependymal tubes on each side of the injury had fused together to re-establish a continuous central canal. It was not possible to correlate the distance axons had regenerated beyond the injury site with functional recovery in this study because the axon tracer appears to fade out after 3 - 4 mm (Figure 4.2K, L). This is true even in the intact spinal cord (data not shown). There is some tolerance for sloppiness in how axons regenerate, for even in animals that had recovered function, wrapping axons were still evident (see Figure S4.4A” and Movie 4.5), some axons appeared to decussate (see Figure S4.4A’ and Movie 4.5), and separate fiber tracts could

be seen traveling along the meninges (Figure 4.2K). Excessive sloppiness or gross misalignments may be the cause of a delay in or a complete failure of functional recovery (see Figure S4.4B-F and Movie 4.6).

4.3.3 Sensory axons do not appear to regenerate

Descending and ascending regenerating axons appear to progress through similar stages (Table 4.1, see also Table S4.1). This was surprising given that sensory axons are not thought to regenerate after a SCI in newts or zebrafish even though these animals recover function (Stensaas, 1983; Becker et al., 1997). To determine if ascending regenerating axons are true sensory axons, rather than axons arising from neurons within the spinal cord, an axon tracer was applied to the sciatic nerve 1 or 4 days prior to tissue harvest (Figure 4.3A). In 6 wk regenerates, descending axons were also labeled with a different tracer. Our goal was to identify tracer-labeled sensory axons wisping into and growing through and beyond the lesion.

Tracer application to the sciatic nerve effectively labels, on the ipsilateral side only, sensory neurons in the spinal ganglia, motor neurons, dorsal column axons, and occasionally axons in a ventral location, which are presumably motor neuron axons exiting the cord to form the ventral root (Figure 4.3B). Labeled sensory and motor neurons were found mostly at the level of S1 and T-1 and occasionally at T-2 (Figure 4.3A).

To determine if sensory axons are among axons wisping into the injury site, 3 wk regenerates received tracer application to the sciatic nerve 4 days prior to tissue harvest (n=3). The spinal cord caudal to the injury site (T-2 to S1) was analyzed in cross section to determine the effectiveness of the tracer application. Sensory and motor neurons and

Figure 4.3. Sensory axons may not regenerate. (**A**) Cartoon showing tracer application sites in relationship to the SCI. Tracer was applied to the sciatic nerve in the hindlimb to label sensory axons (green) and, in 6 wk regenerates, rostral to the injury to label descending axons (magenta). Tracer applied to the sciatic nerve labels primarily neurons in spinal ganglia S1 and T-1 (solid lines) and occasionally neurons in T-2 (dotted lines). **(B)** Cross section through spinal cord and spinal ganglia at T-1, 1 day after SCI and tracer application to the sciatic nerve. The tracer labels sensory neurons in the spinal ganglia (sg), motor neurons (mn), dorsal column axons (dc), and motor neuron axons (mna) exiting to form the ventral root. **(C-E)** Sections through a 3 wk regenerate. Sensory axons were labeled with BDA (green), and all axons were labeled with 3A10 (magenta in D, E). (C) Cross section at T-1. Inset, spinal ganglia on labeled side. (D, E) Longitudinal sections through the SCI at the level of the dorsal columns (D), and a more ventral level where there are wisping axons (E). Schematic cross sections of the spinal cord in the upper right corner show where the section is along the D-V axis. **(F-H)** Cross sections through a 6 wk regenerate that had recovered swimming function at T-1 (F), at T-4, about 500 μm caudal to the SCI (G), and through the center of the SCI at T-4/T-5 (H). Sensory axons were labeled with RDA (green), and descending axons were labeled with BDA (magenta). Inset in (F), spinal ganglia on labeled side. Inset in (H), phase image of injury site. Nuclei are shown in blue. D, dorsal; V, ventral; R, rostral; C, caudal. All scale bars: 200 μm (C-H, same scale; insets in C, F, same scale).

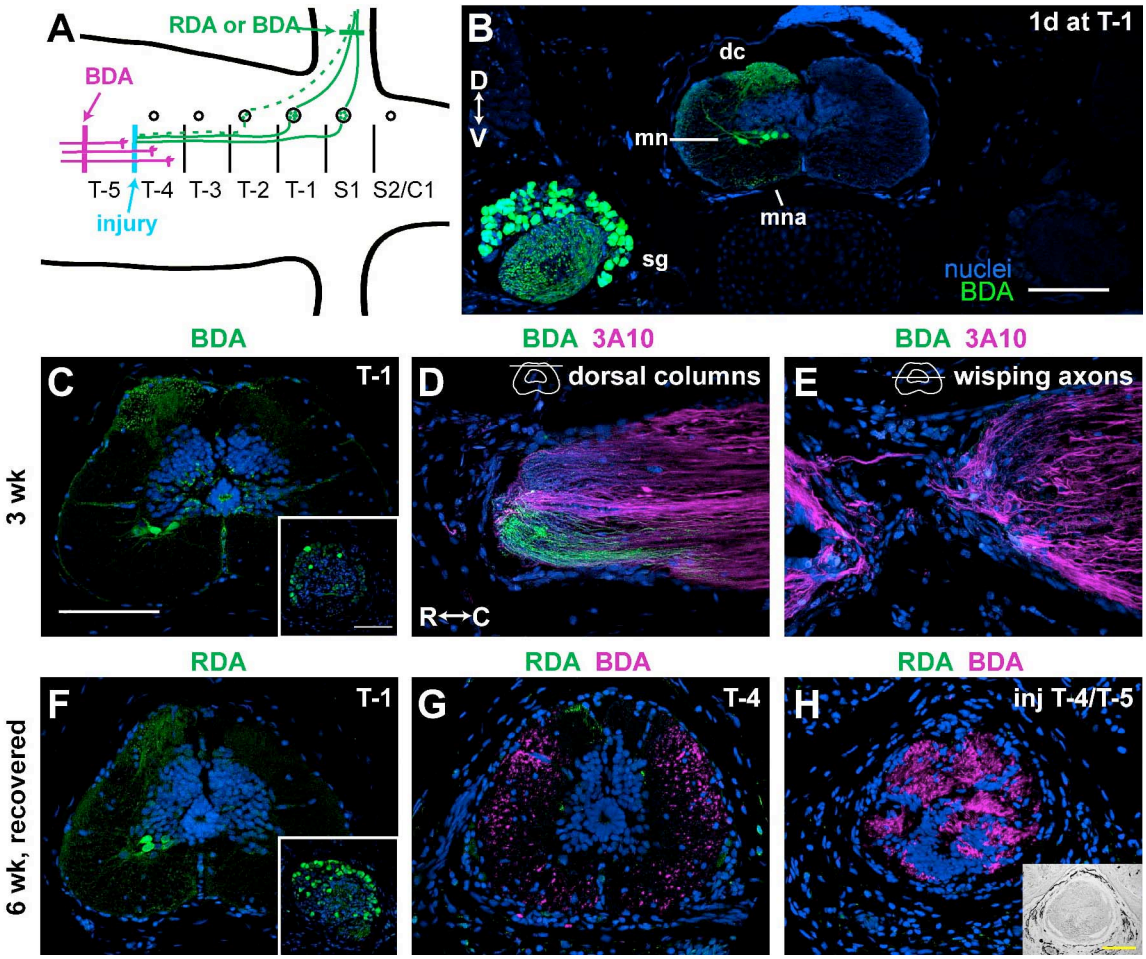
A
RDA or BDA
BDA
T-5
T-4
T-3
T-2
T-1
S1
S2/C1
injury
B
1d at T-1
dc
D
V
mn
mna
sg
nuclei
BDA
BDA
BDA 3A10
BDA 3A10
3 wk
C
T-1
D
dorsal columns
R↔C
E
wisping axons
RDA
RDA BDA
RDA BDA
6 wk, recovered
F
T-1
G
T-4
H
inj T-4/T-5

dorsal column axons were labeled in all three animals (Figure 4.3C). The injury site was analyzed in longitudinal sections to best view wisping axons. In sections through the dorsal columns, tracer-labeled sensory axons could be seen all the way up to the end of the cut cord (n = 2 out of 3; Figure 4.3D). In ventral sections through the region of wisping axons, however, none of the wisping axons were labeled with the tracer (Figure 4.3E).

To determine if sensory axons grow through and beyond an injury site, 6 wk regenerates received rhodamine dextran anime (RDA) application to the sciatic nerve 4 days prior to tissue harvest. BDA was also used to label descending axons. The spinal cord caudal to the lesion and the lesion itself were analyzed in cross section (n = 4). Sensory and motor neurons and dorsal column axons were effectively labeled with RDA in the spinal cord caudal to the lesion in three out of the four animals (Figure 4.3F). Two of the animals in which RDA was effectively applied had recovered function, and BDA-labeled descending axons could be seen growing through and at least 500 μm caudal to the injury site (Figure 4.3G, H). Despite this, RDA labeling in dorsal column axons got progressively weaker towards the injury, and RDA-labeled dorsal column axons were never seen in the injury site in any animal (Figure 4.3G, H).

We were not able to detect tracer-labeled sensory axons wisping into the lesion and growing through or beyond the lesion. This could indicate that sensory axons are either delayed or not regenerating or that the tracer faded out before the injury site. The tracer appears to travel a sufficient distance in four days to label wisping axons because it was seen robustly in dorsal column axons all the way up to the injury site in 3 wk regenerates (Figure 4.3D). If the axons had regenerated, however, it is possible that the

tracer was not detected in the injury site because of a dilution effect. The most likely explanation for why the tracer faded in the dorsal columns of the 6 wk regenerates is because the dorsal column axons were degenerating (Stensaas, 1983). Therefore, sensory information may not be needed for functional recovery in the newt, or sensory information may be transmitted to the brain via a relay circuit that is formed by ascending propriospinal axons that do regenerate across the injury site.

4.3.4 Axons regenerate through white matter to reach functional targets

Axons regenerating beyond the injury site in zebrafish travel preferentially through the grey matter rather than white matter to reach functional targets (Becker and Becker, 2001). Our initial study of axon regeneration in whole-mount preparations suggested that this is not true in newts (see Figure 4.2K, L). To investigate this further, descending axons in three, 6 wk regenerates in the growth beyond the injury site stage were analyzed in cross section about 500 μm caudal to the injury site. All axons in all three animals traveled in the white matter only (Figure 4.3G). Thus, axons do not re-route through the grey matter to reach functional targets in the newt. This suggests that white matter inhibitors (Xie and Zheng, 2008) either are not present in the newt spinal cord during axon regeneration or that newt axon regrowth is not inhibited by these molecules.

4.3.5 Extracellular matrix of the injured newt spinal cord

The ECM associated with an SCI in mammals is inhibitory or repulsive for axon growth cone migration (Silver and Miller, 2004). Chondroitin sulfate proteoglycans (CSPGs) are a major component of this inhibitory ECM. After injury, they are expressed

by a variety of cell types including astrocytes and meningeal cells, and they are expressed in the glial scar and glia limitans that forms at the border between the injury site and the spinal cord. They are also upregulated in the spinal cord itself in a gradient that increases as axons approach the injury site (Davies et al., 1999; Tang et al., 2003). ECM proteins that are canonically permissive for growth cone migration, such as FN (Bundesen et al., 2003; Herrmann et al., 2010), laminin (LM) (Busch et al., 2010) and collagen (Col) (Hermanns et al., 2001), as well as ECM proteins with more ambiguous effects, such as tenascin C (TN-C) (Tang et al., 2003), are also expressed. Overall, however, the ECM is dense and does not support growth cone motility (McKeon et al., 1995; Condic and Lemons, 2002).

Axon regeneration in the newt, then, may be enabled, in part, because the ECM of the injured newt spinal cord is not inhibitory. Consistent with previous studies, our initial axon regeneration experiments suggest that a dense scar does not form in the lesion (see Figure 4.2E-J). To confirm this observation and determine if the ECM in the newt contains permissive rather than inhibitory proteins, we used immunohistofluorescence to analyze the expression of CSPGs, TN-C, FN, LM, and Col in wisping and spiking stage regenerates, the stages in which axons grow across the injury site. Two-and-a-half to three wk regenerates were used to target these stages (see Table S4.1), and axons were labeled either with the axon tracer or an antibody against neurofilament associated protein (3A10).

In the intact spinal cord, CSPGs are not expressed, though they are expressed in the vertebral body in association with chondrocytes (Figure 4.4A). Surprisingly, CSPGs are expressed in the injured newt spinal cord. They are associated with the meninges and

Figure 4.4. Wisping axons are associated with loose ECM made up of canonically inhibitory and permissive proteins. Axons were labeled with 3A10 (B-D, G-H, S-T, V) or the axon tracer (F, J-L, N-P, R) and are shown in magenta. Each ECM protein is shown in green, and nuclei are blue. **(A-D)** CSPG expression in the intact spinal cord (A, cross section) and in wisping stage regenerates (B-D). (B) is a longitudinal section. (C) and (D) are cross sections through the terminal vesicle (C), and axons wisping into the injury site (D) from the same animal. Schematic longitudinal sections of the spinal cord in the upper right corner of (C) and (D) show where the section is in relationship to the injury site. Similarly, the expression of TN-C **(E-H)**, FN **(I-L)**, Col XII **(M-P)**, LM **(Q-T)**, and pigment **(U, V)** is shown. **(W)** A section adjacent to the one shown in (B) treated with chABC before incubation with the CS-56 antibody. **(X)** A section adjacent to the one shown in (E) treated only with secondary antibody; the primary antibody was omitted. D, dorsal; V, ventral; R, rostral; C, caudal. Scale bar: 200 μm (A-X).

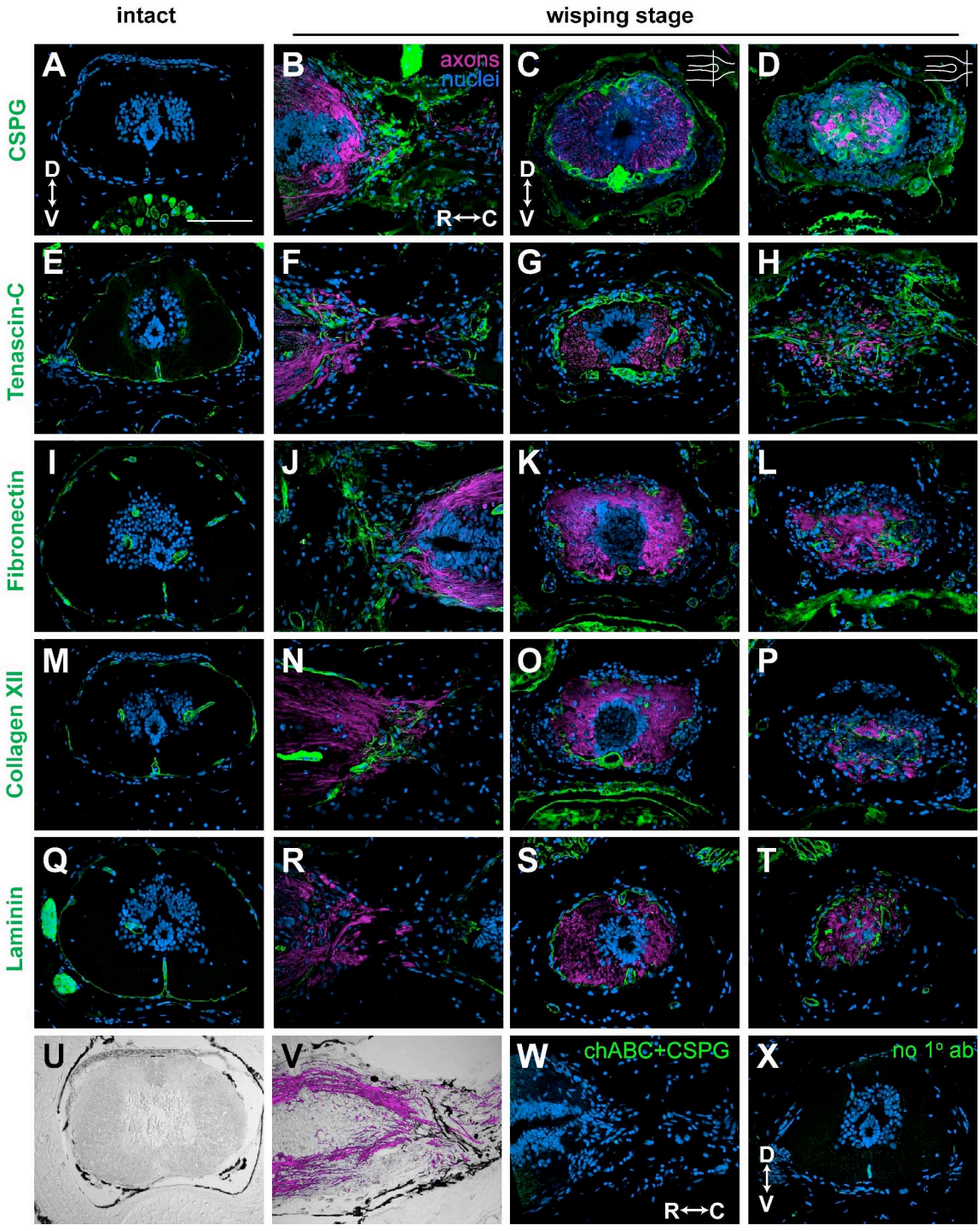
intact
wisping stage
CSPG
Tenascin-C
Fibronectin
Collagen XII
Laminin
A
B
axons
nuclei
C
D
D
V
R↔C
E
F
G
H
I
J
K
L
M
N
O
P
Q
R
S
T
U
V
W
chABC+CSPG
R↔C
X
no 1° ab
D
V

blood vessels (Figure 4.4B, C) and are expressed near wisping axons (Figure 4.4B, D). CSPGs are not found in the grey or white matter of the injured spinal cord and do not form a barrier between the cord and injury site. Thus, astrocytes in the spinal cord do not appear to express CSPGs. CSPGs also do not form a dense scar within the lesion. Unlike CSPGs, TN-C, FN, Col, and LM are expressed in the intact cord in association with the meninges and blood vessels (Figure 4.4E, I, M, Q). After injury all of these proteins are expressed in a pattern similar to CSPGs. They are associated with the meninges and blood vessels (Figure 4.4F, G, J, K, N, O, R, S) and are expressed near wisping axons (Figure 4.4F, H, J, L, N, P, R, T). These proteins are not found within the grey or white matter of the injured spinal cord, do not form a barrier between the cord and injury site, and do not form a dense scar within the injury site. We occasionally detected a weak TN-C signal within the white matter of the spinal cord, but this signal was not significantly above background noise (autofluorescence and non-specific staining). A previous study detected a stronger TN-C signal in the white matter of the intact and regenerating newt tail spinal cord (Caubit et al., 1994). We were unable to reproduce these results, perhaps because we were analyzing a different region of the spinal cord, a different regenerative context, or TN-C expression with different TN-C antibodies.

In summary, similar inhibitory and permissive ECM proteins are expressed in the injured newt and mammalian spinal cords, but the pattern of expression is different. In the newt, the ECM associated with wisping axons is loose and open, and a dense scar does not form. Also, ECM proteins are not present within the grey or white matter of the spinal cord, and the ECM does not form a permanent barrier, or glia limitans, between the

cord and the injury site, though we do have preliminary evidence that such a barrier may exist transiently during the wrapping stage (see Figure S4.5). Overall, even though inhibitory CSPGs are expressed, the ECM of the injured newt spinal cord does appear to be more permissive for axon growth cone migration than that of the injured mammalian spinal cord.

4.3.6 Meningeal and endothelial cells are associated with wisping axons

Given that cells closely associated with axons growing across the injury site and cells that create the permissive ECM are likely to be playing an important role in enabling axon regeneration, we sought to identify these cells. We hypothesized that they may be meningeal and/or endothelial cells because in the intact and regenerating spinal cord, ECM proteins appear to be expressed by cells of the meninges and blood vessels, not by cells in the grey or white matter (Figure 4.4). Thus, astrocytes and EG in the spinal cord do not appear to express ECM, at least not around their cell bodies. Our hypothesis is also supported by the fact that in the intact spinal cord, pigmented cells are only found in the meninges and blood vessels (Figure 4.4U), and pigmented cells are associated with wisping axons (Figure 4.4V). Additionally, many cells associated with wisping axons appear to be meningeal cells because they are continuous with the meninges (Figure 4.2). The meninges appear to regenerate ahead of regrowing axons, and some regrowing axons even appear to follow the regenerating meninges (Figure 4.5D; see also Movie 4.2).

To determine if cells associated with wisping axons and ECM are endothelial cells, we used the endothelial cell marker, von Willebrand Factor (vWF), which appears to specifically label blood vessels in the newt spinal cord (Figure 4.5A). In wisping stage

Figure 4.5. Meningeal and endothelial cells are associated with wisping axons. **(A-D)** Axons were labeled with the axon tracer (B, C) or 3A10 (D) and are shown in magenta, vWF is green (A-C) and nuclei are blue. (A) Cross section through intact spinal cord. (B) Longitudinal section through the SCI of a wisping stage regenerate labeled with anti-FN (white, shown separately in B') and anti-vWF (shown separately in B"). Arrowheads, cells double-labeled with FN and vWF. (C) Cross section through axons wisping into the injury site of a wisping stage regenerate. Schematic longitudinal section of the spinal cord in the upper right corner shows where the section is in relationship to the injury site. (D) Single confocal plane of a longitudinal thick section of a wisping/spiking stage regenerate. Arrowhead, meninges (m). **(E-I)** Longitudinal section through a wisping stage regenerate imaged with EM. (E) Region containing axons wisping ahead of the TV (TV). Asterisks, phagocytic cells. (F) Enlargement of meningeal cells in box F of (E). (G) Enlargement of meningeal-like cell in box G of (E) that is associated with dura mater ECM (ecm). Arrowhead, closed loop formed by meningeal-like cell processes; arrow, process resembling dura mater cell process. (H) Enlargement of meningeal-like cell in box H of (E), rotated 90°. This cell's processes (arrowheads) wrap around a bundle of axons (ax) cut in cross section. (I) Enlargement of box I in (H) showing that this cell's processes (arrowheads) are also associated with ECM (ecm). D, dorsal; V, ventral; R, rostral; C, caudal. Scale bars: 200 μm (A-D), 50 μm (E), 10 μm (F-H), 1 μm (I).

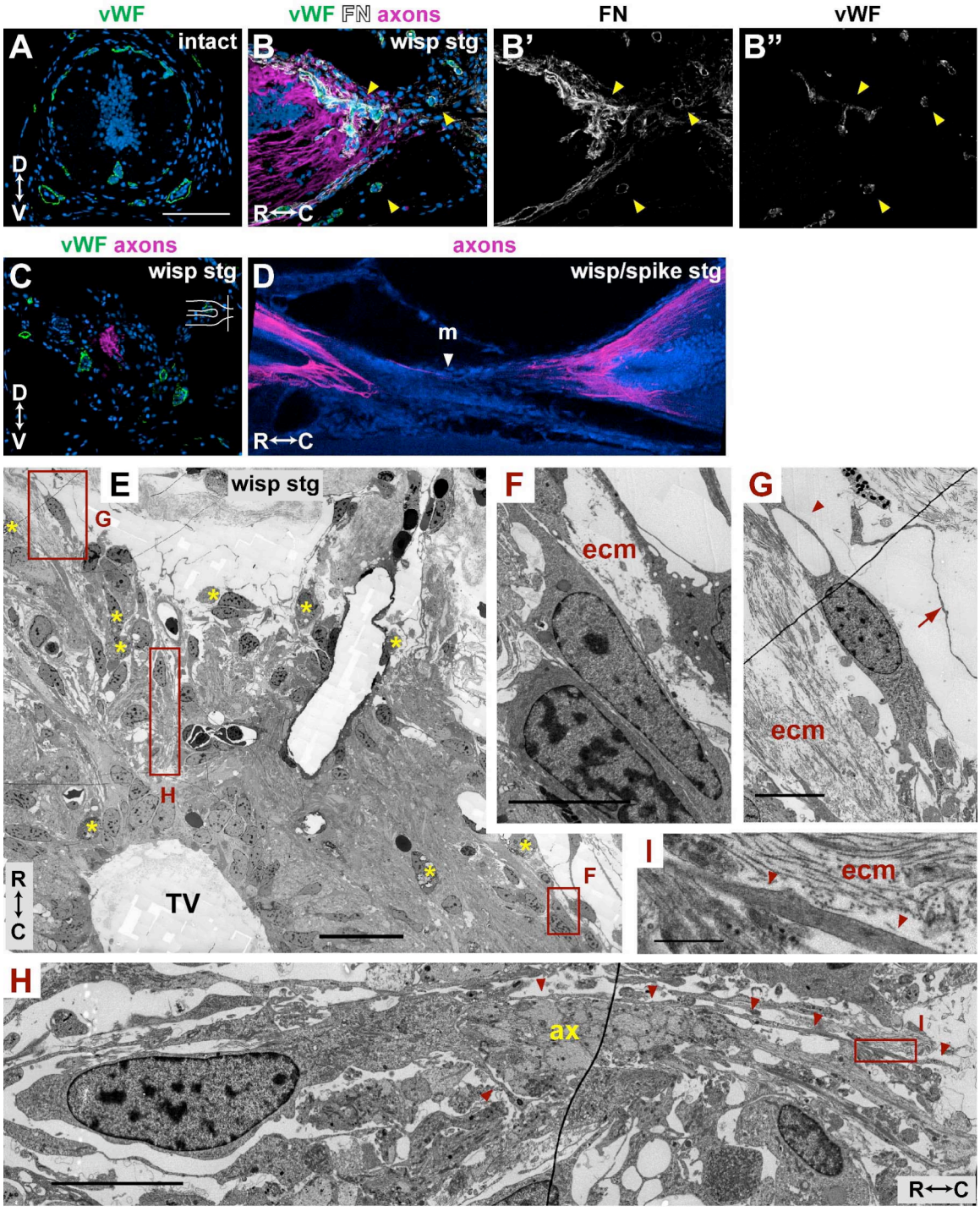
vWF
vWF FN axons
FN
vWF
A
intact
B
wisp stg
B'
B''
D
V
R↔C
vWF axons
axons
C
wisp stg
D
wisp/spike stg
m
E
wisp stg
G
H
TV
F
ecm
I
ax

regenerates, vWF^+ cells can be found in the injury site and near (Figure 4.5B, B") and ahead of (not shown) regenerating axons. These cells are also associated with FN, though not all of the FN is associated with vWF^+ cells (Figure 4.5B, B', B"). It has been hypothesized that blood vessels and nerves, because of their close proximity and parallel tracts, guide each other during development (Larrivee et al., 2009). To determine whether they might guide one another during newt spinal cord regeneration, we analyzed injury sites in cross sections. We found that although vWF^+ cells and axons are in the injury site at the same time, they do not need to be in direct contact with each other (Figure 4.5C). Therefore, regenerating blood vessels and axons do not appear to guide one another across the injury site, at least not through a contact-mediated mechanism.

Many cells in the injury site were not vWF^+, and much of the FN was not associated with vWF^+ cells. We, therefore, sought to determine, more conclusively, if any of the cells closely associated with wisping axons and ECM were meningeal cells. Meningeal cell markers such as RALDH2 and NG2 (Mey et al., 2005) did not produce a signal in our preparations (see Table S4.2), so we used electron microscopy (EM) to analyze cell types based on ultrastructure. In the intact and regenerating spinal cords, meningeal cells, in general, have an electron dense cytoplasm filled with mitochondria, an elongated nucleus with some clumped chromatin, and thin dark processes that are often associated with ECM (Figure 4.5E, F; see also Figure S4.6). None of the other cell types in the intact cord shared these characteristics of meningeal cells (see and compare Figures S4.6 and S4.7). In regenerating spinal cords, we observed cells with meningeal cell characteristics closely associated with regrowing axons. Figure 4.5H shows an enlargement of one of these cells. It has an electron dense cytoplasm filled with

mitochondria, an elongated nucleus with some clumped chromatin, and thin dark processes that appear to wrap around a bundle of axons that has been cut in cross section. Processes from this cell are also associated with ECM (Figure 4.5I). Another meningeal-like cell (Figure 4.5G) was associated with dura mater-like elements, namely ECM and fine, dark cell processes (see Figure S4.6B). Processes from the cell in Figure 4.5G form a closed loop, which suggests they may be attempting to wrap or cup around structures in their environment. Figure 4.6E shows another example of a meningeal-like cell process that is closely associated with regenerating axons as well as ECM.

It is difficult to know with certainty the identity of the meningeal-like cells. Stensaas (1983) suggested that cells with these characteristics were dark astrocytes derived from EG. Morphologically, however, these cells and their processes resemble meningeal cells far more than they do EG and astrocytes (see Figures S4.7 and S4.8). Although these cells appear to wrap around axons, we and Stensaas (1983) saw no evidence of them forming myelin, and therefore we do not think they are oligodendrocytes or Schwann cells. Further support for the idea that these cells may be meningeal cells comes from studies of meningeal cells that are transplanted into injured mammalian spinal cords along with olfactory ensheathing cells (OECs). Such meningeal cells appear to wrap axons into fascicles much like fibroblasts in the perineurium of peripheral nerves wrap axons (Li et al., 1998; Lakatos et al., 2003). These meningeal cells were also associated with ECM and had morphological features similar to our meningeal-like cells.

Figure 4.6. An inflammatory response is present, but not detrimental to axon regeneration. **(A)** Longitudinal section through a wisping stage regenerate. Axons were labeled with 3A10 (magenta), nuclei are in blue, and fluorescent channels were laid over the phase image. **(B)** A section adjacent to (A) stained with H&E. Many small cells with dark blue nuclei are present near wisping axons. **(B')** Enlargement of blue box in (B). Lymphocytes (arrowhead) and monocytes (arrows) can be identified near wisping axons. **(C-E)** Longitudinal section through a wisping stage regenerate imaged with EM. (C) Region containing axons regenerating into the injury site. Many phagocytic cells (asterisks), or macrophages, can be identified near regenerating axons. (D) Enlargement of box D in (C). Processes from this macrophage (m) are in direct contact with regenerating axons (ax). (E) Enlargement of box E in (C). Another example of a meningeal cell-like process (p) that is mingled and closely associated with regenerating axons (ax). ecm, ECM; R, rostral; C, caudal. Scale bars: 200 μm (A, B), 50 μm (B', C), 5 μm (D), 1 μm (E).

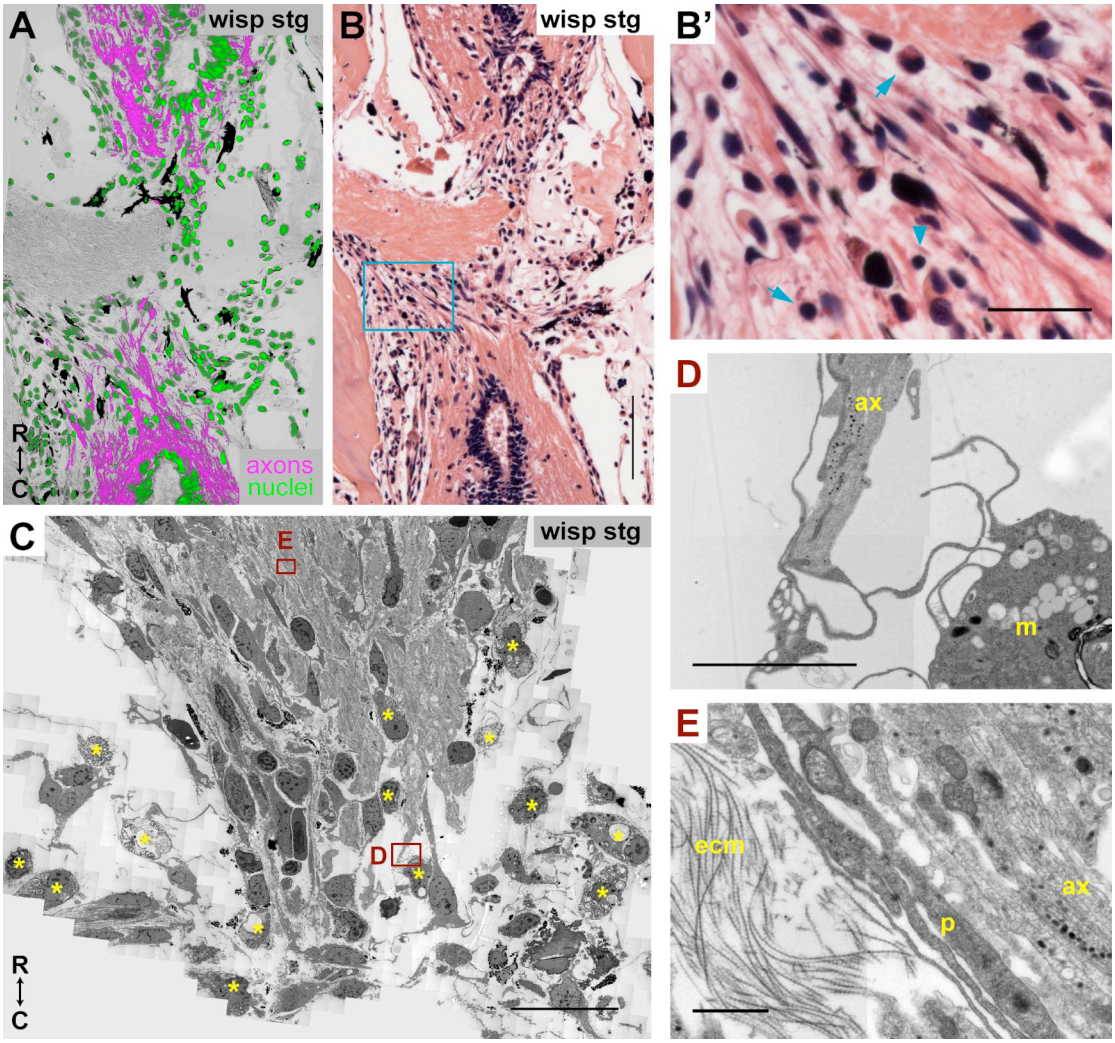
A
wisp stg
axons
nuclei
R
C
B
wisp stg
B'
D
ax
m
C
wisp stg
E
D
R
C
E
ecm
ax
p

4.3 7 Ependymoglial and astrocytic processes are associated with wisping axons

As mentioned above, axons are often seen wisping ahead of the central canal, and thus, a pre-formed ependymal tube does not appear to be required for axon regeneration after an SCI. To determine if EG still might be playing a role in axon regrowth, we used an antibody against glial fibrillary acid protein (GFAP). In the intact newt spinal cord, GFAP weakly labels EG cell bodies, strongly labels astrocytic cell bodies and strongly labels radial processes from both these cell types (Figure 4.7A). Therefore, this cell marker enabled us to observe the astrocytic as well as EG response.

In the injured spinal cord, GFAP expression is maintained in astrocytes and EG around the central canal. It does not appear to be upregulated, and $GFAP^+$ processes do not appear to be thicker than they are in the intact cord (compare Figure 4.7A and B). Therefore, astrocytes do not appear to become hypertrophic. In the injury site, only a few $GFAP^+$ cell bodies can be found (Figure 4.7D, D'). These cells are more likely to be EG than astrocytes because they express GFAP only weakly. Thus, astrocytes do not migrate into the lesion. In wisping stage regenerates, $GFAP^+$ processes are closely associated with wisping axons (Figure 4.7D, D'). These processes likely originate from EG and astrocytes that surround the central canal. Rather than being aligned perpendicular to axons, as they are during tail regeneration however, the $GFAP^+$ processes are aligned more parallel to the direction in which axons travel. This is especially evident in later-stage regenerates (Figure 4.7E). Note also that the $GFAP^+$ processes do not form a glia limitans between the cord and the injury site as they do in mammals (Figure 4.7B, D).

Figure 4.7. Glial processes are associated with wisping axons and do not form inhibitory barriers. Axons were labeled with 3A10 (B, D) or the axon tracer (E) and are shown in magenta. Glia were labeled with anti-GFAP (green), and nuclei are blue (A-D). **(A)** Cross section through intact spinal cord. GFAP labels EG and astrocytes and all of their processes. **(B)** Longitudinal section through the SCI of a wisping stage regenerate. Astrocytes do not become hypertrophic (compare with A). **(C)** Section adjacent to (B) treated only with secondary antibodies, primary antibodies were omitted. **(D)** Longitudinal section through the SCI of a wisping stage regenerate. **(D')** Enlargement of dotted box in (D). $GFAP^+$ processes (arrows) are associated with wisping axons and do not form a glia limitans. Only a few weakly $GFAP^+$ cells (arrowhead) are in the injury site. **(E)** Single confocal plane of a longitudinal thick section of a growth beyond stage regenerate. $GFAP^+$ processes run parallel to axons across the injury site. D, dorsal; V, ventral; R, rostral; C, caudal. Scale bars: 200 μm (A-D; B, C, same scale; D, E, same scale), 50 μm (D').

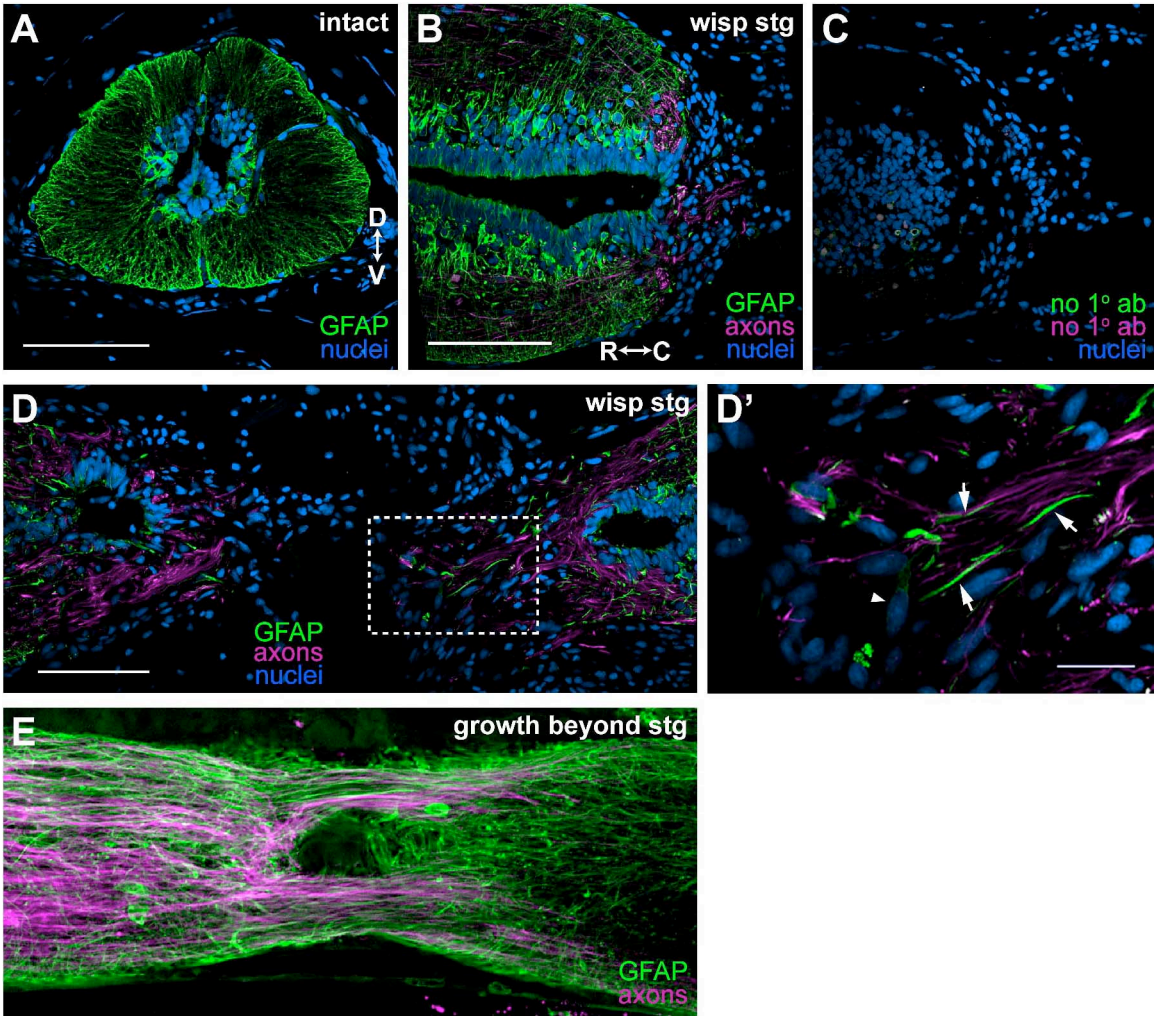
A
intact
D
V
GFAP
nuclei
B
wisp stg
GFAP
axons
nuclei
R↔C
C
no 1° ab
no 1° ab
nuclei
D
wisp stg
GFAP
axons
nuclei
D'
E
growth beyond stg
GFAP
axons

These data demonstrate that, while the EG response after SCI appears to be different than that after tail amputation, EG are still likely to be playing an important role in enabling axon regeneration, because $GFAP^+$ processes are closely associated with axons growing across the injury site. Also, while EG do not appear to migrate into the injury site in large numbers, there are a few that appear to do so.

Furthermore, the astrocytic response in the newt is very much different than that seen in mammals. Newt astrocytes do not appear to become hypertrophic, migrate into the injury site, express ECM, or form a glial limitans or scar. Instead of inhibiting axon regeneration as they do in mammals, newt astrocytes may, like EG, play a supportive role because many of the $GFAP^+$ processes associated with axons likely arise from astrocytes as well as EG.

4.3.8 An inflammatory response is present but does not appear to be detrimental to regeneration

It has been hypothesized that inflammation leads to scarring and nonregenerative wound healing and that it is not present in systems that regenerate (Harty et al., 2003). In support of this, macrophages in the injured mammalian spinal cord contribute to the formation of the scar (Fitch et al., 1999) and have even been shown to physically interact with axons to cause retraction (Horn et al., 2008).

To determine if an inflammatory response might be present in the newt SCI, we used hematoxylin and eosin (H&E) staining. With H&E staining, an inflammatory response is characterized by the appearance of many small round cells that have dark blue nuclei and very little cytoplasm. Lymphocytes have almost no cytoplasm, whereas monocytes have a small rim of cytoplasm. Based on these characteristics, an

inflammatory response does appear to be present in wisping stage regenerates (n=5, Figure 4.6A, B, B'). Figure 4.6B' highlights some of the more obvious examples of lymphocytes and monocytes that are present at this stage. These types of cells are associated with the fibrin clot that forms in the injury site and can be identified as early as one week after injury (see Figure S4.9A, B-B").

To confirm the presence of various types of inflammatory cells, we again tried several cell-type specific antibodies, but these did not produce a reliable signal in our preparations (see Table S4.2). We were, however, able to identify many phagocytic cells, or functional macrophages, in the region of regenerating axons in our EM images. Asterisks in Figures 4.5E and 4.6C mark obvious macrophages. These macrophages could even be seen to be in direct contact with axons (Figure 4.6D).

These data demonstrate that an inflammatory response does appear to be present in the injured newt spinal cord, but does not appear to be detrimental to the regenerative response. In fact, one of the most severe cases of inflammation was seen in a contact stage regenerate (see Figure S4.9C, C'). The inflammation, which was likely present at earlier stages as well, did not prevent regeneration from progressing to this advanced stage. The interaction of newt macrophages with axons, if it also causes axon retraction in newts, does not prevent the net response to be that of axon growth. Perhaps the beneficial effects the immune system can have on regeneration (Donnelly and Popovich, 2008) outweigh any detrimental effects in the newt.

4.4 Conclusions

Axons appear to be able to regenerate after an SCI in the newt, in part, because the environment of the injury site is not inhibitory. Instead of forming a dense inhibitory

scar and interacting to form a glia limitans and as they do in mammals (Shearer and Fawcett, 2001; Bundesen et al., 2003; Silver and Miller, 2004), newt meningeal cells and glia appear to create a permissive environment for axon regeneration. Figure 4.8 summarizes the stages of axon regeneration and the roles these cell types play. After an SCI, axons initially retract from the end of the cut cord and appear dystrophic, but then initiate growth by about 1 wk. Axons wrap around the end of the TV before growing into the lesion, perhaps because meningeal cells create a transient basal lamina. Meningeal and endothelial cells lead the way across the lesion and are associated with a loose extracellular matrix that permits growth cone migration. Axons grow into the injury site next and are closely associated with meningeal cells and glial processes that extend from EG and astrocytic cell bodies surrounding the central canal. Later in the process, ependymal tubes lined with glia extend into the lesion as well. Then, as a unit, meningeal cells, axons, and glia close the gap in the spinal cord. Finally, axons enter the cord on the opposite side of the injury and travel through white matter to reach functional targets. We also noted that although ascending axons do regenerate, sensory axons do not appear to be among them and that, overall, this regenerative process can occur in the presence of an inflammatory response.

4.4.1 Model

Based on our observations, we propose a glia – meningeal cell interaction model of spinal cord regeneration: spinal cord regeneration is enabled when meningeal cells and glia (astrocytes and EG) interact to form a conduit for axon regeneration rather than an inhibitory barrier (scar, glia limitans, and dense ECM). Simpson (1983) hypothesized that successful spinal cord regeneration depends upon an interaction between mesenchymal

Figure 4.8. Cellular model of newt axon regeneration. Schematics of longitudinal sections through the spinal cord are shown. See text for details. et, ependymal tube.

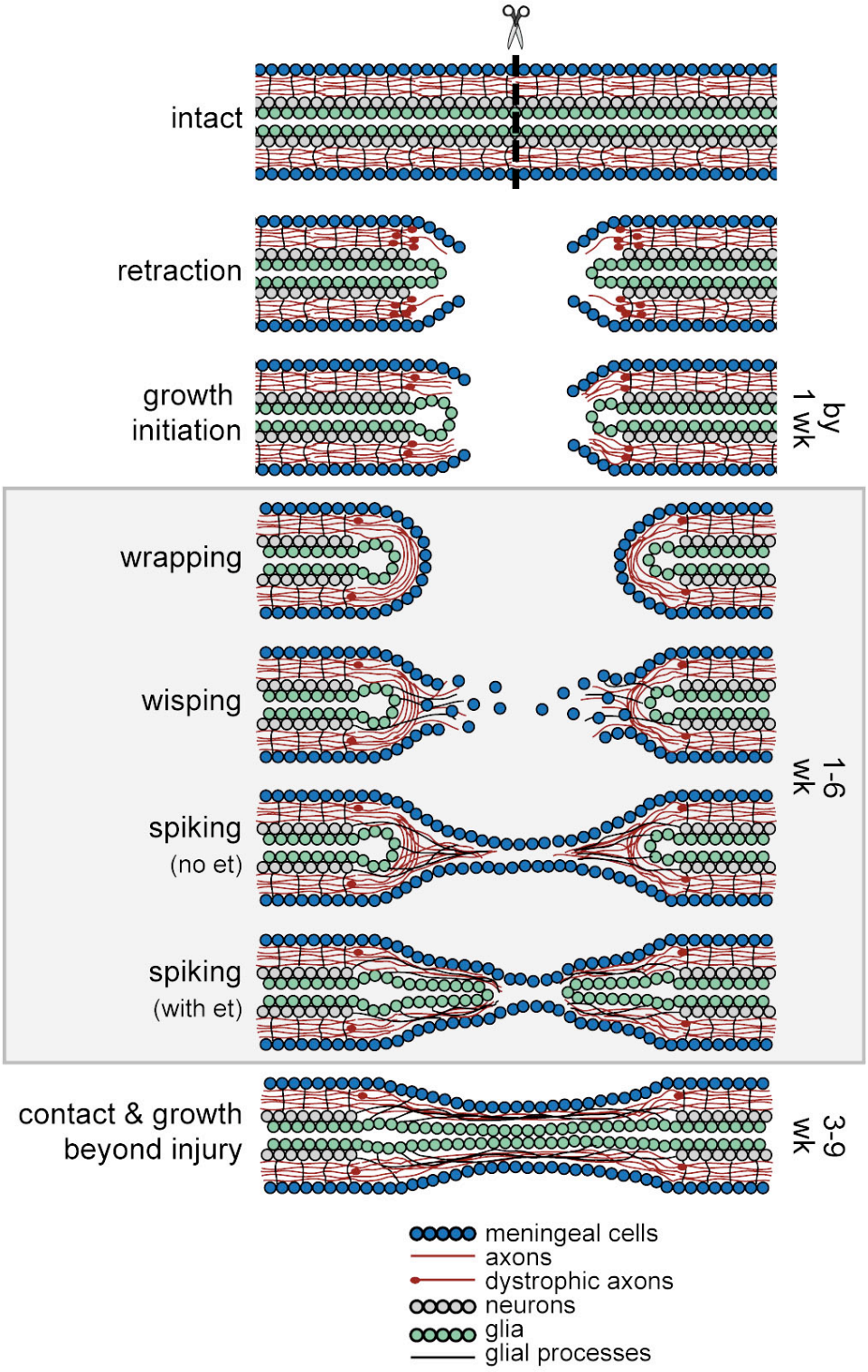
intact
retraction
growth initiation
by 1 wk
wrapping
wisping
spiking (no et)
spiking (with et)
1-6 wk
contact & growth beyond injury
3-9 wk
meningeal cells
axons
dystrophic axons
neurons
glia
glial processes

cells and the ependymal epithelium that stimulates the ependyma to proliferate and form a scaffold, which guides axons across the lesion. Since astrocytes also appear to be an important component in this interaction, we have included astrocytes with the ependymal cells and refer to them as glia. Simpson postulated that blastemal cells are the important mesenchymal cell after tail amputation, but was not specific about which cells play that role after SCI. We suggest that meningeal cells are an important mesenchymal cell after SCI and that they, too, can provide a scaffold for axon growth and guidance.

4.4.2 Glia

Our model of spinal cord regeneration after an SCI is similar to that after tail amputation in that EG play a central role. Their processes are closely associated with regenerating axons and may provide a substratum for growth cone migration and guidance via cell-cell adhesion. Our data also suggest that astrocytes may play a similar role. These astrocytes may be immediate descendants of EG and not the fully mature astrocytes seen in the mammalian spinal cord (Schonbach, 1969), and this may explain, in part, why they respond so differently to SCI. The arrangement of the glial processes, however, is different from the tail regeneration model, at least initially. Instead of extending radially from a pre-formed ependymal tube to form channels through which axons can grow (Singer et al., 1979), they extend longitudinally ahead of the TV and run roughly parallel to the regenerating axons. Such glial support may allow the axons to grow into the injury site in the absence of a pre-formed tube. They may also help guide the EG lining the central canal, and thus the ependymal tube, into the region of wisping axons similar to the way in which radial processes guide newborn neurons to their proper locations in the developing cortex. Soma may translocate as their processes shorten, or

they may migrate along the processes of other EG (Ghashghaei et al., 2007). Given that very few cells in the injury site express GFAP, we do not think many EG undergo an epithelial to mesenchymal transition to migrate freely into the lesion as proposed for axolotls after SCI (O'Hara et al., 1992). This does not rule out the possibility, however, that undifferentiated progeny of EG might migrate into the injury site. Alternatively, given that the mesenchymal cells in the axolotl injury site were also GFAP$^-$ and were associated with FN, such cells could be meningeal and/or endothelial cells.

4.4.3 Meningeal cells

Unlike most previous models of salamander spinal cord regeneration, our model assigns an important role to meningeal cells. Although they are thought to be detrimental to axon regeneration in the injured mammalian spinal cord, meningeal cells are able to stimulate, support, and guide developmental and regenerative processes in other contexts. Meningeal cells are fibroblast-like, and fibroblasts in flesh wounds are responsible for remodeling the ECM into either scar or normal tissue. The difference appears to depend on whether the fibroblasts are stimulated by TGFβ1 or TGFβ3 (Ferguson and O'Kane, 2004). As mentioned previously, meningeal cells harvested from the olfactory bulb, a part of the nervous system that does regenerate, and transplanted into a mammalian SCI along with OECs appear to fasciculate axons into perineurial-like structures and enhance the ability of OECs to remyelinate axons (Li et al., 1998; Lakatos et al., 2003). During development, the meninges serve as substratum for and secrete a chemoattractant, CXCL12, which regulates the migration of Cajal-Retzius cells (Borrell and Marin, 2006). In the developing forebrain, the meninges secrete retinoic acid (RA) which stimulates radial glia to begin producing neurons (Siegenthaler et al., 2009). Meningeal cells in

mammalian SCI express RA and permissive ECM proteins such as LM and FN (Shearer et al., 2003; Mey et al., 2005). RA has been shown to stimulate and possibly be an attractant for neurite outgrowth (Clagett-Dame et al., 2006; Wang and Scott, 2008). While the permissive ECM proteins expressed by meningeal cells *in vitro* tend to form a basal lamina that axons cannot cross, axons appear to grow quite well along it (Shearer et al., 2003). Thus, the basal lamina can either guide or inhibit axon regeneration depending on its orientation. In fact, following a large ablation of the spinal cord in which the meninges were left intact, axons were seen regenerating along the basal lamina of the meninges, which was oriented in a productive direction parallel to axon regrowth (Stensaas, 1983).

4.4.4 Axons

Our model does not exclude the possibility that axons and axon-intrinsic properties also play an important role in newt spinal cord regeneration. The 1 wk required for growth initiation suggests that an intrinsic growth potential is activated. This is supported by the fact that a one week conditioning lesion encouraged neurite outgrowth from newt retinal explants (Becker et al., 1999). Activation of intrinsic growth could also enable axons to overcome any inhibition CSPGs might inflict, similar to the way in which embryonic neurons adapt to CSPGs (Condic et al., 1999; Lemons et al., 2005). Furthermore, matrix metalloproteinases are upregulated during newt spinal cord regeneration (unpublished observations), and if they are expressed in growth cones, they could break down inhibitory ECM molecules and allow the axons to grow through regions that would normally be nonpermissive. Axons may also directly influence the behavior of the cells in their environment. Nerves are required for newt limb

regeneration, and they stimulate Schwann cells to produce anterior gradient protein (AG), a factor that is sufficient to rescue regeneration in de-nervated limbs (Kumar et al., 2007). Regenerating optic nerve axons in the frog appear to stimulate a breakdown of the blood brain barrier at the front of regenerating axons (Tennant and Beazley, 1992). Finally, when degenerated optic nerve fragments containing hypertrophic astrocytes are implanted into an optic nerve injury site in frogs, axons grow into the grafted tissue and appear to stimulate the reactive astrocytes to adopt a more permissive architecture: the astrocytes extend radial processes and form compartments for axon elongation (Reier et al., 1983). Thus, newt axons may play a role in stimulating appropriate glial and meningeal cell responses.

4.4.5 Summary

If meningeal cells and glia support the development and regeneration of the nervous system in some contexts, why do they not do so in all contexts? Although no definitive answer can be put forward, we suspect that the state of differentiation of the cells may play a key role. In the newt spinal cord, EG maintain characteristics of radial glia of the developing cortex (Ferretti et al., 2003), astrocytes may be recent progeny of EG (Schonbach, 1969), and many differentiated cells have the ability to dedifferentiate and become more progenitor-like (Odelberg, 2005). Learning more about how newt cell types are intrinsically different and what factors stimulate their behavior will undoubtedly give us new insights into how to improve spinal cord regeneration in mammals. Identifying effective treatments for spinal cord injury in mammals has been so intractable that it is imperative we take full advantage of the opportunity to learn how nature has already solved this problem in newts.

4.5 Methods

4.5.1 Animals

Adult newts, *Notophthalmus viridescens*, were purchased from Charles D. Sullivan Co. Inc., (Nashville, TN), housed at 22°C in glass aquariums equipped with water filters, and fed live blackworms, *Lumbriculus varietgatus* (Eastern Aquatics, PA). All animal protocols were approved by the University of Utah Institutional Animal Care and Use Committee.

4.5.2 Spinal cord injury

Newts were anesthetized by submersion in 0.1% Tricaine (Ethyl 3-aminobenzoate methanesulfonate salt, Sigma, A5040) in 20 mM Tris-HCl, pH 7.5 for 10 min and placed in ice for 30 min prior to surgery. Complete transection injuries were performed similar to those described in Davis et al (1989; 1990). After swabbing the skin with 10% Providone Iodine, a deep incision was made between vertebral bones about 1 cm rostral to the hindlimbs. Using forceps, the vertebrae were gently and slightly separated and the dorsal lamina of the caudal vertebra was removed to expose the spinal cord. The spinal cord was cut completely with fine spring scissors. Blood was irrigated with sterile 85% phosphate buffered saline (PBS) when necessary. Animals were kept moist during the procedure, placed on ice for 15 min after the surgery, and allowed to recover in bins that were tilted to produce a shallow area of water. Bins were cleaned and filled with fresh de-chlorinated water every day or every other day throughout the recovery period.

4.5.3 Axon tracer application

Our procedure was modified from that used in zebrafish (Becker et al., 1997; Becker and Becker, 2001). Three axon tracers were tried: BDA (3kD, lysine fixable, Invitrogen, D7135), RDA (3kD, lysine fixable, Invitrogen, D3308), and biocytin (Pierce, 28022). RDA appeared to work as well as BDA, but was only used when two tracers were needed in the same animal. Biocytin, which was reported to reveal thin processes better than a 10 kD RDA (Becker et al., 1997), unfortunately did not produce a signal in our preparations, perhaps because of the decalcification step in tissue processing (see below). BDA and RDA were prepared similarly: small pieces of gel foam (Pharmacia & Upjohn Co., MI) were soaked in 1.5 μl of a 10% solution and allowed to air dry 40 min in a tissue culture hood to further concentrate the solution. Fast green dye (Fisher, F-99) was added to the BDA solution at 0.05 mg/ml to make it visible *in vivo*. Biocytin did not readily go into solution at 10%, but a slurry was made. Small pieces of gel foam were soaked in 10 μl of the slurry, air dried completely, and stored at -20°C. To apply tracer to the spinal cord, the cord was transected one vertebral segment (about 2 mm) rostral or caudal to the original injury site using the same procedure described above and a piece of gel foam saturated with tracer was inserted into the gap. To apply tracer to the sciatic nerve, an incision was made along the course of the sciatic blood vessel on the posterior aspect of the hindlimb where the hindlimb joins with the body. Fine forceps were used to tease the nerve from the vessel, and the nerve was transected with fine spring scissors. A piece of gel foam saturated with tracer was applied and the wound was sealed closed with Vetbond tissue adhesive (3M). Excessive bleeding was controlled before tracer application, if necessary, by inserting a piece of gel foam into the wound and allowing

the animal to sit on ice for several minutes. Use of this technique was minimized, however, because it decreased the efficiency of tracer uptake.

4.5.4 Tissue harvest, fixation, and decalcification

Animals were anesthetized as above, placed on ice for at least 15 min, then perfused with about 1.5 ml 85% PBS followed by 3 ml periodate-lysine-paraformaldehyde (PFA) fixative (PLP: 75 mM lysine, 10 mM sodium periodate, 0.5% PFA in 85% PBS, pH 7.4; 0.1 M lysine and 2% PFA stocks were stored at -20°C and ingredients were mixed and used within 2 hours) (McLean and Nakane, 1974). All incubations were performed rocking at room temperature (RT) and rinses were for 20-30 min, three times, unless otherwise specified. The spinal column was harvested in about 4 mm long segments, post-fixed in PLP for 2 hours, rinsed with PBS (137 mM NaCl, 2.7 mM KCl, 8.1 mM Na_2HPO_4, 1.15 mM KH_2PO_4, pH 7.4), rinsed in fresh PBS overnight at 4°C, decalcified with Morse's solution (22.5% formic acid, 10% sodium citrate) for 24 hours, and rinsed with PBS. Some of the spinal cords prepared for paraffin sections were not perfusion fixed and this did not seem to affect the results, though perfusion did make tissue prepared for thick and frozen sections easier to section. An alternative fixative, 4% PFA, was tried, but the quality of sections was not improved, there was more autofluorescence, and some antibodies did not work as well.

4.5.5 Thick sections and fluorescent labeling (spinal cord whole-mounts)

Methods were adapted from previous studies (Klymkowsky and Hanken, 1991; Kardon, 1998) and described in Zukor et al. (2010). All incubations were performed

rocking at RT unless otherwise specified. Decalcified tissue was bleached with formamide bleach (6% hydrogen peroxide, 3% formamide, 0.1% Triton X-100 in PBS) for about 2 hours; rinsed with PBS for 20-30 min, three times; and embedded in 4% agarose. Longitudinal sections containing the whole spinal cord (about 350 μm thick) were cut on a vibratome and collected in ice cold PBS. Sections were transferred to 0.67 ml centrifuge tubes, permeabilized with PBS-TxD (PBS containing 0.5-2% Triton X-100 and 20% DMSO; 0.5% Triton X-100 was sufficient for streptavidin, 2% was necessary for antibodies) overnight and incubated in streptavidin or primary antibody diluted in PBS-TxDB (PBS-TxD containing 1% BSA (EMD, 2960) and 0.1% fish skin gelatin (Sigma, G7765) as blocking reagents) for 7 days for streptavidin or 10 days for antibody penetration. Sections needing incubation with secondary antibodies were rinsed with PBS-Tx (PBS with 2% Triton X-100) for 30 min, five times and incubated in secondary antibody diluted in PBS-TxDB for 10 days. Sections were then rinsed in PBS for 30 min, four times; rinsed in TNT (100 mM Tris-HCl, pH 7.5, 150 mM NaCl, 0.05% Tween-20) for 30 min; incubated in SYTOX green (Invitrogen, S7020) diluted 1/1000 in DMSO, then 1/25 in TNT for 3 hours to stain nuclei; and rinsed in TN (TNT without Tween-20) for 10 min, three times. Sections were transferred to glass vials, dehydrated through a methanol (MeOH)/TN series (20%, 50%, 75%, 100% MeOH; 15 min each); and cleared in BABB (1 part benzyl alcohol, 2 parts benzyl benzoate) overnight at 4°C (not rocking).

4.5.6 Frozen sections

Frozen sections of the injured spinal cord were difficult to obtain presumably because it contains more water than the intact cord and because the spinal column

contains tissues of heterogeneous density: the muscle and bone are rigid and dense, while the spinal cord is quite soft. Therefore, methods were adapted from Tokuyasu (1989). Perfusion-fixed, decalcified tissue was cryoprotected to 2.3 M sucrose in PBS (3 hours in 25%, 3 hours in 50%, overnight in 75%, 24 hours in 100% 2.3 M sucrose; rocking and at RT) and frozen quickly in OCT (Ted Pella, 27050) with liquid nitrogen to minimize freezing artifacts. Sections 16 – 20 μm thick were obtained on a cryostat with the chamber temperature set to -35°C and the object temperature set to -34°C. For intact spinal cord, variables could be somewhat relaxed. Tissue could be cryoprotected to 1.6 M sucrose and perfusion was not critical. Sections were stored at -20°C and, prior to fluorescent labeling, thawed, baked onto the slides for 1 hour at 50°C, and rinsed in PBS for 5 min.

4.5.7 Paraffin sections

All incubations were performed with rocking at RT. Decalcified tissue was dehydrated with ethanol (EtOH, 50% for 30 min, 70% for 30 min, 95% for 30 min, 100% for 30 min, 100% for 1 hour), infiltrated (75% Hemo-De in EtOH for 20 min, 100% Hemo-De for 1 hour, paraffin for 1 hour at 60°C and 15 Hg vacuum), and embedded in paraffin. Sections 10 – 20 μm thick were mounted onto slides, left on a 37°C slide warmer overnight, and stored at 4°C. Prior to fluorescent labeling or staining, sections were dewaxed (Hemo-De for 10 min, two times; 75% Hemo-De in EtOH for 5 min; 100% EtOH briefly and then for 3 min) and rehydrated (95% EtOH for 3 min, 70% EtOH for 3 min, PBS or water for 5 min; PBS was used for fluorescent labeling and water was used for staining).

4.5.8 H&E staining

Paraffin sections rehydrated in water were stained: hematoxylin (Harris modified, with acetic acid, Fisher SH26-500D) 4 min, running tap water 5 min, 70% EtOH briefly, acidified 70% EtOH (10 drops of concentrated HCl to 200 ml 70% EtOH) 1.5 min, bluing solution (10 drops of NH_4OH in 200 ml EtOH) 1 min, Scott's solution (1 g sodium bicarbonate, 10 g magnesium sulfate in 500 ml water) 3 min, running tap water 5 min, 70% EtOH briefly, 0.1% Eosin in 95% EtOH (made from 0.5% Eosin Y Solution, Sigma HT110-1-32) 1 min, 95% EtOH briefly, 100% EtOH 5 min, 75% Hemo-De in EtOH 5 min, 100% Hemo-De 5 min. Coverslips were mounted with Cytoseal 60 (Fisher, 23-244-256).

4.5.9 Fluorescent labeling in paraffin or frozen sections

Sections were blocked in PBS-TxB (PBS with 0.2% Triton X-100, 1% BSA and 0.1% fish skin gelatin) for 1 hour; incubated with primary antibody diluted in PBS-Tx (PBS with 0.2% Triton X-100) overnight at RT; rinsed with PBS for 10 min, three times; incubated with secondary antibody or streptavidin diluted in PBS-Tx for 4 hours; rinsed with PBS for 10 min, two times; rinsed with TNT or TN for 10 min; incubated with SYTOX green (Invitrogen, S7020) diluted 1/1000 in DMSO, then 1/50 in TNT or Hoechst 33342 (Invitrogen, A10027) diluted 1/2000 in TNT for 30 min to stain nuclei; rinsed in TN for 10 min, 50% TN for 10 min, and water for 10 min. Coverslips were mounted with Fluoromount G (Fisher, OB100-01) and sealed with clear nail polish. For some experiments on paraffin sections, incubation with primary antibody was extended to 2 or 3 days at RT. This improved signal without adding noise. Sections treated with

chondroitinase ABC (chABC) were treated before the blocking step. They were equilibrated in tris acetate buffer (50 mM Tris-HCl, pH 8.5, 60 mM Sodium Acetate, 0.02% BSA, 0.5% Triton X-100; made fresh, pH 8.0) for 5 min, treated with chABC solution (7.5 U/ml chABC stock diluted 1:50 in tris acetate buffer; stock was chABC, Sigma C2905, EC 4.2.2.4, reconstituted in 0.01% BSA) for 1 hour at 37°C, and rinsed with PBS for 5 min, three times.

4.5.10 Antibodies and Streptavidins

Primary antibodies and dilutions used are listed in Table 4.2. Additional primary antibodies that were tried are listed in Table S4.2. Secondary antibodies (Invitrogen, whole antibodies, 2 mg/ml, conjugated to Alexa 488, 568, 594, or 633) were diluted 1/100. Streptavidin-Cy5 (Invitrogen, SA1011) and Streptavidin-Alexa 633 (Invitrogen, S21375) were diluted to 4 μg/ml. The FN and Col XII antibodies and one TN-C antibody are newt-specific and have been characterized (Onda et al., 1990; Nace and Tassava, 1995; Wei et al., 1995). The non-newt-specific antibodies appear to be specific in that they produced appropriate expression patterns and are specific in western blots (not shown, not done for vWF and CSPG antibodies). The specificity of the CSPG antibody was verified by treating adjacent sections with chABC and incubating them with the CSPG antibody. The specificity of the secondary antibodies was verified by treating adjacent sections with secondary antibodies in the absence of primary antibodies. Very little non-specific signal was seen in either case (see Figure 4.4W, X), and what little was seen tended to appear in the white matter. The chick-specific TN-C antibody produced an expression pattern similar to the newt-specific antibody, but its signal was much stronger

Table 4.2. Table of antibodies

Antigen	Antibody Type	Company, Cat #	Dilution, Format
CSPGs (chick)	mouse IgM mAb	Sigma, C8035 (CS-56)	1/100, ascites
Tenascin-C (chick)	rabbit pAb	Chemicon, AB19013	1/100, concentrate
Tenascin-C (newt)	mouse IgM mAb	DSHB, MT1	1/25, concentrate
Fibronectin (newt)	mouse IgG mAb	DSHB, MT4	1/50, concentrate
Collagen XII (newt)	mouse IgG1 mAb	DSHB, MT2	1/50, concentrate
Laminin (mouse)	rabbit pAb	Sigma, L9393	1/25, concentrate
Fibrin (human)	mouse IgG1 mAb	ADI, 350	1/50, concentrate
Neurofilament associated protein (chick)	mouse IgG1 mAb	DSHB, 3A10	1/50, supernatant
GFAP (cow)	rabbit pAb	Dako, Z0334	1/200, concentrate
von Willebrand Factor (human)	rabbit pAb	Dako, A0082	1/400, concentrate

and so it was used instead. The antibody against Col XII was used to approximate the expression of Col I since it is found in association with Col I and may enhance the stability of the ECM by bridging collagen fibrils (Reichenberger et al., 2000; Bader et al., 2009). Since paraffin processing may affect CS-56 labeling, CSPGs were analyzed in frozen sections. TN-C, FN, LM, and Col were analyzed in paraffin and frozen sections. Expression patterns were also verified in whole-mount preparations (not shown).

4.5.11Confocal imaging and image processing

Sections labeled with fluorescent dyes were imaged on an Olympus FV300 or FV1000 laser scanning confocal microscope using a 10X or 20X air objective. Images were processed with ImageJ, version 1.40g (W. Rasband; http://rsb.info.nih.gov/ij; NIH, Bethesda, MD) and Adobe Photoshop CS2. Levels were adjusted in Photoshop to maximize the signal to noise ratio but the same adjustments were made to experimental and control images.

4.5.12 Preparation of tissue for EM

Methods were adapted from Anderson et al (2009). Animals were anesthetized as above, then perfused with about 1.5 ml 85% PBS followed by 3 ml EM fixative (2.5% glutaraldehyde, 1% formaldehyde, 3% sucrose, 1 mM $MgSO_4$ in 0.1 M cacodylate buffer (CB), pH 7.4). The spinal column was harvested in about 4 mm long segments; post-fixed in EM fixative overnight at RT; decalcified in cold EDTA solution (0.1 M EDTA, pH 7.2-7.4 with 4% glutaraldehyde) for 4 days at 4°C; rinsed in 0.1 M CB for 20 min, 3 times; rinsed in PBS briefly; and embedded in 4% agarose. Longitudinal sections containing the whole spinal cord (about 350 μm thick) were cut on a vibratome and

collected in ice cold PBS. Sections were returned to 0.1 M CB; osmicated (1% OsO_4 in 0.1 M CB) for 1 hour; rinsed in 0.1 M CB for 10 min, 3 times; partially dehydrated (50%, 75% MeOH; 10 min each); treated with 1% uranyl acetate in 75% MeOH for 1 hour; fully dehydrated (75%, 85%, 95%, 100%, 100% MeOH; 10 min each); infiltrated with resin (100% acetone 10 min, 2 times; 75% resin in acetone overnight; 100% resin 1 hour); embedded in epoxy resin [2 parts dodecenyl succinic anhydride (DDSA, Ted Pella, 18022), 1 part eponate 12 resin (Ted Pella, 18005), 0.06 parts DMP30 accelerator (Ted Pella, 18042)] and cured at 60°C for 2 days. Sections were re-embedded for longitudinal sectioning, and 80 nm sections were collected onto carbon-coated Formvar films in gold, single-hole grids, stained with 5% uranyl acetate for 1 hour and 1% lead citrate for 25 min, and imaged at 80 KeV in a JEOL JEM 1400 electron microscope at 5,000X magnification. Images were captured digitally on a GATAN Ultrascan 4000 16 megapixel 16-bit camera and mosaicked with *ir-tools* (Anderson et al., 2009). Mosaics were viewed and selections were captured with Viking software.

4.6 Supplemental Figures

Figure S4.1. The largest spinal nerves are associated with the S1 and T-1 vertebrae. **(A)** Close-up view of S1, dorsal aspect. The rib associated with this vertebra articulates with the ilium of the pelvis to form the SI joint. **(B)** Ventral side of spinal column showing vertebrae T-4 to S2/C1. The largest spinal nerves (arrowheads) are associated with T-1 and S1. T-2 is intermediate in size. T-4, T-3 and S2/C1 are small. Dotted circles, approximate location of the spinal ganglia; dotted lines, approximate course spinal nerves take to spinal ganglia. Note that the actual location of the SCI in this animal is 1 segment rostral (between T-5 and T-4) to the targeted site (between T-4 and T-3). **(C)** Close-up of T-1 and S1 shown in (B). More flesh has been removed to demonstrate that the vertebra associated with the caudal-most large spinal nerve is indeed S1. The rib associated with it articulated with the pelvis. R, rostral; C, caudal.

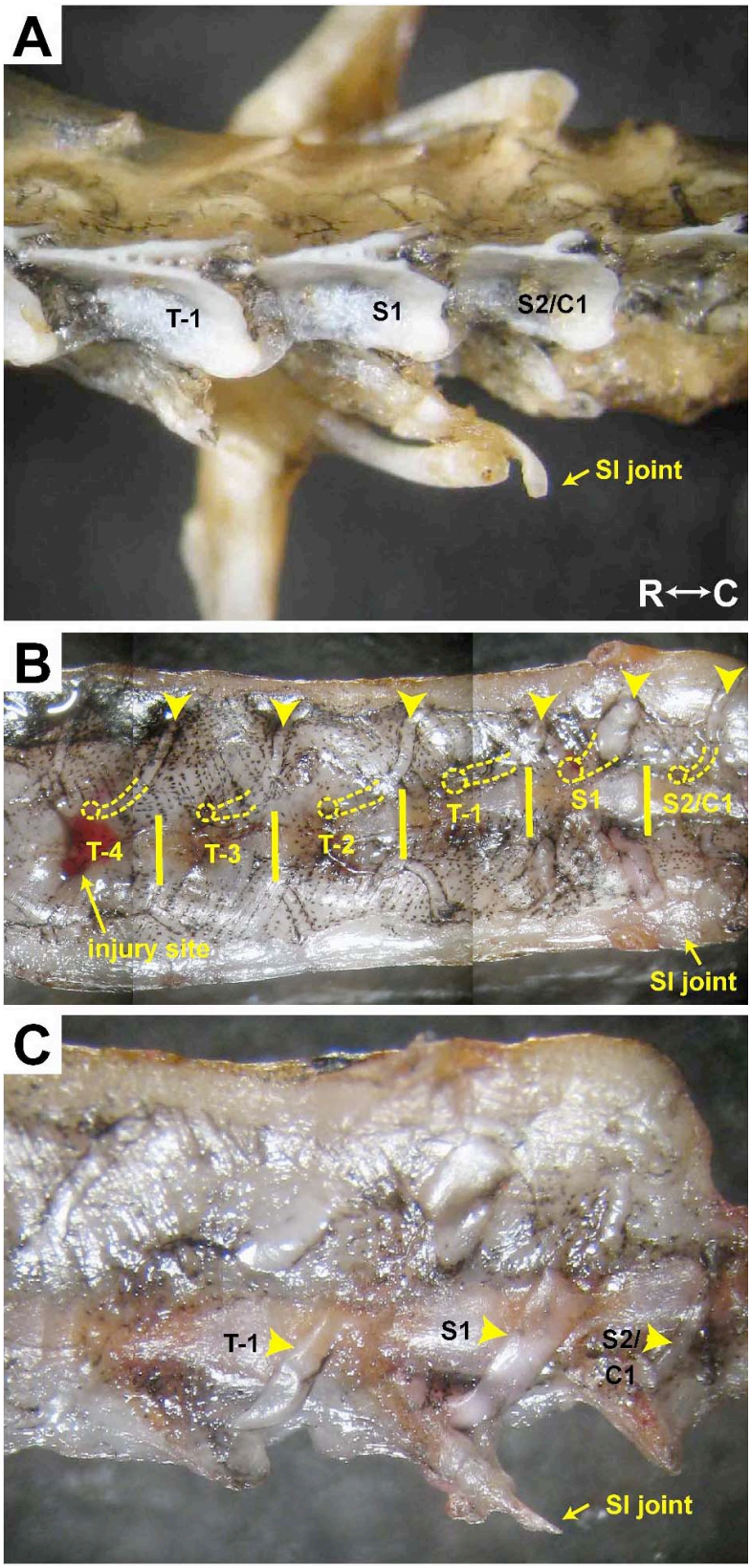
A
T-1
S1
S2/C1
SI joint
R↔C
B
T-4
T-3
T-2
T-1
S1
S2/C1
injury site
SI joint
C
T-1
S1
S2/
C1
SI joint

Figure S4.2. Retraction and growth initiation stage images seen in z-projections. The difference between the retraction and growth initiation stages is apparent throughout the whole spinal cord and is not just a function of which z-plane was chosen for presentation. **(A-D)** Images of retraction (A, B) and growth initiation (C, D) shown in Figure 4.2. All are single confocal planes, except (B), which is a z-projection of 4 planes. **(A'-D')** Z-projections of all planes through the spinal cord, showing just the axon tracer channel, for the same animals in (A-D). In the retraction stage, fewer axons extend to the end of the cut cord (arrowheads). R, rostral; C, caudal. Scale bars: 200 μm (A-D, same scale; A'-D', same scale).

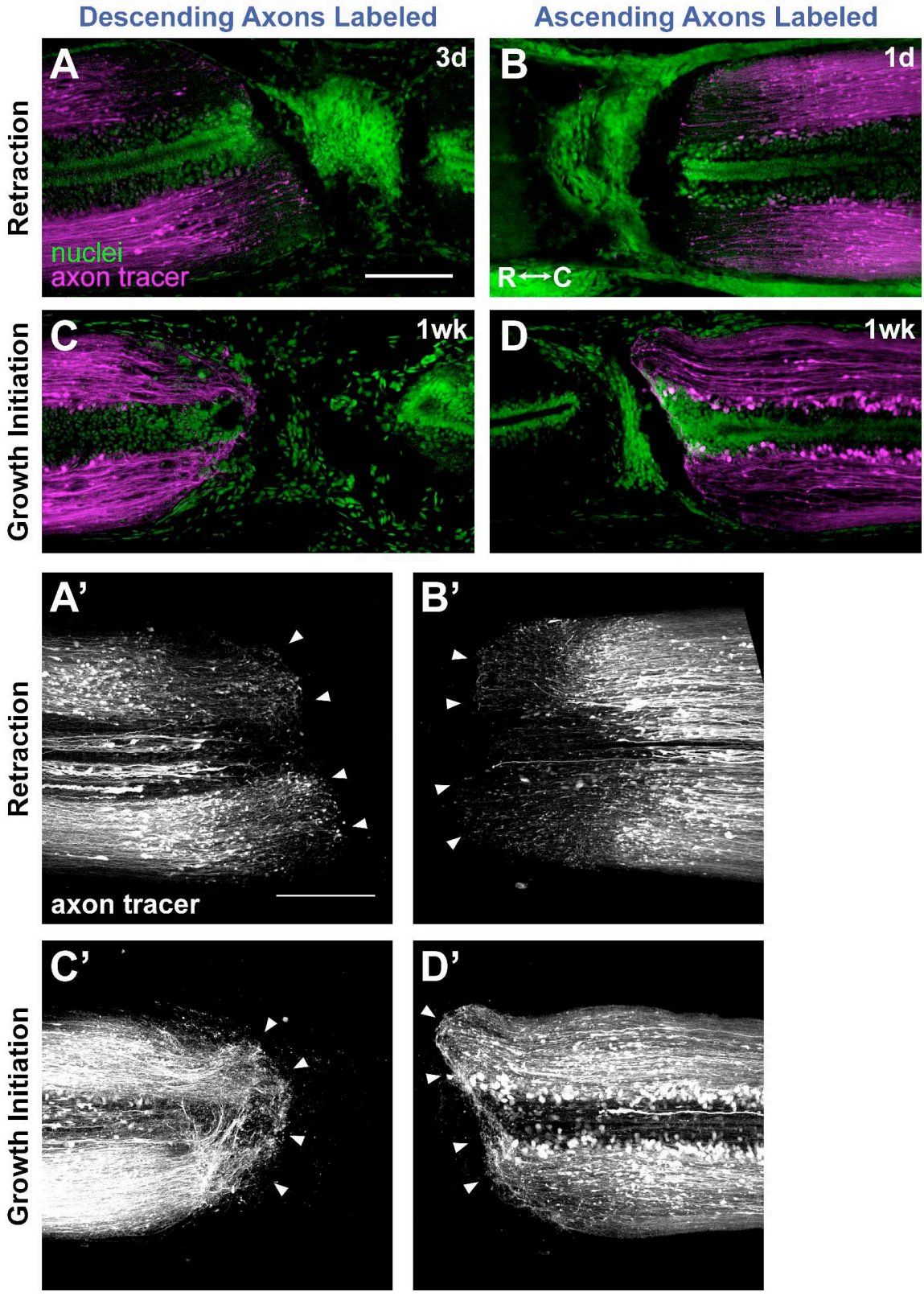
Descending Axons Labeled
Ascending Axons Labeled
Retraction
Growth Initiation
A
3d
nuclei
axon tracer
B
1d
R↔C
C
1wk
D
1wk
A'
axon tracer
B'
C'
D'

Figure S4.3. Size of gap in spinal cord at each stage. Gap size increases before it decreases and is largest during the wrapping stage. *dark lines*, median; *box*, interquartile range (IQR, 25% - 75%); whiskers, most extreme data point that is no more than 1.5 IQT from the box; small circle, outlier. The size of the gap during the wrapping stage is statistically different (asterisk) from that during the retraction stage, with $p < 0.001$ (using Bonferroni correction for multiple t-tests).

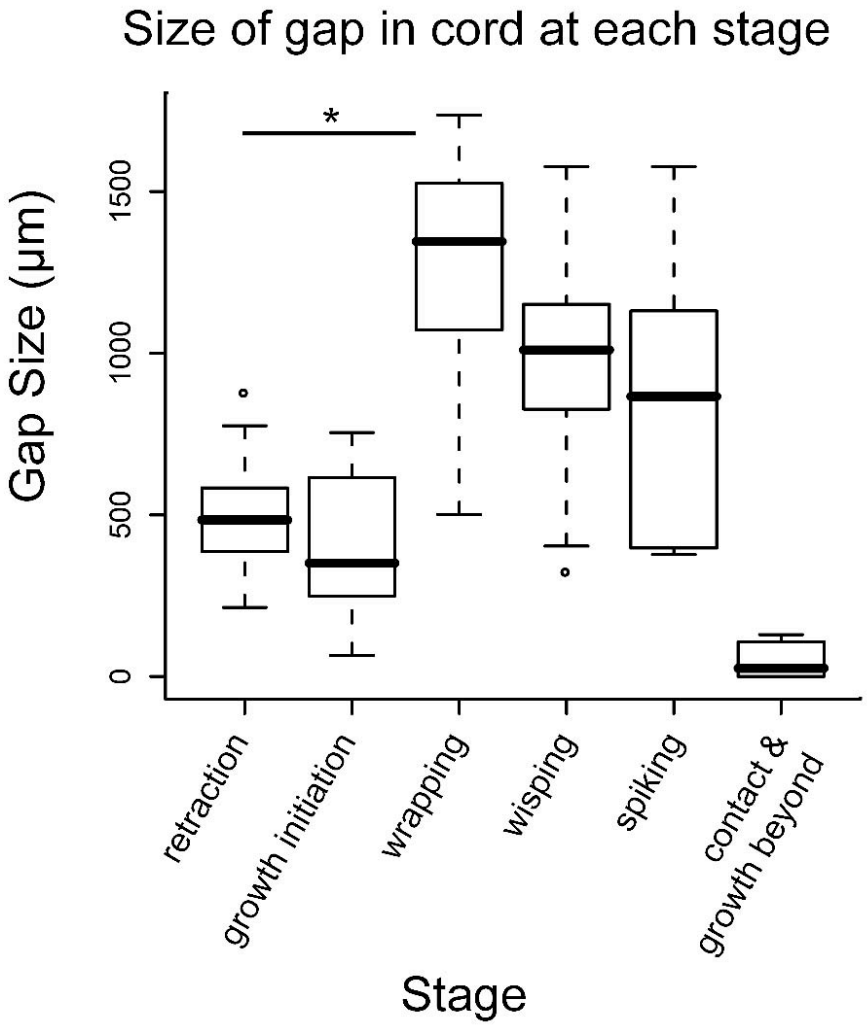
Size of gap in cord at each stage
Gap Size (µm)
0
500
1000
1500
*
retraction
growth initiation
wrapping
wisping
spiking
contact &
growth beyond
Stage

Figure S4.4. Sloppiness and misalignments in axon regeneration. Axon regeneration has some tolerance for sloppiness, but gross misalignments may result in a delay or failure to recover. All images are montages of single confocal planes of longitudinal thick sections, except (F) which is a cross section. Axons in all images were labeled with the axon tracer (magenta), and nuclei are green. **(A, A', A")** A 9 wk regenerate in the growth beyond stage that had recovered swimming function. Gross misalignments are not present. The ependymal tubes have connected to re-establish a continuous central canal (A), yet axon regeneration appears to be a little sloppy in that some axons appear to decussate (arrowhead in A') and wrapping axons are still evident (open arrowhead in A"); however, this has not interfered with functional recovery. **(B)** A 4 wk regenerate in the growth beyond stage that had not recovered function. Similar to (A), axons appear to wrap (open arrowhead) and decussate (arrowhead). This animal may not have recovered yet because it was sacrificed at such an early time point. **(C)** A 9 wk regenerate in the growth beyond stage that had not recovered function. A long spike appears to have elongated from the caudal side (dotted lines), and this may indicate that the gap in the cord was large. Recovery, therefore, may be delayed. **(D)** A 6 wk regenerate in the spiking stage that had not recovered function. The whole spike appears to be veering off in the wrong direction and does not line up properly with the cord on the other side (dotted lines). This gross misalignment may have prevented this animal from ever recovering function. Note that the whole spike, made up of meningeal cells, axons, and EG, is moving as unit in the wrong direction. Arrow, dorsal root to the spinal ganglia. **(E)** A 9 wk regenerate in the growth beyond stage that had not recovered function. Two ependymal tubes (fat arrows) appear to have formed on the rostral side. The more prominent one is misaligned, and the less prominent one is properly aligned. Thus, the less prominent one may be forming to correct the misalignment. Recovery may be delayed as a result. **(F)** Cross section through a 9 wk regenerate in the growth beyond stage that had not recovered function. Axon regeneration appears to be sloppy in that axons are wisping dorsally towards the tissue wound that was created to gain access to the spinal cord. Recovery may be delayed as a result. R, rostral; C, caudal; D, dorsal; V, ventral. Scale bars: 500 μm (A-E, same scale); 200 μm (F).

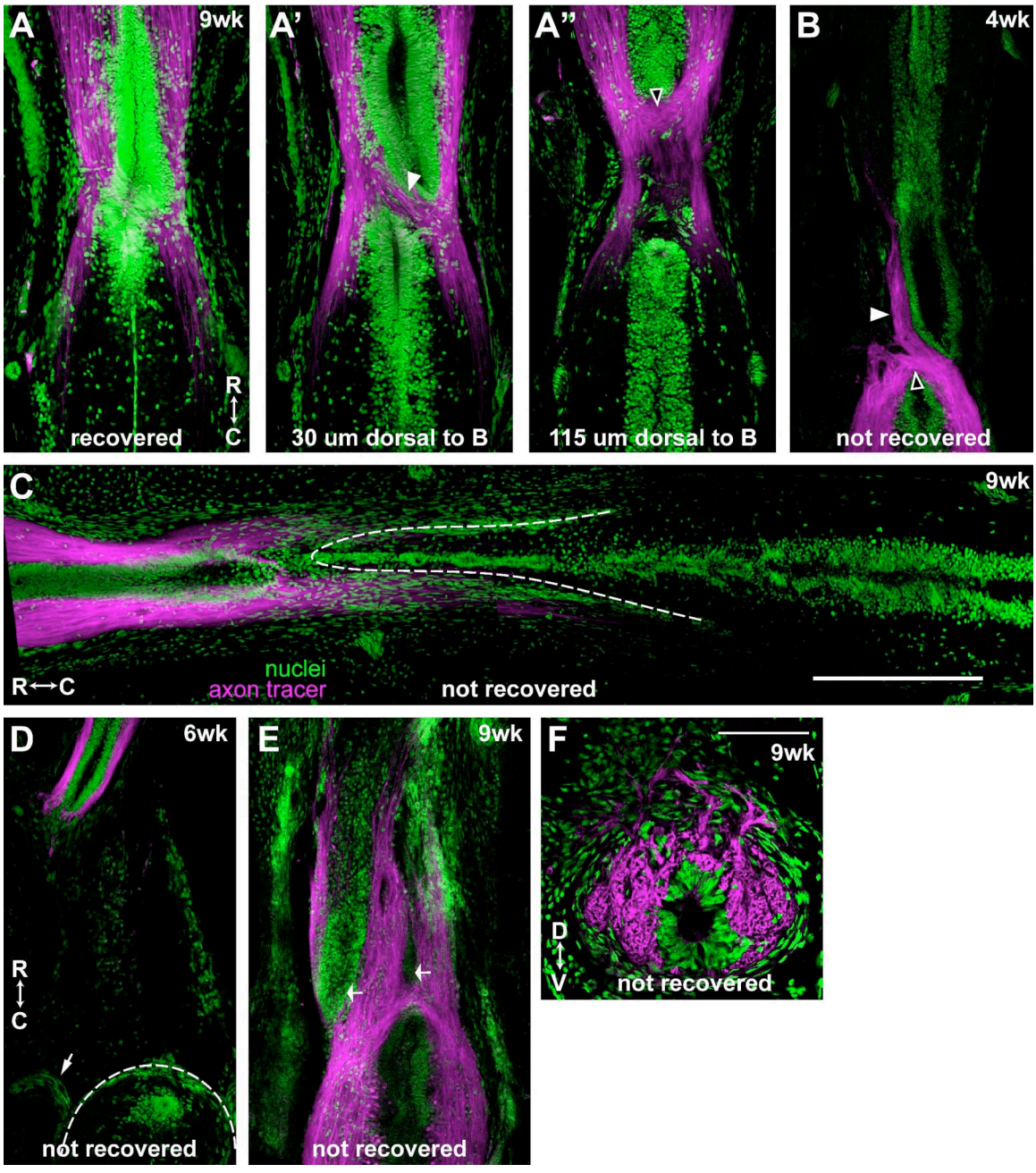
A
9wk
R
C
recovered
A'
30 um dorsal to B
A''
115 um dorsal to B
B
4wk
not recovered
C
9wk
R↔C
nuclei
axon tracer
not recovered
D
6wk
R
C
not recovered
E
9wk
not recovered
F
9wk
D
V
not recovered

Figure S4.5. A glia limitans-like structure may be present during the wrapping stage. Longitudinal sections through wrapping stage regenerates. Axons were labeled with the axon tracer in (C) and (D) and are shown in magenta. Each ECM protein is shown in green, and nuclei are blue. Col XII **(A)**, FN **(B)**, and TN-C **(C)** expression wraps around the end of the cord, while LM **(D)** expression does not. R, rostral; C, caudal. Scale bar: 200 μm (A-D).

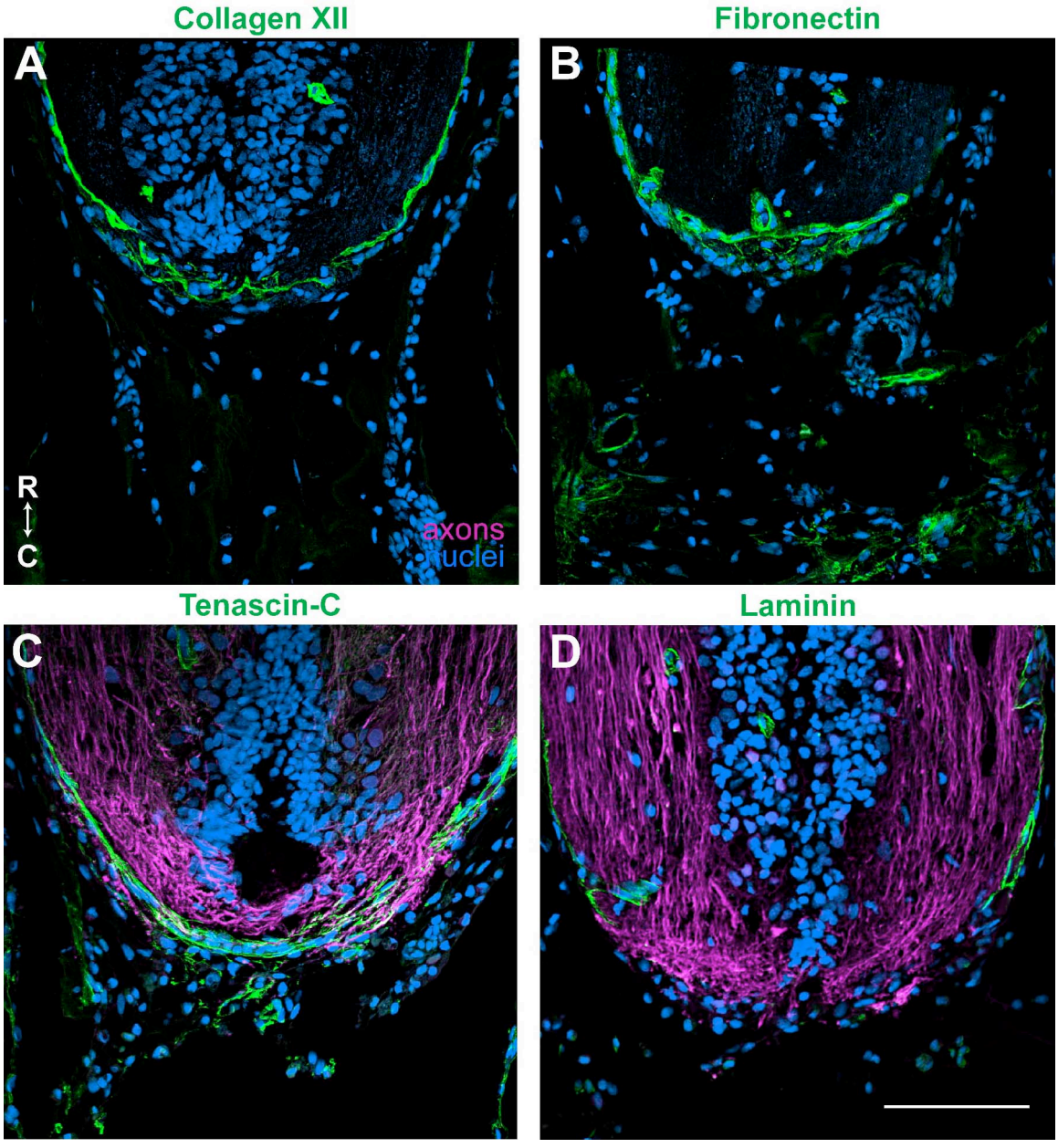
Collagen XII
Fibronectin
A
B
R
C
axons
nuclei
Tenascin-C
Laminin
C
D

Figure S4.6. Meninges of the intact spinal cord. Longitudinal section through the intact spinal cord imaged with EM. **(A)** Region containing the meninges. p, pia mater; a, arachnoid mater; d, dura mater; sas, subarachnoid space; ecm, ECM; ef, glial end feet; o, oligodendrocyte. **(B)** Enlargement of box B in (A) showing skinny, dark processes of dura mater cells (arrows) associated with collagen fibrils (c) of the dura mater. **(C)** Enlargement of box C in (A) showing layers of arachnoid cell processes (a), a skinny process from a dura mater cell (arrow), and collagen (c). **(D)** Enlargement of box D in (A) showing a pia mater cell. **(E)** Enlargement of box E in (A) showing neural collagen (nc). **(F)** Enlargement of box F in (A) showing the basement membrane (arrowhead) at the glia limitans of the spinal cord, collagen (c) and neural collagen (nc). R, rostral; C, caudal. Scale bars: 15 μm (A), 3 μm (D), 1.5 μm (B, C, E, F).

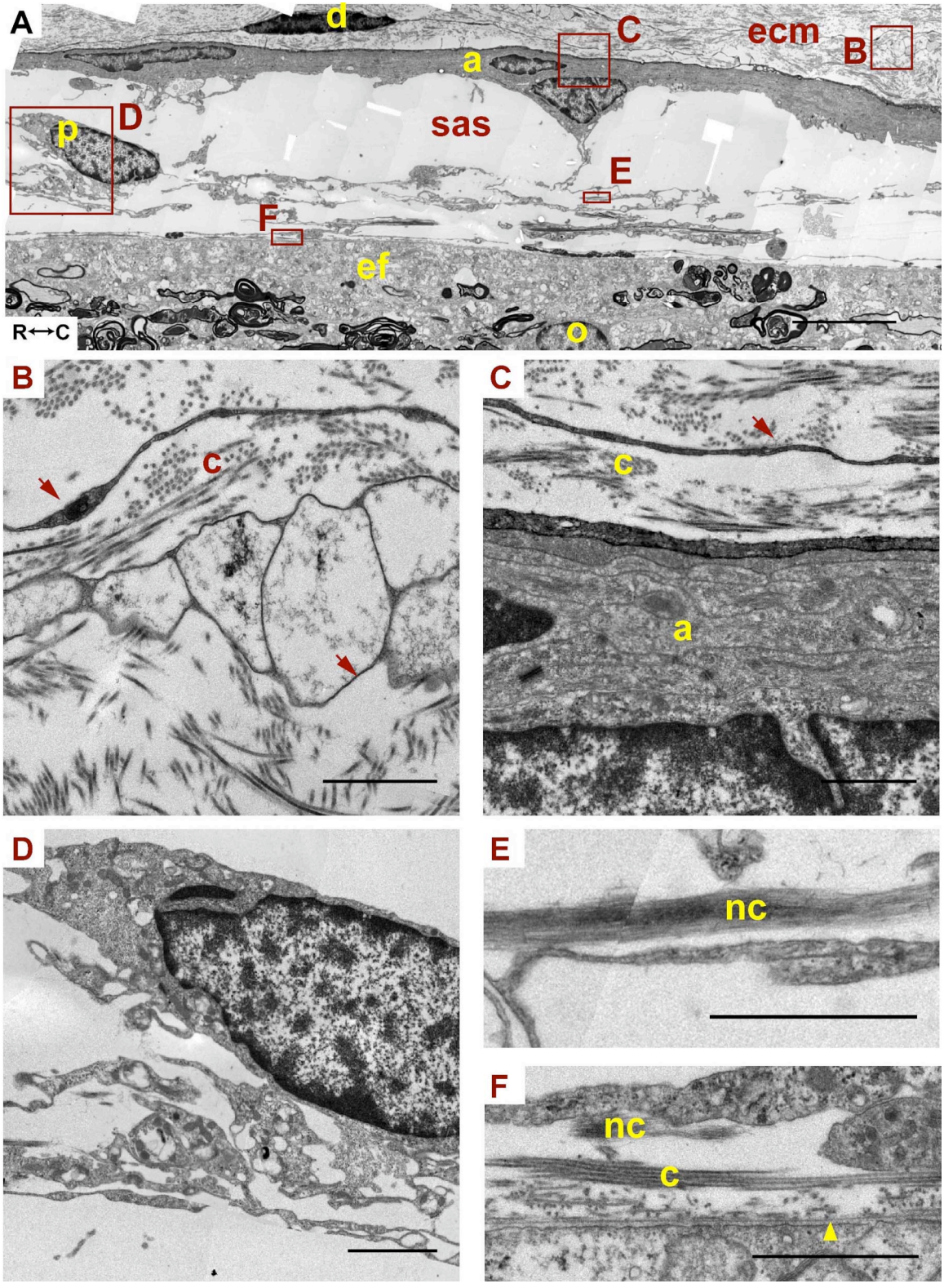
A
d
C
ecm
B
a
D
p
sas
E
F
ef
R↔C
o
B
c
C
c
a
D
E
nc
F
nc
c

Figure S4.7. Other cell types in the intact spinal cord. Longitudinal section through the intact spinal cord imaged with EM. **(A)** Region containing the central canal (cc), EG layer (EG) and a portion of the grey mater (gm). **(B)** Enlargement of box B in (A) showing astrocytes. **(C)** Enlargement of box C in (A) showing the cytoplasm of light EG. **(D)** Enlargement of box D in (A) showing the cytoplasm of dark EG. **(E)** A microglial cell. **(F)** An oligodendrocyte. R, rostral; C, caudal. Scale bars: 15 μm (A, B, F), 5 μm (E), 3 μm (D), 1.5 μm (C).

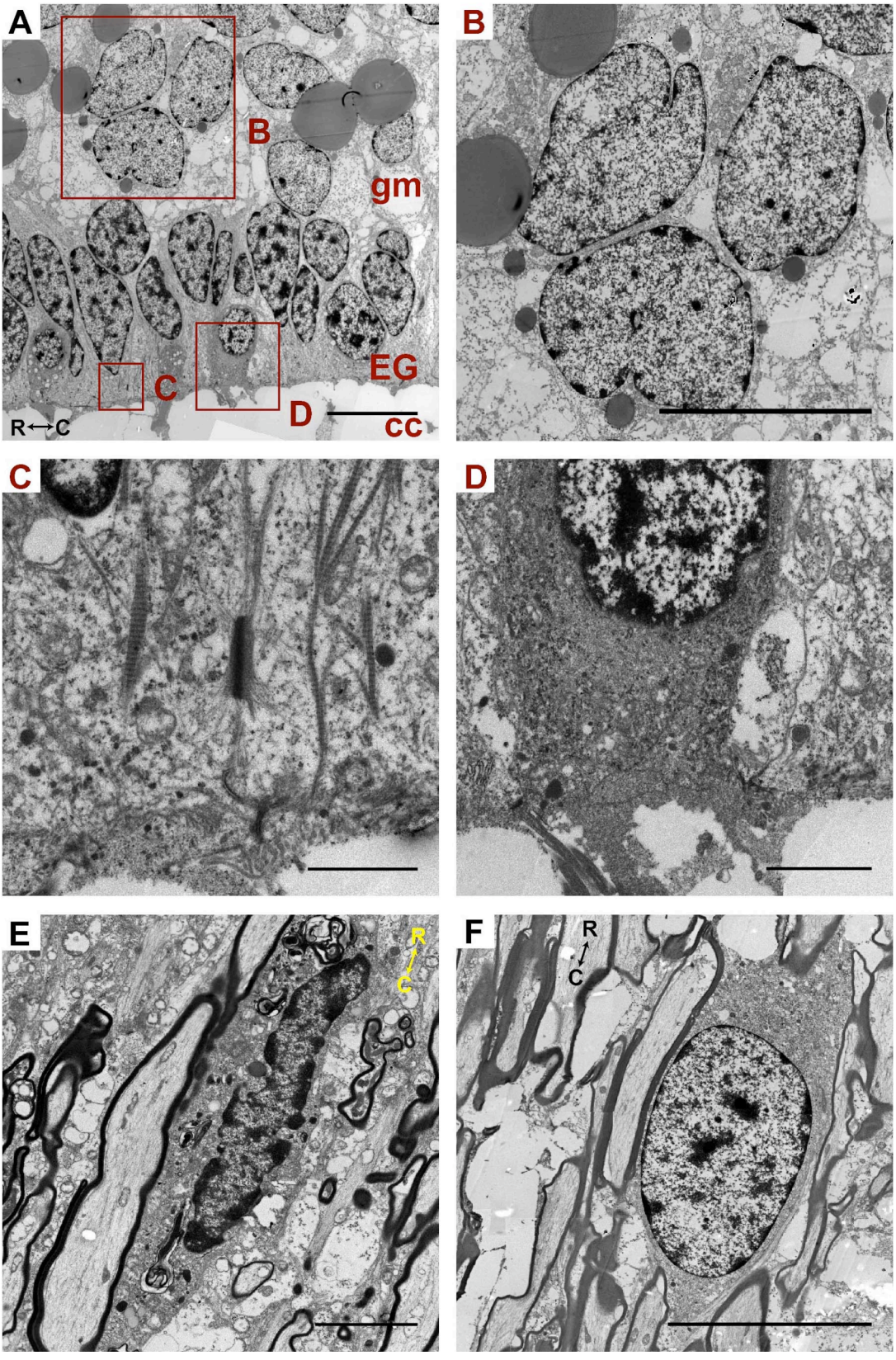
A
B
gm
C
EG
D
cc
R↔C
B
C
D
E
R
C
F
R
C

Figure S4.8. Glia of the regenerating spinal cord. (**A-D**) Longitudinal section through a wisping stage regenerate imaged with EM. **(A)** Region containing axons wisping ahead of the TV (TV). **(B)** Enlargement of box B in (A) showing a light glial process (EG_L) that is associated with regenerating axons (ax). **(C)** Enlargement of box C in (A) showing light (EG_L) and dark (EG_D) EG lining the TV (TV). **(D)** Enlargement of box D in (A) showing a dark EG process (EG_D) associated with axons (ax). R, rostral; C, caudal. Scale bars: 50 μm (A), 15 μm (C), 5 μm (B), 3 μm (D).

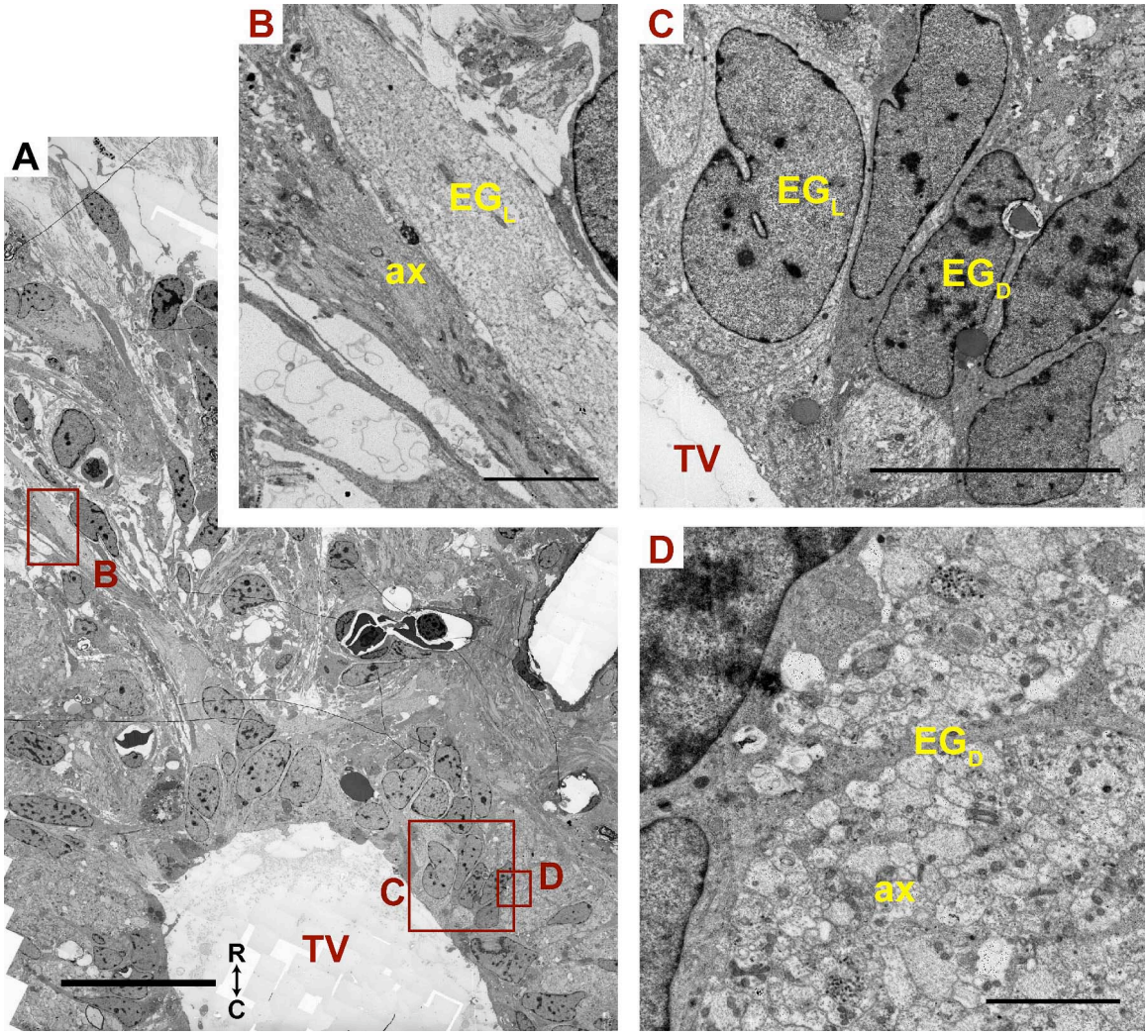
A
B
C
D
EG$_L$
ax
EG$_L$
EG$_D$
TV
B
C
D
TV
R
C
EG$_D$
ax

Figure S4.9. The inflammatory response in early and late stage regenerates. **(A, B**) Adjacent longitudinal sections through a 1 wk regenerate labeled with an anti-fibrin antibody (A) and stained with H&E (B). A fibrin clot is formed in the injury site (A), and inflammatory cells can already be identified in this clot (B). **(B', B")** Enlargement of primed and double primed boxes in (B). Lymphocytes (arrowheads in B') and monocytes (arrow in B") can be identified. Asterisk, fibrin clot. **(C)** Longitudinal section through a contact stage regenerate. A relatively strong inflammatory response has not prevented this animal from progressing to this late stage. **(C')** Enlargement of box in (C). Lymphocytes (arrowhead) and monocytes (arrows) can be identified. R, rostral; C, caudal. Scale bars: 200 μm (A; B, C, same scale), 50 μm (B', B", same scale; C').

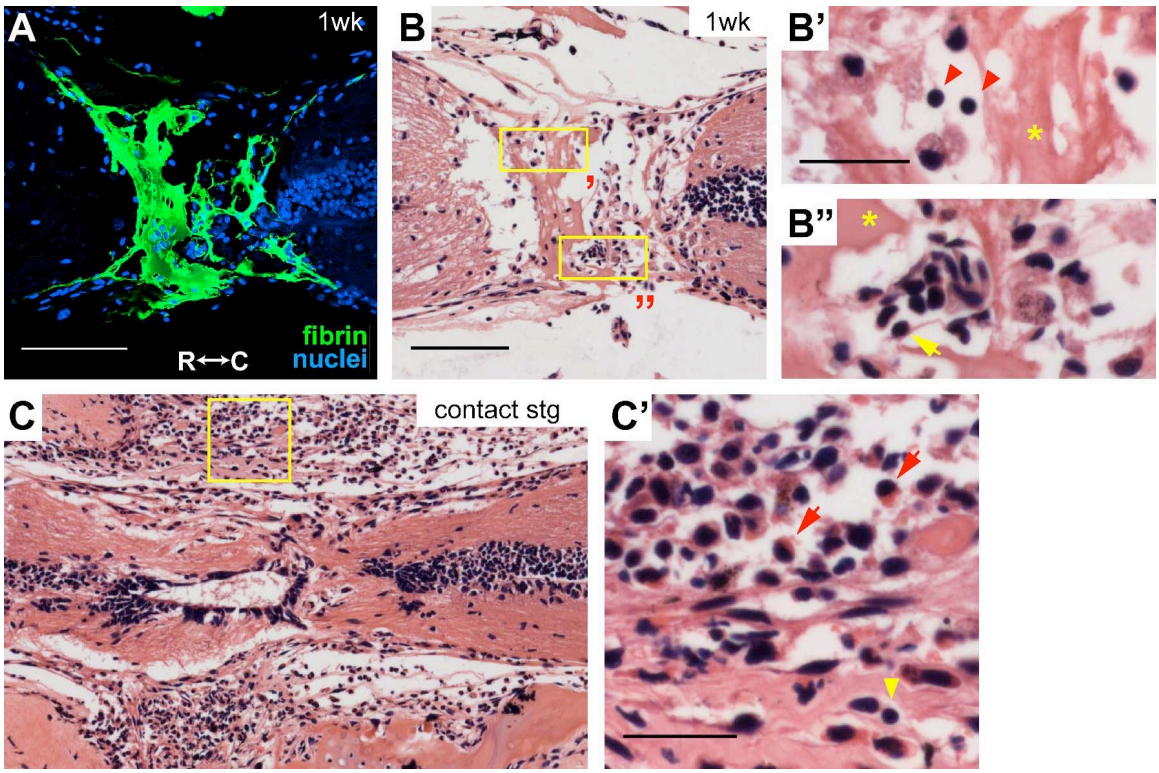
A
1wk
fibrin
nuclei
R↔C
B
1wk
B'
B''
C
contact stg
C'

4.7 Supplemental Tables

Table S4.1. Stages of 2.5 to 3 wk regenerates analyzed after initial study.

Exp-Animal	Prep	Antibody/ Stain	Axon Label	Stage on Rostral Side*	Stage on Caudal Side*
3wk-thick-1-1	thick	FN	rostral BDA app	spiking w/et (wide)	wisping (est)
3wk-thick-1-2	thick	FN	rostral BDA app	contact	contact
3wk-thick-1-3	thick	ColXII	rostral BDA app	growth beyond	growth beyond
3wk-thick-1-4	thick	ColXII	rostral BDA app	spiking w/et (wide)	wisping (est)
3wk-thick-1-5	thick	GFAP/GS	rostral BDA app	growth initiation/wrapping	wisping (est)
3wk-thick-1-6	thick	GFAP/GS	rostral BDA app	growth beyond	growth beyond
3wk-thick-1-7	thick	GFAP/GS	rostral BDA app	spiking w/et (wide)	wisping (est)
3wk-thick-2-1	thick	TN	3A10	spiking w/et	wisping
3wk-thick-2-2	thick	LM	3A10	contact/growth beyond	contact/growth beyond
3wk-thick-2-3	thick	LM	3A10	wrapping/wisping	wisping
3wk-thick-2-4	thick	CSPG	3A10	wisping	wisping
3wk-thick-2-5	thick	TN	3A10	wisping/spiking w/o et	spiking w/o et
3wk-thick-2-6	thick	CSPG	3A10	spiking w/et (wide)	wisping
3wk-thick-2-8	thick	CSPG	3A10	contact	contact
cellID1-3wk-1	pfn long	LM, TN-C, GFAP	rostral BDA app, 3A10	wrapping	–
cellID1-3wk-2	pfn long	CD11b	caudal BDA app, 3A10	wisping	wisping
cellID1-3wk-3	pfn long	IB4, GFAP, LM, TN-C	rostral BDA app, 3A10	wisping	wisping
cellID1-3wk-4	pfn long	FN, ColXII, CSPG	caudal BDA app, 3A10	wisping	wisping
cellID1-3wk-5	pfn long	FN, CSPG, ColXII, IB4	rostral BDA app, 3A10	wisping/spiking w/o et	wisping
cellID1-3wk-6	pfn long	FN, CSPG, ColXII, TN	caudal BDA app, 3A10	wrapping/wisping	wisping
cellID1-3wk-7	pfn long	LM, TN, GFAP, IB4	rostral BDA app, 3A10	wisping	wisping
cellID1-3wk-8	pfn long	LM, TN, GFAP, IB4	caudal BDA app, 3A10	contact	contact
cellID4-3wk-9	cryo long	various	3A10	wisping	spiking w/o et
cellID4-3wk-10	cryo long	various	3A10	wrapping/wisping	wisping
cellID4-3wk-11	cryo long	various	3A10	wrapping/wisping	wisping
cellID4-3wk-12	cryo long	various	3A10	wrapping/wisping	wrapping
cellID6-3wk-13	pfn long	H&E	-	contact (est)	contact (est)
cellID6-3wk-14	pfn long	H&E	-	wisping (est)	wisping (est)

Table S4.1. Continued.

Exp-Animal	Prep	Antibody/ Stain	Axon Label	Stage on Rostral Side*	Stage on Caudal Side*
cellID8-3wk-1	pfn long	H&E, GFAP/GS	-	contact (est)	contact (est)
cellID8-3wk-2	pfn long	H&E, fibrin, GFAP/GS	-	wisping (est)	wisping (est)
cellID8-3wk-3	pfn long	H&E, fibrin, GFAP/GS	-	contact (est)	contact (est)
2.5 wk-1-1	pfn long	vWF/FN, GFAP/fibrin	rostral BDA app, 3A10	wisping	wisping
2.5 wk-1-2	pfn long	vWF/FN, GFAP/fibrin	rostral BDA app, 3A10	wisping	wisping
2.5 wk-1-3	pfn long	vWF/FN, GFAP/fibrin	rostral BDA app, 3A10	wisping	wrapping
2.5 wk-1-4	pfn long	vWF/FN, GFAP/fibrin	3A10	wisping	wisping
2.5 wk-1-5	cryo long	CSPG	3A10	wisping	wisping
2.5 wk-1-6	cryo long	CSPG	3A10	wrapping/wisping	wisping
2.5 wk-1-7	cryo long	CSPG	3A10	wisping	wisping
2.5 wk-1-8	cryo long	CSPG	3A10	wisping	wisping
2.5 wk-1-9	cryo cross	CSPG, vWF/FN	3A10	wisping	wisping
2.5 wk-1-10	cryo cross	CSPG, vWF/FN	3A10	wisping	wisping
2.5 wk-2-11	pfn long	H&E, GFAP, vWF	3A10	wrapping/wisping	wrapping/wisping
2.5 wk-2-12	pfn long	H&E, GFAP, vWF	3A10	wisping	wisping
2.5 wk-2-13	pfn long	H&E, GFAP, vWF	3A10	wisping	wisping
2.5 wk-2-14	pfn cross	GFAP, LM, TN	3A10	wisping (est)	wisping (est)
2.5 wk-2-15	pfn cross	GFAP, LM, TN	3A10	wrapping/wisping (est)	wrapping/wisping (est)
2.5 wk-2-16	pfn cross	GFAP, LM, TN	3A10	wrapping/wisping (est)	wisping (est)
2.5 wk-2-17	pfn cross	FN, ColXII, vWF	rostral BDA app	wisping (est)	wisping (est)
2.5 wk-2-18	pfn cross	FN, ColXII, vWF	rostral BDA app	spiking w/et (est)	wrapping (est)
2.5 wk-2-19	pfn cross	FN, ColXII, vWF	rostral BDA app	wrapping (est)	wisping (est)

* Stage was estimated (*est*) if axons were not labeled with BDA or 3A10 or if the tissue was analyzed in cross sections (*cross*). Staging in thick sections (whole-mount) is more reliable than staging in paraffin (*pfn*) or cryosections (*cryo*) sections. *long*, longitudinal section; *et*, ependymal tube; *app,* application.

Table S4.2. Table of other antibodies tested.

Antigen	Antibody Type	Company, Cat #	Frozen	Paraffin	Thick	Dilution, Format	Notes
Collagen I (human)	goat IgG pAb	Santa Cruz, SC-25974	✖	-	-	1/10, concentrate	non-specific labeling
NCAM (chick)	mouse IgG1 mAb	DSHB, 4D	✖	-	-	1/25, 1/5, concentrate	no bands on reduced & non-reduced WBs
NCAM	mouse IgG1	DSHB, 5B8	-	-	-	ascites	no bands on reduced & non-reduced WBs
Glutamine Synthetase (sheep)	mouse IgG2a	BDTransLab, 610517	✔	✔	✔	~1/1500, concentrate	labels astros & all processes (astros & EG)
Keratin 18 (mammalian)	mouse IgG1 mAb	Santa Cruz, SC-32329	✔	✔	-	1/25, concentrate	labels EG in intact cord, but not regen cord
vimentin	mouse IgM	DSHB, 3CB2	✖	✖	-	1/50, concentrate	tested on intact cord
Sox2 (human)	rabbit IgG pAb	Abcam, ab15830	✔	-	-	1/>25, concentrate	tested on 3wk regen, appears to label neurons
msx 1/2 (chick)	mouse IgG1	DSHB, 4G1	✖ (in SCI)	-	-	1/100, ascites	tested on 3wk regen, no labeling in SCI
22/18	mouse IgM	DSHB, 22/18	✖ (in SCI)	-	-	1/25, concentrate	tested on 3wk regen, no labeling in SCI
Isolectin B4-FITC	-	Sigma, L2895	✔	✔	✔	use at 20 μg/ml	labels microglia, meninges, and many cells in lesion
Iba1	rabbit	Wako, 019-19741	✖	✖	-	1/500	tested on 3wk regen
Iba1 (human)	goat IgG pAb	Abcam, ab5076	✖	-	-	1/200, concentrate	tested on 3wk regen
OX-42	mouse	Serotec, Mca275r	-	✖	-	1/50	tested on 3wk regen
CD11b	rat	Serotec, Mca74ga	✖	✖	-	1/100	tested on 3wk regen
CD11b	rat	BD Pharm, 550282	✖	✖	-	1/50	tested on 3wk regen
F4/80	rat	Serotec, Mca497	-	✖	-	1/10	tested on 3wk regen

Table S4.2. Continued.

NG2	rat	US Biologicals, C5067-70d	✖	✖	-	1/500	tested on 3wk regen
NG2 (human)	goat IgG pAb	Santa Cruz, SC-30923 (G-20)	✖	-	-	1/25, concentrate	tested on 3wk regen
Raldh2 (human)	goat IgG pAb	Santa Cruz, SC-22592 (N-20)	✖	-	-	1/25, concentrate	tested on 3wk regen
Raldh2	rabbit pAb	from P. McCaffery via S. Scott	✖	✖	-	1/100	tested on intact cord
Olig1 (human)	goat IgG pAb	R&D Systems, AF2417	✖	-	-	1/25, concentrate	tested on 3wk regen
Olig2	mouse IgG1	Abcam, ab64547	-	✖	-	1/2000, ascites	tested on 3wk regen
Olig	mouse IgG	DSHB, Olig	✖	✖	-	1/25, concentrate	tested on intact cord
MAG (chick)	mouse IgG1 mAb	Chemicon, MAB1567 (513)	✔	✖	✖	1/100, concentrate	
MAG	mouse mAb	from R. Quarles via M. Filbin	✖	-	-	1/50	tested on intact cord
Nogo-A (human)	rabbit pAb	Santa Cruz, SC-25660 (H-300)	✖	-	-	1/25, 1/10, concentrate	
P0	rabbit pAb	from M. Filbin	✔	-	-	1/50	tested on intact cord, strong label in PNS, weak label in CNS that may be non-specific, multiple bands on WB

astros, astrocytes; *regen*, regenerate or regenerating; *WB*, western blot.

4.8 Movie legends

Movie 4.1. Recovery of swimming function after spinal cord transection injury. When an uninjured newt swims, it propels itself forward by pressing its legs close to its side and undulating its body in an S-shaped motion. When it is finished swimming, it brings its legs forward again, perpendicular to its body axis. One day after a complete transection injury, the hindlimbs are completely paralyzed. Four weeks after injury, this same newt is still paralyzed. When it attempts to swim, it does not use its hindlimbs at all. By 7 wks, this newt has recovered swimming function and swims similarly to an uninjured newt.

Movie 4.2. Movie through confocal z-stack of animal shown in Figure 4.5D, a wisping/spiking stage regenerate. The movie begins on the ventral side of the cord and moves in 2 μm increments through to the dorsal side. Rostral is up. Axons are labeled with 3A10 in magenta, and nuclei are in green. Note the meninges appear to have regenerated across the gap first and that some axons appear to have followed these meninges.

Movie 4.3. Movie through confocal z-stack of animal shown in Figure 4.2J, a spiking stage regenerate. The spike does not contain an ependymal tube in this animal. The movie begins on the ventral side of the cord and moves in 2 μm increments through to the dorsal side. Rostral is up. Descending axons are labeled with the axon tracer in magenta and nuclei are in green.

Movie 4.4. Movie through confocal z-stack of animal shown in Figure 4.2I, a spiking stage regenerate. The spike does contain an ependymal tube in this animal. The movie begins on the ventral side of the cord and moves in 2 μm increments through to the dorsal side. Rostral is up. Descending axons are labeled with the axon tracer in magenta and nuclei are in green.

Movie 4.5. Movie through confocal z-stack of animal shown in Figure S4.4A-A", a recovered animal. This is a 9 wk regenerate in the growth beyond stage that had recovered function. The movie begins on the ventral side of the cord and moves in 2 μm increments through to the dorsal side. Rostral is up. Descending axons are labeled with the axon tracer in magenta and nuclei are in green.

Movie 4.6. Movie through confocal z-stack of animal shown in Figure S4.4E, a nonrecovered animal. This is a 9 wk regenerate in the growth beyond stage that had not recovered function. It begins on the ventral side of the cord and moves in 2 μm increments through to the dorsal side. Rostral is up. Descending axons are labeled with the axon tracer in magenta and nuclei are in green. Note there are two ependymal tubes on the rostral side.

4.9 References

Anderson JR, Jones BW, Yang JH, Shaw MV, Watt CB, Koshevoy P, Spaltenstein J, Jurrus E, U VK, Whitaker RT, Mastronarde D, Tasdizen T, Marc RE (2009) A computational framework for ultrastructural mapping of neural circuitry. PLoS Biol 7:e1000074.

Bader HL, Keene DR, Charvet B, Veit G, Driever W, Koch M, Ruggiero F (2009) Zebrafish collagen XII is present in embryonic connective tissue sheaths (fascia) and basement membranes. Matrix Biol 28:32-43.

Becker CG, Becker T, Meyer RL, Schachner M (1999) Tenascin-R inhibits the growth of optic fibers in vitro but is rapidly eliminated during nerve regeneration in the salamander Pleurodeles waltl. J Neurosci 19:813-827.

Becker T, Becker CG (2001) Regenerating descending axons preferentially reroute to the gray matter in the presence of a general macrophage/microglial reaction caudal to a spinal transection in adult zebrafish. J Comp Neurol 433:131-147.

Becker T, Wullimann MF, Becker CG, Bernhardt RR, Schachner M (1997) Axonal regrowth after spinal cord transection in adult zebrafish. J Comp Neurol 377:577-595.

Borrell V, Marin O (2006) Meninges control tangential migration of hem-derived Cajal-Retzius cells via CXCL12/CXCR4 signaling. Nat Neurosci 9:1284-1293.

Bundesen LQ, Scheel TA, Bregman BS, Kromer LF (2003) Ephrin-B2 and EphB2 regulation of astrocyte-meningeal fibroblast interactions in response to spinal cord lesions in adult rats. J Neurosci 23:7789-7800.

Busch SA, Horn KP, Cuascut FX, Hawthorne AL, Bai L, Miller RH, Silver J (2010) Adult NG2+ cells are permissive to neurite outgrowth and stabilize sensory axons during macrophage-induced axonal dieback after spinal cord injury. J Neurosci 30:255-265.

Butler EG, Ward MB (1967) Reconstitution of the spinal cord after ablation in adult *Triturus*. Dev Biol 15:464-486.

Caubit X, Riou JF, Coulon J, Arsanto JP, Benraiss A, Boucaut JC, Thouveny Y (1994) Tenascin expression in developing, adult and regenerating caudal spinal cord in the urodele amphibians. Int J Dev Biol 38:661-672.

Chernoff EA, Stocum DL, Nye HL, Cameron JA (2003) Urodele spinal cord regeneration and related processes. Dev Dyn 226:295-307.

Clagett-Dame M, McNeill EM, Muley PD (2006) Role of all-trans retinoic acid in neurite outgrowth and axonal elongation. J Neurobiol 66:739-756.

Condic ML, Lemons ML (2002) Extracellular matrix in spinal cord regeneration: getting beyond attraction and inhibition. Neuroreport 13:A37-48.

Condic ML, Snow DM, Letourneau PC (1999) Embryonic neurons adapt to the inhibitory proteoglycan aggercan by increasing integrin expression. J Neurosci 19:10036-10043.

Davies SJ, Goucher DR, Doller C, Silver J (1999) Robust regeneration of adult sensory axons in degenerating white matter of the adult rat spinal cord. J Neurosci 19:5810-5822.

Davis BM, Duffy MT, Simpson SB, Jr. (1989) Bulbospinal and intraspinal connections in normal and regenerated salamander spinal cord. Exp Neurol 103:41-51.

Davis BM, Ayers JL, Koran L, Carlson J, Anderson MC, Simpson SB, Jr. (1990) Time course of salamander spinal cord regeneration and recovery of swimming: HRP retrograde pathway tracing and kinematic analysis. Exp Neurol 108:198-213.

Donnelly DJ, Popovich PG (2008) Inflammation and its role in neuroprotection, axonal regeneration and functional recovery after spinal cord injury. Exp Neurol 209:378-388.

Ferguson MW, O'Kane S (2004) Scar-free healing: from embryonic mechanisms to adult therapeutic intervention. Philos Trans R Soc Lond B Biol Sci 359:839-850.

Ferretti P, Zhang F, O'Neill P (2003) Changes in spinal cord regenerative ability through phylogenesis and development: lessons to be learnt. Dev Dyn 226:245-256.

Fitch MT, Doller C, Combs CK, Landreth GE, Silver J (1999) Cellular and molecular mechanisms of glial scarring and progressive cavitation: in vivo and in vitro analysis of inflammation-induced secondary injury after CNS trauma. J Neurosci 19:8182-8198.

Francis ETB (2002) The anatomy of the salamander. Salt Lake City: Society for the Study of Amphibians and Reptiles.

Ghashghaei HT, Lai C, Anton ES (2007) Neuronal migration in the adult brain: are we there yet? Nat Rev Neurosci 8:141-151.

Harty M, Neff AW, King MW, Mescher AL (2003) Regeneration or scarring: an immunologic perspective. Dev Dyn 226:268-279.

Hermanns S, Reiprich P, Muller HW (2001) A reliable method to reduce collagen scar formation in the lesioned rat spinal cord. J Neurosci Methods 110:141-146.

Herrmann JE, Shah RR, Chan AF, Zheng B (2010) EphA4 deficient mice maintain astroglial-fibrotic scar formation after spinal cord injury. Exp Neurol 223:582-598.

Horn KP, Busch SA, Hawthorne AL, van Rooijen N, Silver J (2008) Another barrier to regeneration in the CNS: activated macrophages induce extensive retraction of dystrophic axons through direct physical interactions. J Neurosci 28:9330-9341.

Kardon G (1998) Muscle and tendon morphogenesis in the avian hind limb. Development 125:4019-4032.

Klymkowsky MW, Hanken J (1991) Whole-mount staining of Xenopus and other vertebrates. In: Methods in Cell Biology, pp 419-441: Academic Press, Inc.

Kumar A, Godwin JW, Gates PB, Garza-Garcia AA, Brockes JP (2007) Molecular basis for the nerve dependence of limb regeneration in an adult vertebrate. Science 318:772-777.

Lakatos A, Smith PM, Barnett SC, Franklin RJ (2003) Meningeal cells enhance limited CNS remyelination by transplanted olfactory ensheathing cells. Brain 126:598-609.

Larrivee B, Freitas C, Suchting S, Brunet I, Eichmann A (2009) Guidance of vascular development: lessons from the nervous system. Circ Res 104:428-441.

Lemons ML, Barua S, Abanto ML, Halfter W, Condic ML (2005) Adaptation of sensory neurons to hyalectin and decorin proteoglycans. J Neurosci 25:4964-4973.

Li Y, Field PM, Raisman G (1998) Regeneration of adult rat corticospinal axons induced by transplanted olfactory ensheathing cells. J Neurosci 18:10514-10524.

McKeon RJ, Hoke A, Silver J (1995) Injury-induced proteoglycans inhibit the potential for laminin-mediated axon growth on astrocytic scars. Exp Neurol 136:32-43.

McLean IW, Nakane PK (1974) Periodate-lysine-paraformaldehyde fixative. A new fixation for immunoelectron microscopy. J Histochem Cytochem 22:1077-1083.

Mey J, D JM, Brook G, Liu RH, Zhang YP, Koopmans G, McCaffery P (2005) Retinoic acid synthesis by a population of NG2-positive cells in the injured spinal cord. Eur J Neurosci 21:1555-1568.

Nace JD, Tassava RA (1995) Examination of fibronectin distribution and its sources in the regenerating newt limb by immunocytochemistry and in situ hybridization. Dev Dyn 202:153-164.

O'Hara CM, Egar MW, Chernoff EA (1992) Reorganization of the ependyma during axolotl spinal cord regeneration: changes in intermediate filament and fibronectin expression. Dev Dyn 193:103-115.

Odelberg SJ (2005) Cellular plasticity in vertebrate regeneration. Anat Rec B New Anat 287:25-35.

Onda H, Goldhamer DJ, Tassava RA (1990) An extracellular matrix molecule of newt and axolotl regenerating limb blastemas and embryonic limb buds: immunological relationship of MT1 antigen with tenascin. Development 108:657-668.

Piatt J (1955) Regeneration of the spinal cord in the salamander. J Exp Zool 129:177-207.

Ramon y Cajal S (1928) Degeneration and regeneration of the nervous system. London: Oxford UP.

Reichenberger E, Baur S, Sukotjo C, Olsen BR, Karimbux NY, Nishimura I (2000) Collagen XII mutation disrupts matrix structure of periodontal ligament and skin. J Dent Res 79:1962-1968.

Reier PJ, Stensaas LJ, Guth L (1983) The astrocytic scar as an impediment to regeneration in the central nervous system. In: Spinal Cord Reconstruction (Kao CC, Bunge RP, Reier PJ, eds), pp 163-196. New York: Raven Press.

Schonbach C (1969) The neuroglia in the spinal cord of the newt, Triturus viridescens. J Comp Neurol 135:93-120.

Shearer MC, Fawcett JW (2001) The astrocyte/meningeal cell interface--a barrier to successful nerve regeneration? Cell Tissue Res 305:267-273.

Shearer MC, Niclou SP, Brown D, Asher RA, Holtmaat AJ, Levine JM, Verhaagen J, Fawcett JW (2003) The astrocyte/meningeal cell interface is a barrier to neurite outgrowth which can be overcome by manipulation of inhibitory molecules or axonal signalling pathways. Mol Cell Neurosci 24:913-925.

Siegenthaler JA, Ashique AM, Zarbalis K, Patterson KP, Hecht JH, Kane MA, Folias AE, Choe Y, May SR, Kume T, Napoli JL, Peterson AS, Pleasure SJ (2009) Retinoic acid from the meninges regulates cortical neuron generation. Cell 139:597-609.

Silver J, Miller JH (2004) Regeneration beyond the glial scar. Nat Rev Neurosci 5:146-156.

Simpson SB, Jr. (1983) Fasciculation and Guidance of Regenerating Central Axons by the Ependyma. In: Spinal Cord Reconstruction (Kao CC, Bunge RP, Reier PJ, eds), pp 151-162. New York: Raven Press.

Singer M, Nordlander RH, Egar M (1979) Axonal guidance during embryogenesis and regeneration in the spinal cord of the newt: the blueprint hypothesis of neuronal pathway patterning. J Comp Neurol 185:1-21.

Stensaas LJ (1983) Regeneration in the spinal cord of the newt *Notopthalamus (Triturus) pyrrhogaster.* In: Spinal Cord Reconstruction (Kao CC, Bunge RP, Reier PJ, eds), pp 121-149. New York: Raven Press.

Tang X, Davies JE, Davies SJ (2003) Changes in distribution, cell associations, and protein expression levels of NG2, neurocan, phosphacan, brevican, versican V2, and tenascin-C during acute to chronic maturation of spinal cord scar tissue. J Neurosci Res 71:427-444.

Tennant M, Beazley LD (1992) A breakdown of the blood-brain barrier is associated with optic nerve regeneration in the frog. Vis Neurosci 9:149-155.

Tokuyasu KT (1989) Use of poly(vinylpyrrolidone) and poly(vinyl alcohol) for cryoultramicrotomy. Histochem J 21:163-171.

Tom VJ, Steinmetz MP, Miller JH, Doller CM, Silver J (2004) Studies on the development and behavior of the dystrophic growth cone, the hallmark of regeneration failure, in an in vitro model of the glial scar and after spinal cord injury. J Neurosci 24:6531-6539.

Wang G, Scott SA (2008) Retinoid signaling is involved in governing the waiting period for axons in chick hindlimb. Dev Biol 321:216-226.

Wei Y, Yang EV, Klatt KP, Tassava RA (1995) Monoclonal antibody MT2 identifies the urodele alpha 1 chain of type XII collagen, a developmentally regulated extracellular matrix protein in regenerating newt limbs. Dev Biol 168:503-513.

Xie F, Zheng B (2008) White matter inhibitors in CNS axon regeneration failure. Exp Neurol 209:302-312.

Zukor KA, Kent DT, Odelberg SJ (2010) Fluorescent whole-mount method for visualizing three-dimensional relationships in intact and regenerating adult newt spinal cords. Dev Dyn 239:3048-3057.

CHAPTER 5

CONCLUSION

The broad aim of this dissertation was to add to our understanding of how naturally occurring regenerative processes take place so that, one day, we may know how to stimulate those regenerative processes in our own species. I used the newt as a model system because it represents the vertebrate with the most extensive regenerative abilities in its adult form. The newt also has the advantage that, unlike fish, it is a tetrapod. Work presented herein focuses mainly on spinal cord regeneration, but also touches on limb regeneration. In Chapter 2, I presented data suggesting that a novel newt chemokine may have a role in stimulating cell proliferation and migration after limb amputation, and thus, may have a role in the formation and growth of the regeneration blastema. In Chapter 3, I demonstrated how whole-mount fluorescent labeling and imaging techniques were adapted for use in the newt spinal cord. This method greatly improved our ability to visualize the cellular and extracellular environment and understand 3-dimensional relationships in the intact and injured cord. In Chapter 4, I used the new methods to identify stages of axon regeneration after a complete transection spinal cord injury (SCI) to the lower trunk region of the animal and found that axons appear to be able to regenerate through the lesion, in part, because the environment permits axon regeneration. This is in contrast to what is already known to occur in the injured mammalian spinal cord, where the environment is inhibitory for axon regeneration.

5.1 Models of spinal cord regeneration

After an SCI in the newt, meningeal and endothelial cells migrate into the lesion before axons do and are associated with a loose extracellular matrix (ECM) that permits axon regeneration. Axons regenerate into the lesion next and are closely associated with meningeal cells and glial processes. An ependymal tube lined by glial cells extends into the lesion last. Then the meningeal cells, axons, and glia move as a unit to close the gap in the cord. Because meningeal cells and glia appear to assist axon regeneration rather than form barriers, such as a glia limitans and dense scar, I hypothesize that this is a primary reason why regeneration is successful in the newt. Endothelial cells are not as closely associated with regenerating axons as the meningeal cells and glia, but they may assist axons by providing trophic support and/or by contributing to the formation of the permissive ECM. Phagocytic cells and leucocytes are also present in the lesion, and these may assist axon regeneration by clearing debris and releasing factors that stimulate beneficial cellular responses.

Newt spinal cord regeneration after an SCI differs from that after tail amputation (Nordlander and Singer, 1978; 1983) in that axons precede the ependymal tube into the lesion rather than vice versa. Thus, an ependymal tube is not required to provide a scaffold for axon regeneration. Instead, meningeal cells and glial processes may fill this role. Spinal cord regeneration after an SCI may also be different between the newt and axolotl in that unlike axolotl ependymoglia (EG), newt EG do not appear to undergo a massive epithelial to mesenchymal transition and fill the injury site with cells that re-epithelialize to form an ependymal tube which then supports axon regeneration (O'Hara et al., 1992; Chernoff et al., 2003). On the other hand, it is possible that events after an

SCI in the axolotl are actually similar to those after an SCI in the newt, and these events were interpreted differently by the investigators. For example, the $GFAP^-$, FN^+ cells in the injury site that they identified as EG could have been meningeal cells. Regeneration after an SCI in the eel appears to proceed similarly to that in the newt (Dervan and Roberts, 2003). The authors described the bridge of tissue across the lesion as consisting of "regrowing axons enwrapping a central canal and enclosed in a meningeal sheath." They also note that axons grow into the lesion before the ependymal cells elongate a central canal. Regeneration after an SCI in zebrafish or frog tadpoles has not been examined at this level of detail. It will be interesting in the future to do comparative analyses between regeneration-competent and regeneration-incompetent animals to determine which factors and events are common to successful spinal cord regeneration and which are common to regeneration failure. For example, events after SCI in zebrafish, goldfish, lamprey, eel, axolotl, newt and frog tadpole could be compared to those in the regeneration-incompetent lizard and adult frog. Given that cold-blooded animals have a greater regenerative capacity than warm-blooded animals, it would also be interesting to determine if the naked mole rat, a mammal that has re-gained cold-bloodedness, has a greater regenerative capacity than mice and rats.

5.2 Implications for spinal cord regeneration in mammals

Now that we know more about the cellular and extracellular responses to SCI in the newt, we can compare them to those in mammals and begin to consider why these differences exist and how they may guide future strategies in regenerative medicine.

In both newts and mammals, initially after an SCI, axons retract from the end of the cut cord and appear dystrophic. This indicates that axon retraction does not preclude successful regeneration. Instead, it may even promote neuronal survival. The acute injury site may be harmful to axotomized neurons, and the axotomized neuron may need time to mount an intrinsic regenerative response before traversing the injury site. Therefore, instead of seeking ways to prevent axon retraction in mammals, it may be more useful to discover how to activate intrinsic growth potential. A recent study deleted the tumor suppressor gene, phosphatase and tensin homolog (PTEN), in mouse corticospinal neurons, and this enabled them to regenerate axons across a transection SCI (Liu et al., 2010). This regeneration, however, was not sufficient to restore function and was only seen at the edges of the cord. It would be interesting to determine if the intrinsic growth potential of newt neurons is activated by a similar mechanism and what the downstream effects of activation are. For example, receptors that mediate inhibition may be downregulated (Keleman et al., 2002), internal levels of cyclic nucleotides may be increased (Cai et al., 2001; Qiu et al., 2002), and expression of proteins that promote growth cone motility may be upregulated, such as integrin β1 and MMPs (Condic et al., 1999; Condic, 2001; Hayashita-Kinoh et al., 2001). These questions can be partially answered with expression studies, but to test the requirement for or sufficiency of various factors, it would be useful to have a robust system for growing newt neurons *in vitro*, as well as genetic tools for manipulating gene expression *in vivo*. These tools are not currently available for the newt model system and will be discussed more fully below. Learning more about how the intrinsic growth potential of newt neurons is activated may enable us to more fully activate growth in mammalian neurons.

Once growth is initiated, newt axons appear to be able to overcome inhibitory factors, such as chondroitin sulfate proteoglycans (CSPGs), in their environment. Their environment, however, does not present physical barriers to regeneration. I hypothesize that if such barriers were created, then newt axons, like mammalian axons, would not be able to regenerate across the lesion in sufficient numbers to restore function. To address this issue, I attempted to make the newt SCI site more inhibitory by adding CSPG protein or by blocking matrix metalloproteinase (MMP) function with the drug GM6001. These studies were inconclusive, however, because I was never able to demonstrate that the manipulation affected the nature of the lesion ECM. Similar experiments have been more successfully attempted in the optic nerve of frog tadpoles (Reier et al., 1983) and in the spinal cord of goldfish (Bernstein and Bernstein, 1967). In these experiments, axons were able to regenerate through the "glial scars" that were created, but it is unclear how similar these scars are to those that are formed in mammals. These studies also did not assess functional recovery nor did they determine if axons emerged from the scar to penetrate the optic nerve or spinal cord on the opposite side of the scar. While these studies suggest that intrinsic growth potential is likely vital for successful regeneration, they also indicate that regeneration is suboptimal if there are barriers in the environment. Indeed, if the two ends of the newt spinal cord are misaligned, functional recovery does not occur (Davis et al., 1990; see also Chapter 4). The misalignment, in effect, creates a physical barrier to regeneration. Thus, it may be fruitful to develop strategies in mammals that induce cells to create a pathway for axon regeneration rather than barriers. If we can combine such strategies with those that induce intrinsic growth potential, such as the PTEN-deletion

strategy used in the study mentioned above (Liu et al., 2010), then we may be able to induce functional spinal cord regeneration in mammals.

After an SCI in mammals, meningeal cells and glia create physical barriers in order to wall off the area and re-establish the blood brain barrier (BBB) (Silver and Miller, 2004). This serves to minimize the extent of the injury. For example, when reactive astrocytes are ablated from a mouse SCI site, the BBB is not repaired, the inflammatory response is elevated, there is more cell death, and functional deficits are more severe (Faulkner et al., 2004). In contrast, newt meningeal cells and glia do not appear to wall off the injury site, at least not as aggressively as their mammalian counterparts. How is the BBB repaired in the newt? How long does it take? I would predict that the BBB is repaired more slowly in the newt. This can be tested by injecting molecules into the blood stream that cannot cross the BBB (such as rhodamine-bovine serum albumin) and then assessing how long after injury these molecules are able to leak into the nervous tissue (Tennant and Beazley, 1992). The consequences of prolonged BBB disruption may be more severe in warm-blooded animals, and this may explain why mammalian astrocytes and meningeal cells evolved such strong reactions to central nervous system (CNS) injuries. It will be important to understand the differences in the mechanisms of BBB repair between newts and mammals as well as how the dynamics of BBB permeability differentially affect the extent of secondary damage if we are to discover a way to effectively remove the barriers to regeneration in mammals.

This may make finding therapies in mammals using information gleaned from newts a challenging endeavor. Nonetheless, there are hints that mammalian cells may retain the capacity to respond to an SCI in ways that support axon regeneration, similar to

the way newt cells do. When PTEN is deleted from mouse corticospinal neurons, the axons regenerate across an SCI lesion in association with $GFAP^+$ processes (Liu et al., 2010). These $GFAP^+$ "bridges" are found at the edges of the spinal cord. In other words, they are found in regions that are closest to the meninges. Thus, mammalian astrocytes and meningeal cells may be able to cooperate to form these bridges. It would be interesting to determine if these bridges always form or if they only form when axonal growth potential is activated. If the latter is true, this would suggest that axons themselves have a role in directing cell behaviors at the injury site and would be consistent with results seen in the frog tadpole studies mentioned above. When axons grew into an implanted glial scar, the hypertrophic astrocytes within the scar adopted a more permissive architecture (Reier et al., 1983). Learning more about who the cell players are in the newt, where they come from and what roles they play may help us learn how to cultivate those types of behaviors in mammalian cells. To do this, however, we will need to develop more tools for the newt model system.

5.3 Tools needed for the newt model system

5.3.1 Basic tools

Basic tools, such as newt specific antibodies and mRNA *in situ* hybridization probes, should be relatively simple to develop. These would allow us to identify, classify and characterize newt cell types better than before and determine which cells express transcripts or proteins that might have a role in shaping the environment or directly stimulating, supporting, or guiding axon regeneration. More markers are needed that can specifically identify EG, astrocytes, meningeal cells, de-differentiated cells, inflammatory

cells, microglia, oligodendrocytes, oligodendrocyte precursor cells, and neurons. Proteins of interest, and transcripts encoding those proteins, would include ECM proteins, cell-cell and cell-ECM adhesion proteins, cell-cell signaling proteins, MMPs, guidance cues and their receptors, and growth factors and their receptors.

5.3.2 Computational molecular phenotyping

Computational molecular phenotyping (CMP) may also be useful for characterizing cell types in the newt. This method classifies cells based on their relative expression of small molecules and metabolites like glutamate, glycine, and glutathione (Marc et al., 1995). Because these small molecules are invariant between species (newt glutamate is the same as mouse glutamate), the probes used are not species specific. Preliminary evidence suggests that CMP will be useful for characterizing the cell types present in the intact newt spinal cord, cellular responses to injury, and for interspecies comparative analyses, but that it may not be useful for identifying reactive cell types present in the middle of an SCI lesion (Odelberg lab, unpublished observations). After an SCI, cells in the lesion tend to adopt the same, bland profile of small molecule expression and could not easily be separated into classes or correlated with classes that were present in the intact cord. This may occur because cells in the lesion have dedifferentiated to a progenitor-like state as they do after limb amputation or because the cells lose their unique signatures after being disrupted and activated by the injury.

5.3.3 Neuronal culture system

As mentioned above, the development of a robust neuronal culture system would also greatly add to our understanding of the requirements for and mechanisms of axon

regeneration in the newt. I tried to develop such a system, using methods informed by the literature (Olsen and Bunge, 1986; Ferretti and Brockes, 1988; Wetzel et al., 1989; Chernoff et al., 1990; Benraiss et al., 1996; Tonge et al., 1997; Tonge et al., 1998; Becker et al., 1999; Bauduin et al., 2000; Tonge and Leclere, 2000; Ikegami et al., 2002; Dmetrichuk et al., 2005), but I was unable to find a system that would reliably allow newt neurons or explants to attach to the dish or grow healthy neurites with growth cones. Table 5.1 shows what parameters I tried and which appeared to work the best. Given how well newt neurons grow axons *in vivo*, it was surprising that they did not grow neurites very well *in vitro*. Mature, adult neurons, however, are typically harder to culture than developing, young neurons. Also, most media/supplement systems available have been optimized for warm-blooded, developing mammalian neurons and not cold-blooded, adult, amphibian neurons. It is likely the two types of neurons have different requirements.

5.3.4 Genetic tools

Clearly, the newt's regenerative capacities make it an intriguing model system. The mechanisms governing its regenerative processes have been very difficult to dissect, however, because there are very few tools available for perturbing or following these processes.

Occasionally, a drug inhibitor will produce useful results. The MMP inhibitor, GM6001, alters limb regeneration when applied to the water in which the animal swims (Vinarsky et al., 2005). AraC, a proliferation inhibitor, is effective at blocking proliferation when injected intraperitoneally (Parish et al., 2007). Fluorescent dyes can be

Table 5.1. Parameters tested for the development of a newt neuronal cell culture system

Variable	Parameters Tested	Best	Future
neuron type	brainstem spinal cord spinal ganglia preconditioning lesion dissociated & explant	spinal ganglia explant	CNS explant, preconditioned, with meninges left on
dissociation	collagenase & dispase 0.25 – 0.05% trypsin 10 min – 100 min with or without DNase	0.125% trypsin, 100 min with DNAse	
purification	preplate cell strainer & centrifugation percoll gradient	unpurified (if purified, yield is LOW)	
substrata	laminin (LM) aggrecan+LM fibronectin collagen 3D collagen 3D collagen+LM tenascin nitrocellulose millipore membranes poly-L/D-lysine (PDL) nitrocellulose+PDL+LM glass	LM millipore membrane+LM *but attachment is poor* (if more attached, then neurites don't grow)	LM or millipore memb+LM or matrigel or meningeal cells
medium (adjusted to ~ 250 mOsm, pH 7.4)	L-15 F12H DMEM F12/DMEM neurobasal	all about the same, but most use L-15 for amphibian cultures	70% L-15
supplements	Sigma's N1 Sigma's N2 Sigma's B27 glucose newt galectin & chemokine serum NGF & NT3 growth factors	all about the same	

manually injected into cells to follow their fate after injury (Lo et al., 1993; Echeverri et al., 2001), but these markers are not permanent and not all cell types are amenable to this type of analysis.

The ideal and most versatile way to manipulate biological function is with genetic tools. The newt is not a very practical model system for transgenic experiments because newts require 3 to 5 years to become sexually mature adults, and a system for breeding them in the lab has not been developed. Newts used in laboratory experiments are collected from the wild. Plasmids have been used for gain-of-function experiments (Kumar et al., 2007) and to express fluorescent tags (Echeverri and Tanaka, 2002), but expression is only transient and electroporation must be used to allow the plasmid to enter cells. This can complicate results because electroporation itself has been shown to cause a cellular response. Namely, it causes cells to de-differentiate (Atkinson et al., 2006). Morpholinos work with only limited efficiency *in vivo* in the axolotl (Schnapp and Tanaka, 2005) and do not appear to be effective in the newt (Odelberg lab, unpublished observations). Morpholinos also require electroporation to enhance their efficacy.

Viral vectors, especially lentiviral vectors, may be the best option for manipulating gene expression in adult newt tissues. Lentiviral vectors can integrate in the genome of dividing and non-dividing cells to produce stable changes in gene expression. This is advantageous for regenerative processes that occur over the course of weeks to months. Lentiviral vectors can be used for overexpression/gain-of-function as well as loss-of-function/RNA interference studies (Szulc et al., 2006; Szulc and Aebischer, 2008). Lentiviral and retroviral vectors pseudotyped with the VSV-G envelope protein are able to induce expression of reporter proteins in newt cell lines *in vitro* (Kumar et al.,

2000; and unpublished observations), but do not appear to be effective when injected *in vivo* (unpublished observations). When lentivirus was added to newt muscle or blastemal cell lines at a multiplicity of infection of 1000, 47% and 100% of the cells, respectively, expressed low levels of the enhanced green fluorescent protein (EGFP) reporter (driven by the CMV promoter) when analyzed via fluorescence-based flow cytometry 5 days after transduction. When 1 μl of the lentivirus (titer 8 x 10^8 infection-forming units/ml) was injected into intact and regenerating newt limbs, EGFP expression could not be seen in whole limbs. This is not because it is impossible to see EGFP expressed in whole limbs. EGFP expression driven by the CMV promoter can be seen in whole limbs when expressed from electroporated plasmids (Atkinson et al., 2006). Either the virus is unable to readily enter newt cells, or the virus enters the cells and integrates into the genome but is silenced. This is worth further investigation. There are viruses that infect newts (Larsen, 1969; Balseiro et al., 2009). Discovering what envelope protein(s) these viruses use to gain entry into newt cells may enable us to develop a viral tool that can transduce newt tissues more efficiently.

Until versatile genetic tools are available for use in the newt, we will be unable to definitively answer many questions about what factors stimulate and direct cell behaviors, what factors are required for a given process, or which cell lineages give rise to reactive or new cell types. It will also be very difficult to determine what roles candidate genes identified via microarray and expression analyses, such as the novel newt chemokine discussed in Chapter 2, play during regeneration. Finally, if the newt can be transformed into a model system amenable to genetic manipulations, it will be

advantageous to sequence its genome and establish a facility to raise newts for laboratory studies, so that natural populations are not depleted.

5.4 Alternative model systems

An alternative, or complementary, strategy for learning more about the mechanisms of regeneration is to translate findings in the newt to model systems that are already more amenable to genetic manipulations, such as the axolotl or zebrafish. Though axolotl tissues may be less mature than newt tissues and zebrafish do not have four limbs, regenerative pathways in these organisms are likely to be similar to those in the newt. The advantage of being able to probe their biology more deeply outweighs the disadvantage of them being less similar to an adult mammal. Axolotls and zebrafish are bred for lab use, they develop faster, and transgenic lines are available. Axolotls are transparent enough for *in vivo* imaging, and it is therefore possible to observe cellular events at multiple time points in the same animal. The zebrafish is a well-established model system, much is known about its developmental biology, mutant lines are available, protocols have been developed for many techniques, morpholino tools are available, and its genome has been sequenced (Becker and Becker, 2007).

5.5 Summary

Regeneration is a fascinating and challenging subject, and the regenerative abilities of the newt give us hope that it may be possible to stimulate limb and spinal cord regeneration in humans. While we are still a long way from achieving this goal, the work presented in this dissertation has taken us one step closer. We have more methods for analyzing newt tissues. We now know that a chemokine may play a role in stimulating

cells to proliferate and migrate to form the regeneration blastema, the self-organizing structure capable of directing epimorphic regeneration of limbs and tails. We also now have a clearer picture of the cellular events and the extracellular environment associated with spinal cord regeneration after an SCI. Spinal cord regeneration appears to be enabled, in part, because the environment is permissive for axon regrowth. Meningeal cells and glia appear to play an important role in creating this permissive environment. Future experiments can test these hypotheses, when more tools become available. These hypotheses also hint that it may be fruitful to look for ways to alter meningeal cell and glial responses in spinal cord injured mammals so that they are more like those in the newt.

5.6 References

Atkinson DL, Stevenson TJ, Park EJ, Riedy MD, Milash B, Odelberg SJ (2006) Cellular electroporation induces dedifferentiation in intact newt limbs. Dev Biol 299:257-271.

Balseiro A, Dalton KP, Del Cerro A, Marquez I, Parra F, Prieto JM, Casais R (2009) Outbreak of common midwife toad virus in alpine newts (Mesotriton alpestris cyreni) and common midwife toads (Alytes obstetricans) in Northern Spain: A comparative pathological study of an emerging ranavirus. Vet J.

Bauduin B, Lassalle B, Boilly B (2000) Stimulation of axon growth from the spinal cord by a regenerating limb blastema in newts. Brain Res Dev Brain Res 119:47-54.

Becker CG, Becker T (2007) Zebrafish as a model system for successful spinal cord regeneration. In: Model organisms in spinal cord regeneration (Becker CG, Becker T, eds). Weinheim: Wiley-VCH.

Becker CG, Becker T, Meyer RL, Schachner M (1999) Tenascin-R inhibits the growth of optic fibers in vitro but is rapidly eliminated during nerve regeneration in the salamander Pleurodeles waltl. J Neurosci 19:813-827.

Benraiss A, Caubit X, Arsanto JP, Coulon J, Nicolas S, Le Parco Y, Thouveny Y (1996) Clonal cell cultures from adult spinal cord of the amphibian urodele Pleurodeles

waltl to study the identity and potentialities of cells during tail regeneration. Dev Dyn 205:135-149.

Bernstein JJ, Bernstein ME (1967) Effect of glial-ependymal scar and teflon arrest on the regenerative capacity of goldfish spinal cord. Exp Neurol 19:25-32.

Cai D, Qiu J, Cao Z, McAtee M, Bregman S, Filbin MT (2001) Neuronal cyclic AMP controls the developmental loss of ability of axons to regenerate. J Neurosci 21:4731-4739.

Chernoff EA, Stocum DL, Nye HL, Cameron JA (2003) Urodele spinal cord regeneration and related processes. Dev Dyn 226:295-307.

Chernoff EAG, Munck CM, Mendelsohn LG, Egar MW (1990) Primary culture of axolotl spinal cord ependymal cells. Tissue and Cell 22:601-613.

Condic ML (2001) Adult neuronal regeneration induced by transgenic integrin expression. J Neurosci 21:4782-4788.

Condic ML, Snow DM, Letourneau PC (1999) Embryonic neurons adapt to the inhibitory proteoglycan aggercan by increasing integrin expression. J Neurosci 19:10036-10043.

Davis BM, Ayers JL, Koran L, Carlson J, Anderson MC, Simpson SB, Jr. (1990) Time course of salamander spinal cord regeneration and recovery of swimming: HRP retrograde pathway tracing and kinematic analysis. Exp Neurol 108:198-213.

Dervan AG, Roberts BL (2003) Reaction of spinal cord central canal cells to cord transection and their contribution to cord regeneration. J Comp Neurol 458:293-306.

Dmetrichuk JM, Spencer GE, Carlone RL (2005) Retinoic acid-dependent attraction of adult spinal cord axons towards regenerating newt limb blastemas in vitro. Dev Biol 281:112-120.

Echeverri K, Tanaka EM (2002) Ectoderm to mesoderm lineage switching during axolotl tail regeneration. Science 298:1993-1996.

Echeverri K, Clarke JD, Tanaka EM (2001) In vivo imaging indicates muscle fiber dedifferentiation is a major contributor to the regenerating tail blastema. Dev Biol 236:151-164.

Faulkner JR, Herrmann JE, Woo MJ, Tansey KE, Doan NB, Sofroniew MV (2004) Reactive astrocytes protect tissue and preserve function after spinal cord injury. J Neurosci 24:2143-2155.

Ferretti P, Brockes JP (1988) Culture of newt cells from different tissues and their expression of a regeneration-associated antigen. J Exp Zool 247:77-91.

Hayashita-Kinoh H, Kinoh H, Okada A, Komori K, Itoh Y, Chiba T, Kajita M, Yana I, Seiki M (2001) Membrane-type 5 matrix metalloproteinase is expressed in differentiated neurons and regulates axonal growth. Cell Growth Differ 12:573-580.

Ikegami Y, Mitsuda S, Araki M (2002) Neural cell differentiation from retinal pigment epithelial cells of the newt: an organ culture model for the urodele retinal regeneration. J Neurobiol 50:209-220.

Keleman K, Rajagopalan S, Cleppien D, Teis D, Paiha K, Huber LA, Technau GM, Dickson BJ (2002) Comm sorts robo to control axon guidance at the Drosophila midline. Cell 110:415-427.

Kumar A, Velloso CP, Imokawa Y, Brockes JP (2000) Plasticity of retrovirus-labelled myotubes in the newt limb regeneration blastema. Dev Biol 218:125-136.

Kumar A, Godwin JW, Gates PB, Garza-Garcia AA, Brockes JP (2007) Molecular basis for the nerve dependence of limb regeneration in an adult vertebrate. Science 318:772-777.

Larsen JH, Jr. (1969) Ultrastructural study on cell-virus relationships in the thyroid of a salamander (Ambystoma macrodactylum Baird). Z Zellforsch Mikrosk Anat 95:511-519.

Liu K, Lu Y, Lee JK, Samara R, Willenberg R, Sears-Kraxberger I, Tedeschi A, Park KK, Jin D, Cai B, Xu B, Connolly L, Steward O, Zheng B, He Z (2010) PTEN deletion enhances the regenerative ability of adult corticospinal neurons. Nat Neurosci 13:1075-1081.

Lo DC, Allen F, Brockes JP (1993) Reversal of muscle differentiation during urodele limb regeneration. Proc Natl Acad Sci U S A 90:7230-7234.

Marc RE, Murry RF, Basinger SF (1995) Pattern recognition of amino acid signatures in retinal neurons. J Neurosci 15:5106-5129.

Nordlander RH, Singer M (1978) The role of ependyma in regeneration of the spinal cord in the urodele amphibian tail. J Comp Neurol 180:349-374.

O'Hara CM, Egar MW, Chernoff EA (1992) Reorganization of the ependyma during axolotl spinal cord regeneration: changes in intermediate filament and fibronectin expression. Dev Dyn 193:103-115.

Olsen CL, Bunge RP (1986) Requisites for growth and myelination of urodele sensory neurons in tissue culture. J Exp Zool 238:373-384.

Parish CL, Beljajeva A, Arenas E, Simon A (2007) Midbrain dopaminergic neurogenesis and behavioural recovery in a salamander lesion-induced regeneration model. Development 134:2881-2887.

Qiu J, Cai D, Dai H, McAtee M, Hoffman PN, Bregman BS, Filbin MT (2002) Spinal axon regeneration induced by elevation of cyclic AMP. Neuron 34:895-903.

Reier PJ, Stensaas LJ, Guth L (1983) The astrocytic scar as an impediment to regeneration in the central nervous system. In: Spinal Cord Reconstruction (Kao CC, Bunge RP, Reier PJ, eds), pp 163-196. New York: Raven Press.

Schnapp E, Tanaka EM (2005) Quantitative evaluation of morpholino-mediated protein knockdown of GFP, MSX1, and PAX7 during tail regeneration in Ambystoma mexicanum. Dev Dyn 232:162-170.

Silver J, Miller JH (2004) Regeneration beyond the glial scar. Nat Rev Neurosci 5:146-156.

Simpson SB, Jr. (1983) Fasciculation and Guidance of Regenerating Central Axons by the Ependyma. In: Spinal Cord Reconstruction (Kao CC, Bunge RP, Reier PJ, eds), pp 151-162. New York: Raven Press.

Szulc J, Aebischer P (2008) Conditional gene expression and knockdown using lentivirus vectors encoding shRNA. Methods Mol Biol 434:291-309.

Szulc J, Wiznerowicz M, Sauvain MO, Trono D, Aebischer P (2006) A versatile tool for conditional gene expression and knockdown. Nat Methods 3:109-116.

Tennant M, Beazley LD (1992) A breakdown of the blood-brain barrier is associated with optic nerve regeneration in the frog. Vis Neurosci 9:149-155.

Tonge D, Edstrom A, Ekstrom P (1998) Use of explant cultures of peripheral nerves of adult vertebrates to study axonal regeneration in vitro. Prog Neurobiol 54:459-480.

Tonge DA, Leclere PG (2000) Directed axonal growth towards axolotl limb blastemas in vitro. Neuroscience 100:201-211.

Tonge DA, Golding JP, Edbladh M, Kroon M, Ekstrom PE, Edstrom A (1997) Effects of extracellular matrix components on axonal outgrowth from peripheral nerves of adult animals in vitro. Exp Neurol 146:81-90.

Vinarsky V, Atkinson DL, Stevenson TJ, Keating MT, Odelberg SJ (2005) Normal newt limb regeneration requires matrix metalloproteinase function. Dev Biol 279:86-98.

Wetzel DM, Lee VM, Erulkar SD (1989) Long-term cultures of neurons from adult frog brain express GABA and glutamate-activated channels. J Neurobiol 20:255-270.